I. EDGE DIFFRACTION OF A CONVERGENT WAVE

II. DIFFRACTION OF LAGUERRE GAUSSIAN BEAMS BY A CIRCULAR APERTURE

Thesis by

Alexander Constantine R. Livanos

In Partial Fulfillment of the Requirements

For the Degree of

Doctor of Philosophy

California Institute of Technology

Pasadena, California

1975

(Submitted September 25, 1974)

ACKNOWLEDGMENTS

I would like to thank my advisor, Dr. Nicholas George, for suggesting these problems to me, and for his constant encouragement and guidance throughout the course of this work.

I wish to thank the staff of the computing center, and especially Albert Chang for his expert help and advice on my numerical calculations.

I would also like to thank Dr. Julio Varsi and Dr. Vince Menichelli for their support in the early stages of my work.

Finally my very special thanks to Dian Rapchak for doing such a beautiful job on typing this thesis with all those equations.

This research has been supported in part by the Electronic and Solid State Sciences Division of the Air Force Office of Scientific Research.

ABSTRACT

PART 1

Closed form solutions have been derived for the focal plane diffraction patterns of (a) a convergent spherical wave illuminating a segment of a circular aperture and (b) a convergent Gaussian beam diffracted by an infinite edge. The theoretical results agree with the experiments showing that the edge produces a spike of light with intensity variation inversely proportional to the squared distance from the center, that the pattern is symmetric in the focal plane, and that in the case of the uniform illumination the intensity has high spatial frequency components while for the Gaussian case the pattern does not ring when the edge is positioned symmetrically in the beam.

In addition, the near focus intensity distribution for a convergent uniform amplitude wave illuminating a semicircular aperture is presented, and it is shown that the fact that the radiation pattern is symmetric only at the focal plane can be used very effectively to determine the exact location of that plane.

PART II

The diffraction of a Laguerre Gaussian beam ($TEM_{p,\ell}$ mode of a laser resonator) by a circular aperture is presented here. We calculate the electric field for the Fresnel region, and study the loss of power as a function of relative aperture size and mode index, showing that the conventional rule of thumb in selecting apertures by "going out a few times w_o" is not accurate for large mode indices.

TABLE OF CONTENTS

PART I

TABLE OF CONTENTS

PART II

PART I

EDGE DIFFRACTION OF A CONVERGENT WAVE

CHAPTER 1

INTRODUCTION

1.1 Statement of the Problem

The diffraction of an electromagnetic wave by an edge is a basic problem in optics. The experimental detection of the observed patterns as well as the theoretical solution has been a subject of numerous studies in the past[1-17], closely related with the evolution of the theory of diffraction.

Important motivations for calculating the focal plane diffraction patterns of a spherically curved wave incident on an edge appeared in discussions of optical transforms and optical processing[18], as applied in pattern recognition[19,20], and on line inspection systems[21].

To get a qualitative feeling for the type of transform that we intend to analyze consider a plane wave of uniform amplitude incident on a lens. If the lens aperture is unobstructed, then at the focal plane we will see the conventional Airy pattern (see Fig. 4-3). Positioning an edge at the lens so as to reduce the opening produces a different pattern whose basic characteristics are an intense spike of energy appearing at right angles to the edge and a high spatial frequency content. Fig. [4-2] shows the pattern that was produced when the edge blocked half of the lens aperture.

In the work reported here we obtain approximate solutions for the light distribution on the focal plane for a) a spherically convergent, uniform amplitude wave truncated by a segment of a circular aperture and b) a spherically convergent, Gaussian amplitude wave truncated by an infinite edge. The results show that the truncation produces a spike of high intensity, at right angles to the edge, with an envelope falling off in proportion to the square of the distance from the center of the pattern, i.e. the geometrical focal point. For the uniform amplitude the pattern exhibits high spatial frequencies consistent with the ratio of the wavelength to the aperture opening, while for the Gaussian amplitude the pattern does not ring when the edge is positioned symmetrically in the beam. In addition the focal plane intensity distribution is symmetrical about the origin in the focal plane.

This particular property, namely that the pattern has polar symmetry in the focal plane, provides a useful way of determining that plane. The determination of the exact location of the focal plane is of particular importance for systems that perform optical Fourier transforms, as well as in setting the receiving plane of image-forming systems.

The field distribution near the focus of a well corrected lens has been analyzed extensively[22-34]. The results show that the light intensity is symmetric about the optical axis. Because of this particular symmetry the exact determination of the focal plane can be difficult.

In this work we analyze the near focus intensity distribution for a lens of which half has been blocked, and show that the light distribution is symmetric only at the focal plane, and that this symmetry is very sensitive to the translation of the lens along the optical axis. Furthermore we determine the dependence of this asymmetry, as we move away from the focal plane, as a function of the ratio of the diameter of the lens to its focal length.

1.2 Historical Perspective

Although the first reference of diffraction phenomena appears in the work of Leonardo Da Vinci (1452-1519)[1], the problem of the diffracting edge was first introduced by the Jesuit father Francesco Maria Grimaldi who in his book (1665),"Physicomathesis De Lumine Coloribus Et Iride"[2], describes the fringes he observed from a narrow bar. In 1678 Huygens in his book "Traité de la Lumière" becomes the first proponent of the wave theory of light. Newton in 1704 in his "Opticks", Book 3, Observation 1, tries to explain the appearance of fringes due to a diffracting edge in the following manner: "Are not the Rays of Light in passing by the edges and sides of Bodies, bent several times backwards and forwards, with a motion that of an Eel? And do not the three fringes of colour'd Light above-mention'd arise from three such bendings?"[3] Between 1700-1800 the problem of diffraction by narrow bars and rods was principally investigated by Delisle[4], Maraldi[5], Mairan[6], Du Sejeour[7] and Marat[8]. These works were very much influenced by the corpuscular theories of Newton and in effect do not improve upon the original fringes observed by Grimaldi.

The revival of the wave theory of light was made by T. Young who in 1802 in a paper published in the Philosophical Transactions discusses the diffraction effects of a narrow bar. It was not until 1818 that Fresnel in his "Mèmoire Couronné" established the principles of diffraction, and discussed the problem of the diffraction of a plane wave by a straight edge. His solution was given in terms of Fresnel integrals which he tabulated for different values of the upper limit. The idea of plotting the integrals and using the graphs for solving other diffraction problems was first conceived in 1874 by A. Cornu[9] and for this reason the spiral bears his name. Kirchhoff in 1882 put Fresnel analysis on a sound mathematical basis.

The first rigorous solution of the diffraction of a plane wave by a semi-infinite plane screen was given in 1896 by A. Sommerfeld[10], where the wave equation with the appropriate boundary conditions was solved with the method of images.

Another approach was developed by Copson[11] and by Schwinger[12] which involves the formulation of the problem in terms of integral equations and their exact solution using the Wiener-Hopf method[13]. More recently, Keller has treated this problem using his geometrical theory of diffraction[14], and he compares his result with Sommerfeld's exact solution. Related boundary- value-problem solutions for perfectly conducting slits are described by Braunbek and Laukien[15] and Borgnis and Papas[16]. Edge diffraction of Gaussian laser beams has been analyzed in the Fresnel zone by Pearson et al.[17].

The near focus intensity distribution for a lens was first discussed by Lommel[22] in 1885, who expressed the field in terms of infinite series of Bessel functions which since have been referred to as Lommel functions of two variables[23]. Struve[24], one year later, published a similar account and gave some useful approximations. K. Schwarzschild[25] in 1898 derived some asymptotic expansions for the description of the intensity many wavelengths away from the focus.

In 1909 Debye[26] published his solution to the near focus problem and his method is not limited to Kirchhoff's approximation but is based on the fundamentals of wave optics. His solution according to Sommerfeld,"can claim the same degree of exactness as, for instance, our treatment of the problem of the straight edge"[27]. F. Zernike and B. R. A. Nijboer[28] in 1949 developed a different expansion of Debye's integral but their final results are essentially the same. The work of E. H. Linfoot and E. Wolf in the early fifties[29,30] presented accurate calculations for the intensity distribution in a meridional plane, as well as some power and phase calculations. Later these treatments were incorporated in E. H. Linfoot's book on "Recent Advances in Optics"[31]. Finally Boivin et al. in 1965 and 1967[33-34] calculated, on the basis of electromagnetic theory, diagrams showing contours of electric energy density and of energy flow.

1.3 Summary of Research

In the following chapters we discuss the focal plane diffraction patterns for the uniform and Gaussian amplitude converging waves, we experimentally demonstrate these calculations, and finally we present the near-focus analysis for a convergent, unit amplitude wave, illuminating a semicircular aperture.

In Chapter 2 we calculate the intensity distribution at the focal plane for a converging uniform amplitude wave illuminating an aperture consisting of a segment of a circle. The general solution is particularized to the semicircular aperture case, and expressions pertaining to on axis calculations, with the corresponding asymptotic expansions, are given. The numerical evaluation of these solutions is presented and the general features of the pattern are discussed.

In Chapter 3 the focal plane diffraction of a convergent Gaussian amplitude wave illuminating an infinite edge is presented. The general result for the focal plane electric field is given as well as the one for an asymmetrical slit. The important properties of this class of diffraction patterns are discussed, and the numerical evaluation of the solutions is given.

In Chapter 4 we describe the experimental set-up used for the recording of the diffraction patterns discussed in Chapters 2 and 3, and present photographs for the important cases.

In Chapter 5 the near focus intensity distribution patterns for a semicircular aperture illuminated by a convergent wave of uniform amplitude are presented as well as the generalization of the solution to include the Gaussian amplitude case. Contour plots of constant intensity for various planes including the meridional and back focal are shown and discussed.

Chapter 6 contains a summary of the important formulas involved as well as the conclusions drawn from the evaluations of these solutions.

CHAPTER 1

REFERENCES

1. M. Born, F. Wolf, Principles of Optics, (Pergamon Press, London, 1970), p. 370.
2. J. Priestly, History of Vision Light,and Colours, (London, 1772), p. 171.
3. C. F. Meyer, The Diffraction of Light, X-rays, and Material Particles, (University of Chicago, Chicago, 1934), p. 6.
4. Delisle, Mem. Acad. Roy., (Paris, 1715), pp. 147-166.
5. Maraldi, Mem. Acad. Roy., (Paris, 1723), p. 111.
6. Mairan, Mem. Acad. Roy., (Paris, 1738) p. 53.
7. Du Sejeour, Mem. Acad. Roy., (Paris, 1775), p. 265.
8. Marat, Décourvetes Sur la Lumière, (Londres, 1780).
9. A. Cornu, Jour. de Phys., 3, (Paris 1874) pp. 1-44.
10. A. Sommerfeld, Mathem. Ann., 47, (1896), p. 317.
11. E. T. Copson, Quart. J. Maths. 17, (1946), p. 19.
12. J. Schwinger, H. Levine, Phys. Rev. 73, (1948), p. 383.
13. E. C. Titchmarsh, Introduction to the Theory of Fourier Integrals (Clarendon Press, Oxford, 1937), p. 339 .
14. J. B. Keller, J. Opt. Soc. Am. 52, (1962), 116.
15. W. Braunbek and G. Laukien, Optik 9, (1952), 174.
16. F. E.Borgnis and C. H. Papas, Randwertprobleme Der Mikrowellenphysik, (Springer-Verlag, Berlin, Göttingen Heidelberg, 1955), p. 101-157.
17. J. E. Pearson, T. C. McGill, S. Kurtin and A. Yariv, J. Opt. Soc. Am. 59, (1969), 1440.

18. H. Lipson, Optical Transforms (Academic Press, London, New York, 1972).

19. G. Lendaris and G. L. Stanley, SPIE Pattern Recognition Studies, Seminar Proceedings 18, (1969), p. 127.

20. N. George, J. T. Thomasson, J. Opt. Soc. Am., 62, (1972), p. 1380.

21. J. D. Cuthbert, D. F. Munro, and D. L. Fehrs, Abstracts of Conference on Optical Methods in Scientific and Industrial Measurements, (Tokyo, 1974), (to be published).

22. E. Lommel, Abh. Bayer Akad. 15, Abth, 2, (1885), 233.

23. G. H. Watson, A Treatise on the Theory of Bessel Functions, (Cambridge University Press, Cambridge, 1966), p. 537.

24. H. Struve, Mèm. de l'Acad. de St. Petersbourgh 34, (1886), 1.

25. K. Schwarzschild, Sitzb. München. Akad. Wiss., Math.-Phys. Kl., 28, (1899), p.271.

26. P. Debye, Ann. d. Physik., 30, (1909), p. 775.

27. A. Sommerfeld, Optics (Academic Press, New York and London, 1967), p. 319.

28. F. Zernike, B. R. A. Nijboer, La Théorie des Images Optiques, (Revue d'Optique, Paris, 1949), p. 227.

29. E. H. Linfoot, E. Wolf , Proc. Phys. Soc. 69, (1956), p. 823.

30. E. Wolf, Proc. Roy. Soc., 204, (1951), p. 542.

31. E. H. Linfoot, Recent Advances in Optics, (Clarendon Press, Oxford, 1955).

32. A. Boivin, E. Wolf, Phys. Rev., 138, (1965), p. 1561.

33. A. Boivin, J. Dow, E. Wolf, J. Opt. Soc. Amer. 57, (1967), p. 1171.

CHAPTER 2

CONVERGENT WAVE OF UNIFORM AMPLITUDE

2.1 Introduction

In this chapter we calculate the diffraction patterns, at the focal plane, for a converging unit amplitude incident wave illuminating a segment of a circular aperture.

The diffracting aperture is expressed in terms of the conventional circ and sgn functions, and the incident wave is written in the well-known paraxial form. Sommerfeld's diffraction theory integral is used with the Fresnel approximation to generate the electric field at the focal plane. The general solution is expressed in terms of infinite sums of Bessel functions. The solution is particularized to the case of a semicircular aperture, and expressions are derived for the on axis electric fields, and for their appropriate asymptotic forms.

Numerical evaluation of the solutions is presented showing that the introduction of the edge causes an intense spike of energy to appear in the focal plane at right angles to the edge symmetric about the origin. The intensity has an envelope falling off in proportion to the square of the distance from the center of the pattern; i.e. from the geometrical focus. Furthermore the pattern exhibits spatial frequencies proportional to the characteristic dimensions of the aperture.

2.2 General Theory

Consider an aperture located in the plane $z = 0$ having a transmittance function $T(\xi,\eta)$ given by:

$$T(\xi,\eta) = \text{circ}\left[\frac{(\xi^2+\eta^2)^{\frac{1}{2}}}{a}\right]\left[\frac{1}{2} + \frac{\text{sgn}(\xi-d)}{2}\right] , \qquad (2.1)$$

where ξ,η are cartesian coordinates at plane $z = 0$, a is the radius of the aperture, and d is the distance between the point (0,0,0) and the chord (see Fig. [2-1]). The circ and sgn functions are defined by:

$$\text{circ}\left[\frac{(\xi^2+\eta^2)^{\frac{1}{2}}}{a}\right] \begin{cases} = 1 & \text{when} \quad \dfrac{\xi^2+\eta^2}{a^2} \leq 1 \\ = 0 & \text{otherwise} \end{cases} \qquad (2.2)$$

and

$$\text{sgn}(\xi-d) \begin{cases} = 1 & \text{when} \quad \xi-d > 0 \\ = -1 & \text{when} \quad \xi-d < 0 \end{cases} \qquad (2.3)$$

The wave incident on the aperture is monochromatic, plane-polarized spherical wave with radius of convergence s. This transverse, scalar component $U(\xi,\eta)$ of the electric field is written in the well-known paraxial form, suppressing the time dependence (written for $\exp(i\omega t)$) and unessential phase terms as follows:

$$U(\xi,\eta) = \exp\left[\frac{i\pi}{\lambda s}(\xi^2+\eta^2)\right] \qquad (2.4)$$

The calculation of the electric field at point (x,y,z) in the right half space involves the solution of Sommerfeld's diffraction

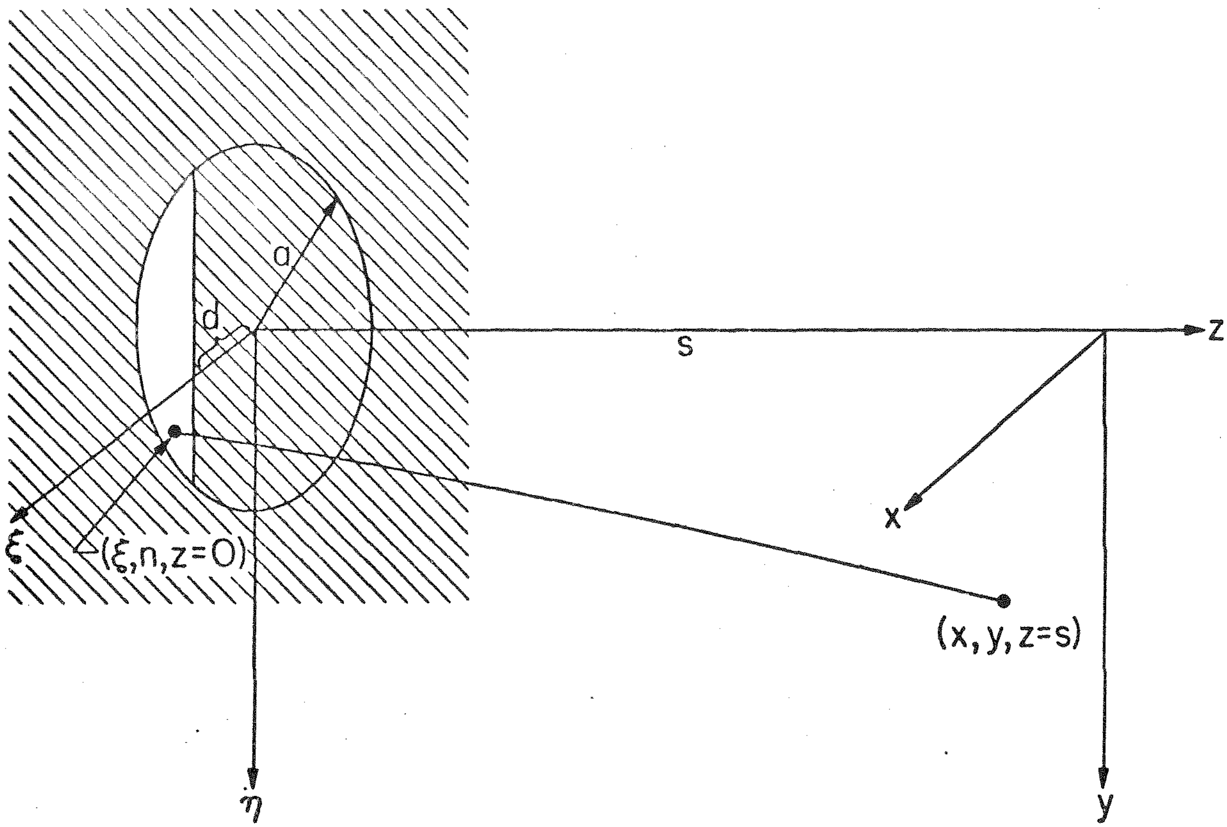

Fig. [2-1]. Geometry of relationships between the aperture, consisting of a segment of a circle, and the back focal plane.

theory integral (written for $\exp(i\omega t)$ dependence)[1]

$$V(x,y,z) = \frac{1}{2\pi} \iint_{-\infty}^{+\infty} U'(\xi,\eta,0) \frac{e^{-kR_1}}{R_1} \left(ik + \frac{1}{R_1}\right) \frac{z}{R_1} \, d\xi d\eta \qquad (2.5)$$

where U' is the aperture distribution, and R_1 is the distance between the point $(\xi,\eta,0)$ in the aperture plane and (x,y,z) in the observation screen expressed in terms of ξ,η,x,y,z as follows:

$$R_1 = [(\xi-x)^2 + (\eta-y)^2 + z^2]^{1/2} \quad . \qquad (2.6)$$

Assuming that the observation screen is the focal plane and using the conventional Fresnel approximation, Eq. (2.5) can be rewritten in the form:

$$V(x,y,z=s) = \frac{i \exp(-i2\pi s/\lambda)}{\lambda s} \iint_{-\infty}^{+\infty} U' \exp(- \frac{i\pi}{\lambda s} [(\xi-x)^2 + (\eta-y)^2] d\xi d\eta \qquad (2.7)$$

Furthermore adopting some of Kirckhoff's assumptions namely that the field distribution across the aperture is the same as it would have been in the absence of the aperture, and that the field is identically zero over the geometrical shadow of the aperture, U' can be written as

$$U'(\xi,\eta) = T(\xi,\eta) U(\xi,\eta) \quad . \qquad (2.8)$$

Combining Eqs. (2.2), (2.3), (2.4), (2.7) and (2.8) gives

$$V(x,y,z=s) = i \exp[-i2\pi s/\lambda - i\pi(x^2+y^2)/(\lambda s)]\cdot\{I_1+I_2\} \qquad (2.9)$$

where

$$I_1 \equiv \frac{1}{2}\iint_{-\infty}^{\infty} \mathrm{circ}\left[\frac{(\xi^2+\eta^2)^{\frac{1}{2}}}{a}\right] \exp[i2\pi(x\xi+y\eta)/(\lambda s)]d\xi d\eta \qquad (2.10)$$

and

$$I_2 = \frac{1}{2}\iint_{-\infty}^{\infty} \mathrm{circ}\left[\frac{(\xi^2+\eta^2)^{\frac{1}{2}}}{a}\right] \mathrm{sgn}(\xi-d)\exp[i2\pi(x\xi+y\eta)/(\lambda s)]d\xi d\eta \qquad (2.11)$$

We note that the restriction $z = s$ results in the cancellation of the quadratic terms $[\exp -i\pi(\xi^2+\eta^2)/(\lambda s)]$ and Eqs. (2.10) and (2.11) represent the two-dimensional Fourier transform of the circ function and the product of the circ with the offset sgn function. The calculation of the first integral is the Airy pattern and is evaluated in Goodman[(2)]. The result is:

$$I_1 = \pi a^2 \; \frac{J_1(\alpha\sqrt{x^2+y^2})}{\alpha\sqrt{x^2+y^2}} \quad , \qquad (2.12)$$

in which $\alpha = 2\pi a/(\lambda s)$ and J_1 is the Bessel function of the first kind and first order. Physically this result can be interpreted as the focal plane intensity distribution resulting from an open circular aperture with amplitude transmission of 0.5 across the full aperture.

The second integral in Eq. (2.11) physically represents the focal plane distribution for an open aperture with an offset phase mask that varies from 0 to π radians, stepwise, at $\xi = d$. In calculating I_2 since the Fourier transform of the circ and the sgn function is known, one could calculate the convolution of $J_1(\alpha\sqrt{x^2+y^2})/\alpha(x^2+y^2)^{1/2}$ with $i\lambda s \cdot \exp(i2\pi xd/(\lambda s))/x$. This type of approach, although straightforward from a Fourier analysis point of view, presents difficult problems. For this reason we have evaluated Eq. (2.11) by integrating with respect to the η variable first, and then expanding the integrand in terms of Bessel functions and integrating term by term. This approach gives a result in terms of infinite sums of Bessel functions that can be readily adapted for numerical calculations.

Integrating Eq. (2.11) with respect to η gives

$$I_2 = \frac{1}{2}\frac{\lambda s}{\pi y}\int_{-a}^{+a} \mathrm{sgn}(\xi-d)\sin\left(\frac{2\pi y}{\lambda s}[a^2-\xi^2]^{\frac{1}{2}}\right)\exp[i2\pi x\xi/(\lambda s)]d\xi \qquad (2.13)$$

Note that because of the definition of the circ function the limits of integration for x have been restricted from -a to +a. Furthermore substituting $u = \xi/a$ in Eq. (2.13), splitting the integral into its real and imaginary parts, using the properties for the integration of even and odd functions within the given interval, yields the following form:

$$I_2 = a^2\pi\,\frac{2}{\pi\alpha y}\left\{ i\int_{\frac{d}{a}}^{1} \sin(\alpha y[1-u^2]^{\frac{1}{2}})\sin(\alpha xu)du - \int_{0}^{\frac{d}{a}} \sin(\alpha y[1-u^2]^{\frac{1}{2}})\cos(\alpha xu)du\right\} \qquad (2.14)$$

Letting $u = \sin\theta$ in Eq. (2.14) gives:

$$I_2 = a^2\pi \frac{2}{\pi\alpha y}\left\{ i \int_{\sin^{-1}(\frac{d}{a})}^{\pi/2} \sin(\alpha y\cos\theta)\sin(\alpha x\sin\theta)\cos\theta\, d\theta - \int_{0}^{\sin^{-1}(\frac{d}{a})} \sin(\alpha y\cos\theta)\cos(\alpha x\sin\theta)\cos\theta\, d\theta \right\} \tag{2.15}$$

To evaluate Eq. (2.15) we use the identities that can be derived from the generating function for the Bessel series A.S. 9.1.43, namely that:

$$\sin(z\sin\theta) = 2\sum_{k=o}^{\infty} J_{2k+1}(z)\sin\{(2k+1)\theta\}$$

$$\sin(z\cos\theta) = 2\sum_{k=o}^{\infty} (-1)^k\, J_{2k+1}(z)\cos\{(2k+1)\theta\}$$

$$\cos(z\sin\theta) = J_o(z) + 2\sum_{k=1}^{\infty} J_{2k}(z)\cos(2k\theta)$$

Exchanging the order of integration and summation in Eq. (2.15) leads to the following form:

$$I_2 = a^2\pi \frac{2}{\pi\alpha y}\left\{ 4i \sum_{n=o}^{\infty}(-1)^n J_{2n+1}(\alpha y)\sum_{m=o}^{\infty} J_{2m+1}(\alpha x)\cdot \int_{\sin^{-1}(\frac{d}{a})}^{\pi/2} \cos\{(2n+1)\theta\}\sin\{(2m+1)\theta\} \right.$$

$$\left. - 4\sum_{n=o}^{\infty}(-1)^n J_{2n+1}(\alpha y)\sum_{m=o}^{\infty}\frac{(-1)^m}{(1+\delta_{om})} J_{2m}(\alpha x)\int_{0}^{\sin^{-1}(\frac{d}{a})} \cos\{(2n+1)\theta\}\cos(2m\theta)\cos\theta\, d\theta \right\} \tag{2.16}$$

where the Kronecker delta $\delta_{om} = 1$ for $m = 0$ and is zero for $m \neq 0$. Evaluation of the integrals in Eq. (2.16) can be easily made and the result is:

$$I_2 = a^2\pi\cdot\frac{2}{\pi\alpha y}\cdot\left\{\sum_{n=o}^{\infty}(-1)^n J_{2n+1}(\alpha y)\cdot\left[i\sum_{m=o}^{\infty}J_{2m+1}(\alpha x)\cdot g_1(m,n)\right.\right. +$$

$$\left.\left. - \sum_{m=o}^{\infty}(1-\frac{1}{2}\delta_{om})(-1)^m J_{2m}(\alpha x)\cdot g_2(m,n)\right]\right\} \qquad (2.17)$$

where g_1 and g_2 are given by

$$g_1(m,n) = \frac{\cos[(2m+2n+3)\sin^{-1}(\frac{d}{a})]}{2m+2n+3} + \frac{\cos[(2m+2n+1)\sin^{-1}(\frac{d}{a})]}{2m+2n+1}$$

$$+ \frac{\cos[(2n-2m+1)\sin^{-1}(\frac{d}{a})]}{2n-2m+1} + \frac{\cos[(2m-2n+1)\sin^{-1}(\frac{d}{a})]}{2m-2n+1} \qquad (2.18)$$

$$g_2(m,n) = \frac{\sin[(2m+2n+2)\sin^{-1}(\frac{d}{a})]}{2m+2n+2} + \frac{\sin[(2m+2n)\sin^{-1}(\frac{d}{a})]}{2m+2n}$$

$$+ \frac{\sin[(2n-2m+2)\sin^{-1}(\frac{d}{a})]}{2n-2m+2} + \frac{\sin[(2m-2n)\sin^{-1}(\frac{d}{a})]}{2m+2n} \qquad (2.19)$$

The general result for the electric field, V, is found by substitution of Eqs. (2.12) and (2.17) into Eq. (2.9), as follows:

$$V(x,y,z=s) = \frac{i}{\lambda s}\exp(-iks)\exp[-i\pi(x^2+y^2)/(\lambda s)]\pi a^2\left[J_1[\alpha(x^2+y^2)^{\frac{1}{2}}/[\alpha(x^2+y^2)^{\frac{1}{2}}]\right.$$

$$+ \frac{2}{\pi\alpha y}\left\{\sum_{n=o}^{\infty}(-1)^n J_{2n+1}(\alpha y)\left[i\sum_{m=o}^{\infty}J_{2m+1}(\alpha x)\cdot g_1(m,n)\right.\right.$$

$$\left.\left.\left. - \sum_{m=o}^{\infty}(1-\frac{1}{2}\delta_{om})(-1)^m J_{2m}(\alpha x)g_2(m,n)\right]\right\}\right] \qquad (2.20)$$

where $k = 2\pi/\lambda$.

2.3 Semicircular Aperture, On Axis Calculations, Asymptotic Expansions

A case of particular interest occurs when the edge is positioned symmetrically, i.e. when d = 0. This corresponds physically to the focal plane diffraction patterns produced from a semicircular aperture.

In this case Eq. (2.20) reduces to the following:

$$V(x,y,z=s) = \frac{i}{\lambda s}\exp(-iks)\exp[-i\pi(x^2+y^2)/(\lambda s)]\pi a^2\Big\{J_1[\alpha(x^2+y^2)^{\frac{1}{2}}]/[\alpha(x^2+y^2)^{\frac{1}{2}}]$$

$$+\frac{2i}{\pi\alpha y}\sum_{n=o}^{\infty}\sum_{m=o}^{\infty}(-1)^n J_{2n+1}(\alpha y)J_{2m+1}(\alpha x)g_o(m,n)\Big\}\ . \qquad (2.21)$$

Also since $\sin^{-1}\frac{d}{a} = 0$ for d = 0, Eq. (2.19) gives $g_2 = 0$ and g_1 from Eq. (2.18) reduces to the form in Eq. (2.22) which we denote by $g_o(m,n)$

$$g_o(m,n) = \frac{1}{2(m+n)+3} + \frac{1}{2(m+n)+1} - \frac{1}{2(n-m)+1} + \frac{1}{2(m-n)+1} \qquad (2.22)$$

Eq. (2.21) is well suited for numerical calculations since algorithms for Bessel functions are readily available and since the summations can be truncated when the index exceeds the argument. It is of academic interest to present an alternate solution formulated in terms of Struve functions. Returning to Eq. (2.14) and setting d = 0 gives

$$I_2 = a^2\pi\,\frac{2}{\pi\alpha y}\ \ i\int_0^1 \sin(\alpha y[1-u^2]^{1/2})\sin(\alpha xu)du \qquad (2.23)$$

Now we expand $\sin(\alpha y[1-u^2]^{1/2})$ in an infinite power series and exchange the order of summation and integration

$$I_2 = \pi a^2 \frac{2i}{\pi} \sum_{m=o}^{\infty} (-1)^m \frac{(\alpha y)^{2m}}{(2m+1)!} \int_0^1 (1-u^2)^{m+1)-1/2} \sin\alpha xu \, du \quad (2.24)$$

By A.S. 12.1.6 Eq. (22) can be written as

$$I_2 = \pi a^2 \frac{i}{\sqrt{\pi}} \sum_{m=o}^{\infty} \frac{\left(\frac{-\alpha y^2}{2x}\right)^m}{(2m+1)!} \Gamma(m+3/2)\mathscr{H}_{m+1}(\alpha x) \quad (2.25)$$

where $\mathscr{H}_{m+1}$ is the Struve function of order m+1, and $\Gamma(m+3/2)$ is the conventional gamma function.

Using the duplication formula for the gamma function A.S. 6.1.18 we get the result

$$I_2 = \pi a^2 \frac{1}{\alpha x} \sum_{m=o}^{\infty} \frac{\left(\frac{-\alpha y^2}{4x}\right)^{km}}{m!} \mathscr{H}_{m+1}(\alpha x) \quad (2.26)$$

and the electric field is given by:

$$V(x,y,z=s) = \frac{i}{\lambda s} \exp(-iks)\exp[-i\pi(x^2+y^2)/(\lambda s)]\pi a^2 \left\{ \frac{J_1(\alpha[x^2+y^2]^{\frac{1}{2}})}{\alpha[x^2+y^2]^{\frac{1}{2}}} + \right.$$

$$\left. + \frac{i}{\alpha x} \sum_{m=o}^{\infty} \frac{\left(-\frac{\alpha y^2}{4x}\right)^m}{m!} \mathscr{H}_{m+1}(\alpha x) \right\} . \quad (2.27)$$

Although this result looks simpler than the double sum of Eq. (2.21) it is not particularly suited for numerical calculations because it is a very slowly converging series exhibiting the serious numerical problem of generating very large initial terms.

However the above expression is particularly useful for calculating the on x axis intensity distribution namely for $y = 0$. Then Eq. (2.27) becomes

$$V(x,0,z=s) = \frac{i}{\lambda s} \exp(-iks)\exp(-i\pi x^2/\lambda s)\pi a^2 \left\{\frac{J_1(\alpha|x|)}{\alpha|x|} + \frac{i}{\alpha x}\mathcal{H}_1(\alpha x)\right\} \tag{2.28}$$

The Struve function of order 1 is tabulated (A.S. Table 12.1) so that an axis calculation can be readily performed. Furthermore for typical cases, i.e. $a = .5$ cm, $z = 20$ cm, $\lambda = 6328$ Å, $\alpha \sim 2{,}500$. Thus for $x \geq 40$ μm the asymptotic expansion for $\mathcal{H}_1$ can be used A.S. 12.1.31. It follows that:

$$V(x,0,z=s) \simeq \frac{i}{\lambda s} \exp(-iks)\exp(-i\pi x^2/\lambda s)\pi a^2 \left\{\frac{H_1^{(1)}|\alpha x|}{\alpha x} + \right.$$

$$\left. + \frac{2i}{\pi\alpha x} \quad 1 + \frac{1}{(\alpha x)^2} - \frac{3}{(\alpha x)^4} + \cdots\right\} \tag{2.29}$$

where $H_1^{(1)}$ is the first order Hankel function of the first kind. This expression is valid for $\pm x$ with the use of the $|\alpha x|$ argument in the Hankel function and the property that $\mathcal{H}_1(\alpha x) = \mathcal{H}_1(-\alpha x)$. This form can also be shown from Eq. (2.21) and (2.22) by combining the $J_{2n+1}(\alpha y)/\alpha y$ terms, taking the limit as y goes to zero, regrouping the Bessel summation and using recurrence formula A.S. 9.1.27.

An alternative form of Eq. (2.28) can be derived useful for small values of αx. Using A.S. 12.1.20 Eq. (2.28) can be written as

$$V(x,0,z=s) = \frac{i}{\lambda s} \exp(-iks)\exp[-i\pi x^2/(\lambda s)]\pi a^2 \left\{ \frac{J_1(\alpha x)}{\alpha x} + \frac{4i}{\pi dx} \sum_{m=1}^{\infty} \left[\frac{4m^2}{4m^2-1}\right] J_{2m}(\alpha x) \right\} \tag{2.30}$$

This expression is useful for small αx since the series can be truncated at $m \sim \alpha x$ with a few terms added for improved accuracy since $J_n(x) \to 0$ for $n > x$ (A.S. 9.3.1).

Furthermore when we consider the radiation pattern for the semi-circular aperture along the y-axis (with $x = 0$) we have the result:

$$V(o,y,z=s) = \frac{i}{\lambda s} \exp(-iks)\exp[-i\pi y^2/(\lambda s)]\pi a^2 \frac{J_1(\alpha|y|)}{\alpha|y|} \tag{2.31}$$

This result physically is interpreted as the intensity distribution at the focal plane of a circularly symmetric aperture with amplitude transmittance of 1/2 across the aperture.

Finally because of the semicircular symmetry of the problem it is interesting to express the electric field for the semicircular aperture in cylindrical coordinates. We will present the final result only, since the derivation is very similar to the one presented in Chapter 5.

$$V(\rho,\phi,z=s) = \frac{i}{\lambda s} \exp(-iks)\exp(-i\pi\rho^2/\lambda s)\pi a^2 \left\{ \frac{J_1(\frac{k\rho a}{s})}{(\frac{k\rho a}{s})} + \right.$$

$$\left. + \frac{2i}{\pi}\left(\frac{k\rho a}{s}\right) \sum_{m=o}^{\infty} \frac{\left(\frac{-k^2\rho^2 a^2}{4s^2}\right)^m \sin[(2m+1)\phi]}{2m+1} \sum_{n=o}^{\infty} \frac{\left(\frac{-k^2\rho^2 a^2}{4s^2}\right)^n}{n!(2m+n+1)!} \frac{1}{(2m+2n+3)} \right. \tag{2.32}$$

2.4 Numerical Calculations

In this section we present the numerical evaluation of Eq. (2.21) for a number of interesting cases. First we plot the intensity along the x axis for y = 0, and along the y axis for x = 0. Then we plot the intensity as a function of x and y (three dimensional plots) for the neighborhood of the focus and for an area at larger values of x.

The important points in the calculation of VV^* from Eq. (2.21) are outlined below:

For a given value of αx and αy the number of terms in the m and n summations was calculated. The criterion for truncation was that the last term in either sum be smaller than 10^{-25}. Consequently a function subroutine calculated in double precision the sequence of Bessel functions for the given argument. The functions were multiplied by the weighting factor $g_0(m,n)$ and a function subprogram sorted the terms in 43 groups and summed them in double precision. Double precision was used throughout the program to minimize the inherent errors that can occur when an intermediate partial sum is much larger in magnitude than the final sum or when the intermediate sums become much larger in magnitude than individual addends but not larger than the final sum.

The subroutine used to calculate the Bessel functions in double precision was obtained from the Argonne computer library facilities. The function subprogram for the calculation of the summations is a modified version, that we have developed, of an algorithm generated by M. A. Malcom (Stanford University)[3]. The complete program is included in Appendix A.

Fig. [2-2] shows the intensity distribution along the major lobe of the radiation pattern. Curve (A) is for the semicircular aperture showing the log of VV^* from Eq. (2.30) normalized by $[\pi a^2/(\lambda s)]^2$ versus $2\pi ax/(\lambda s)$. Note that at the origin $I_1 = 0.5$ and $I_2 = 0$; hence the normalized intensity peaks at the value of 0.25.

From Eqs. (2.9) and (2.12) we see that for a circular aperture the intensity $V_o V_o^*$ is given by

$$V_o V_o^* = \left[\frac{\pi a^2}{\lambda s} \; \frac{J_1(\alpha\sqrt{x^2+y^2})}{\alpha\sqrt{x^2+y^2}} \right]^2 , \tag{2.33}$$

where by Eq. (1) this implicitly assumes that the amplitude transmission is only 0.5 across the full aperture. Curve (B) shows $V_o V_o^*$ from Eq. (2.33) normalized by $[\pi a^2/(\lambda s)]^2$ versus the same normalized x abscissa and with $y = 0$.

Comparing (A) and (B) in Fig. [2-2], we note that the nulls are filled in when the edge is present, the intensity at large x is orders of magnitude higher, and that the relative maxima occur at approximately one-half the frequency of that for the open aperture.

We also note that Eq. (2.31) gives an intensity identical to Eq. (2.33) when $x = 0$. The significance of this is that the curve (B) in Fig. [2-2], introduced for comparing the departure of the x-axis pattern caused by the edge, serves also to describe the intensity along the y-axis when the edge is present.

Three dimensional computer plots are shown in Figs. [2-3], [2-4] for a semicircular aperture illuminated by a converging wave of uniform amplitude. Specifically in Fig. [2-3] the center point of the

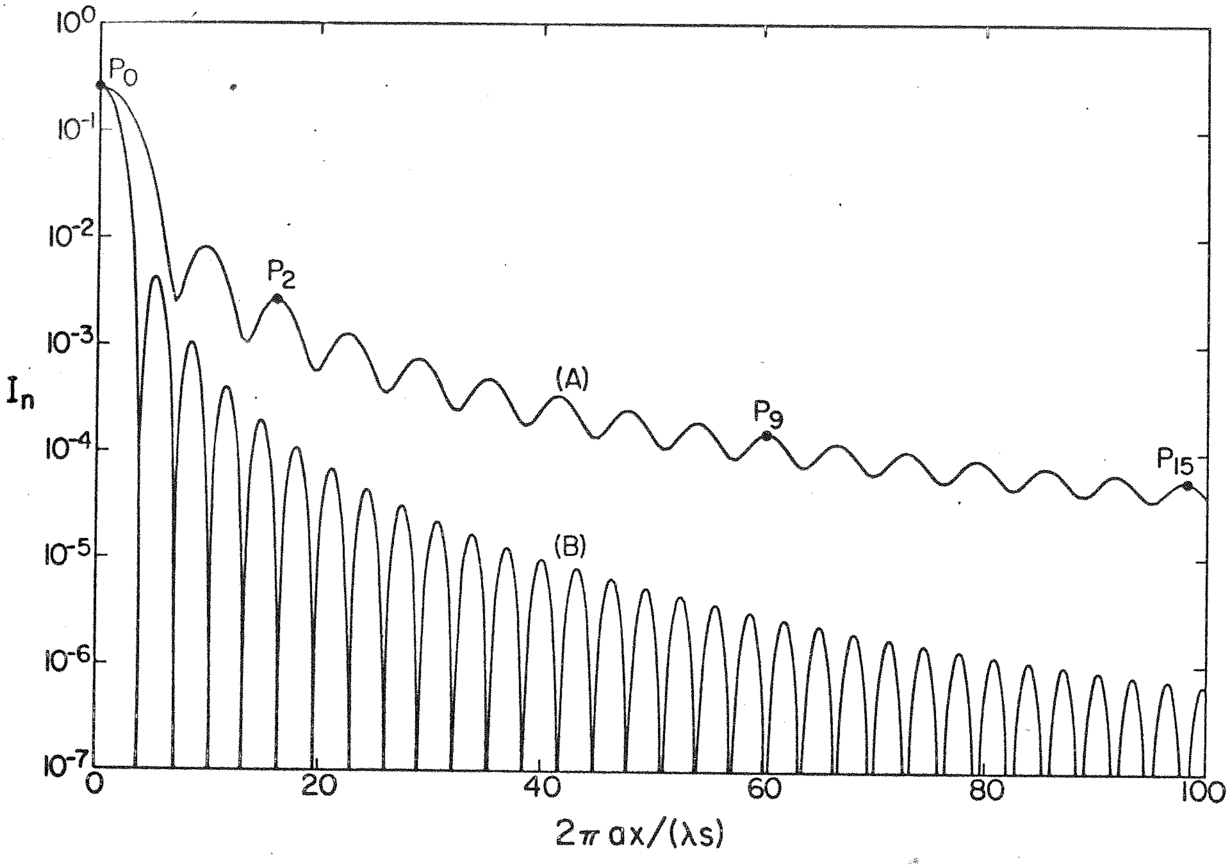

Fig. [2-2]. Normalized transmitted irradiance I_n is plotted logarithmically vs αx with $y=0$ for a semicircular aperture curve (A), illuminated with a convergent wave of unit amplitude, and for a circular aperture, curve (B), illuminated with a convergent wave with amplitude equal to 0.5.

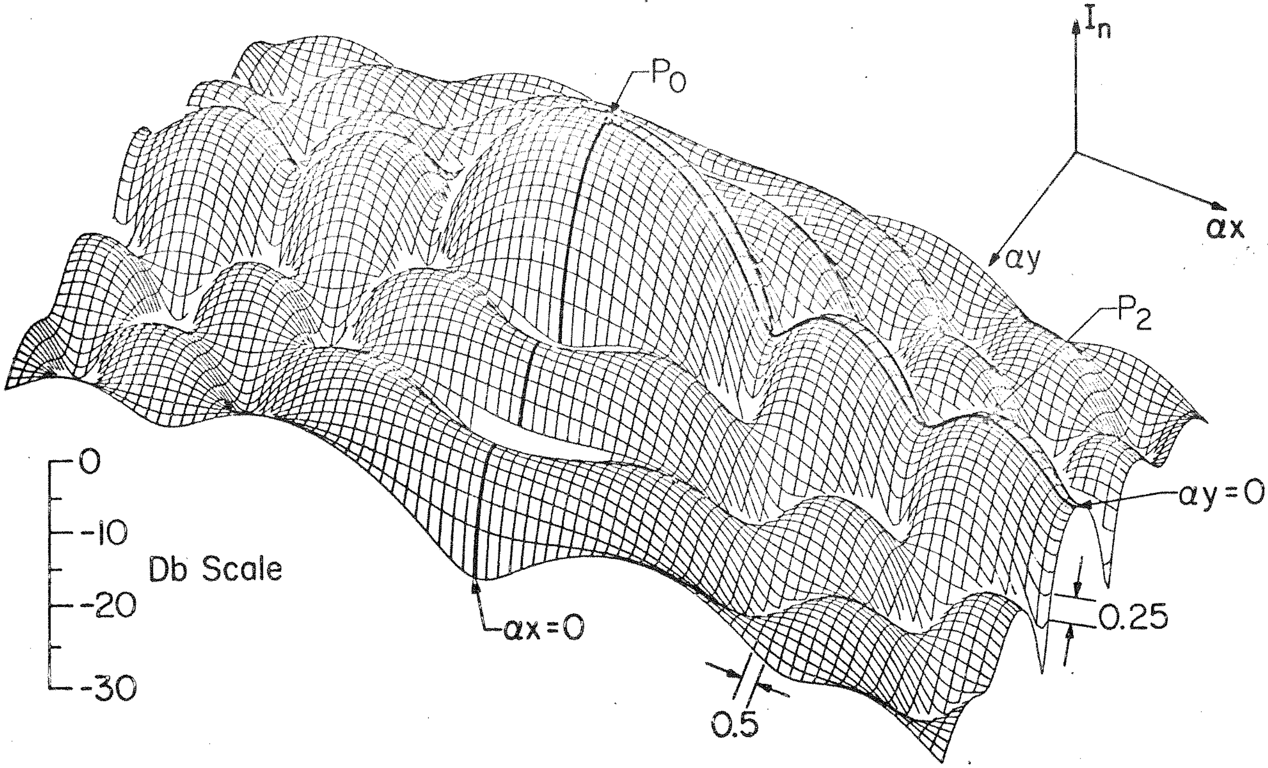

Fig. [2-3]. Normalized transmitted irradiance I_n is plotted logarithmically vs αx and αy with d=0, for a semi-circular aperture illuminated with a convergent unit amplitude wave. P_o corresponds to a normalized irradiance of 0.25, the range in αy is from -10 to +10 and in αx from -20 to +20.

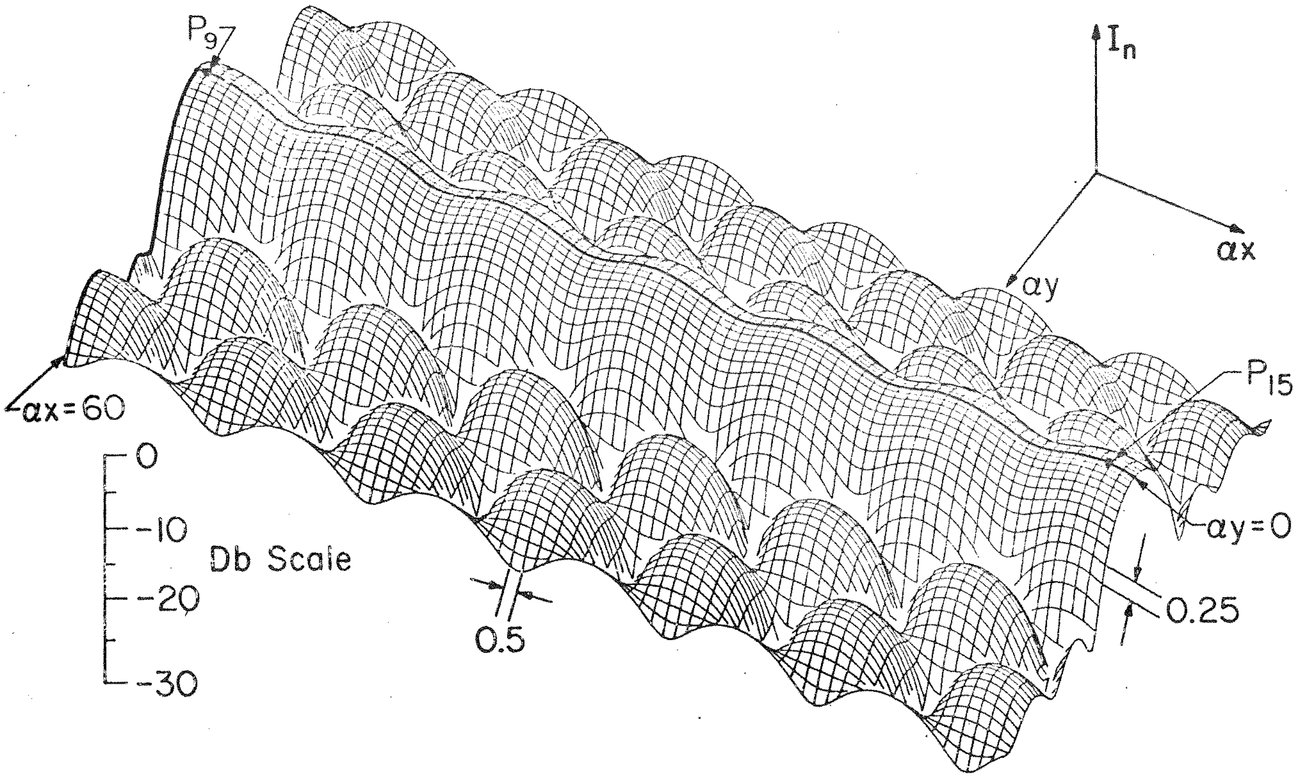

Fig. [2-4]. Normalized transmitted irradiance I_n plotted logarithmically vs αx and αy with d=0, for a semi-circular aperture illuminated with a convergent unit amplitude wave. The interval along the αy axis is from $-10 \leq \alpha y \leq 10$, and αx spans the relative maxima from P_9 through P_{15}; the point P_9 corresponds to a normalized irradiance of 1.4×10^{-4}.

radiation pattern (geometrical focus) is labeled P_0 and is also shown on Fig. [2-2]. Likewise, to provide orientation, the second relative maximum along x is labeled P_2. A logarithmic intensity scale is used, as labeled, with P_0 corresponding to a normalized absolute intensity of 0.25. Contour intervals in αx of 0.5 and in αy of 0.25 are used. Thus, in Fig. [2-3] the entire plot encompasses the region $-20 \leq \alpha x \leq 20$ and $-10 \leq \alpha y \leq 10$.

The details of the radiation spike at larger values of αx are shown in Fig. [2-4]. Again a logarithmic intensity scale is used, and P_9 corresponds to a normalized intensity of 1.4×10^{-4}. The span in αx encompasses the relative maxima from P_9 through P_{15}; the interval along the y axis is again from $-10 \leq \alpha y \leq 10$. The contour intervals in αx of 0.5 and in αy of 0.25 have been used as in Fig. [2-3].

To create the 3-D plots log of VV^* normalized was calculated as described previously, and the data stored on a disk. This way various parameters, such as viewing angles, contour intervals, etc. could be changed at will. The subroutine that performed the transformations was the one developed by D. L. Nelson (University of Maryland)[4].

The complete programs of these subroutines are included in Appendix B.

2.5 Summary and Conclusions

We have analyzed several cases of edge diffraction of convergent waves of uniform amplitude. The electric field in the focal plane for the case of an infinite edge, positioned off-center in a circular aperture is given in Eq. (2.20). The corresponding result for a 0-π radian phase plate can be written directly from Eqs. (2.9) and (2.16). The particular case of the semicircular aperture is presented in Eq. (2.21).

The dominant feature of the focal plane pattern due to the edge is the large spike of energy diffracted at right angles to the edge. The intensity in the spike falls off asymptotically as $1/x^2$ where x is the distance from the focal point. This can be seen directly from Eq. (2.29). In addition to the fall-off there is a fractional ripple of the spike even at large values of x, but without sharp nulls. Quantitatively, the fractional ripple is seen by Eq. (2.29) to be of the order of $|H_1^{(1)}(|\alpha x|)|^2$.

Another important aspect of the patterns is the ringing at an angular spacing consistent with the ratio of the wavelength λ to the aperture opening.

Finally we note that the intensity VV^* computed from Eq. (2.21) for the offset edge has polar symmetry. This follows from noting by Eqs. (2.10) and (2.11) that I_1+I_2 is the Fourier transform of a real valued function. This polar symmetry can also be shown by a direct calculation using Eq. (2.20).

CHAPTER 2

REFERENCES

1. A. Sommerfeld, Optics, (Academic Press, London, 1967), p. 201.

2. J. W. Goodman, Introduction to Fourier Optics, (McGraw-Hill, San Francisco, 1968), p. 64.

3. M. A. Malcolm, CACM, 14, (1971), p. 731.

4. D. L. Nelson, University of Maryland Technical Report, 553.

A.S. M. Abramowitz and I. A. Stegun, Handbook of Mathematical Functions, (Nat. Bureau of Standards, Washington, 1970).

CHAPTER 3

CONVERGENT WAVE OF GAUSSIAN AMPLITUDE

3.1 Introduction

The calculation of the focal plane diffraction patterns for a convergent wave of Gaussian amplitude, diffracted by an offset infinite edge, is presented here.

In this case the incident wave, in addition to the converging term, has a quadratic amplitude distribution, and the diffracting screen can be written in terms of a displaced sgn function. The application of Sommerfeld's integral, within the Fresnel approximation, produces focal plane electric fields that can be expressed in terms of w functions. An asymptotic form for this solution is derived and the electric field for an infinite slit is also presented. It is shown that the Gaussian amplitude taper produces a radial spike of high intensity perpendicular to the edge, having symmetry (in intensity) about the origin in the focal plane, and an inverse-squared-distance dependence of intensity similar to the case of the unit amplitude wave. However when the edge is positioned symmetrically in the Gaussian beam no ringing occurs.

3.2 Theory

Consider an infinite edge located at plane z = 0 offset by the distance d along the z axis. For a transmission function we write

$$T(\xi,\eta) = \frac{1}{2}\,[1 + \mathrm{sgn}(\xi-d)] \quad . \tag{3.1}$$

The incident wave is again monochromatic, plane polarized but with a Gaussian amplitude variation and it can be written in the form

$$U_g(\xi,\eta) = \exp[i\pi(\xi^2+\eta^2)/(\lambda s) - (\xi^2+\eta^2)/w_o^2] \tag{3.2}$$

where w_o is the radius at which the incident intensity has dropped to its $1/e^2$ value. The assumed field distribution U' is given by the product of Eq. (3.1) and (3.2). As in the previous chapter Kirchoff's assumptions have been used for the aperture distribution.

Substitution of $U' = TU_g$ in Eq. (2.7) gives the following result:

$$V_g(x,y,z=s) = \frac{i}{2\lambda s}\exp(-i2\pi s/\lambda)\exp(-i\pi(x^2+y^2)/(\lambda s)]\cdot$$

$$\int_{-\infty}^{+\infty}\int_{-\infty}^{+\infty} \mathrm{sgn}(x-d)\exp[-(\xi^2+\eta^2)/w_o^2]\exp[i2\pi(x\xi+y\eta)]d\xi d\eta\ +$$

$$+\int_{-\infty}^{+\infty}\int_{-\infty}^{+\infty} \exp[-(\xi^2+\eta^2)/w_o^2]\exp[i2\pi(x\xi+y\eta)]d\xi d\eta \quad . \tag{3.3}$$

Using A.S. 7.4.6 the integration with respect to η can be performed, and using Eq. (2.3) the above expression can be written as:

$$V_g(x,y,z=s) = \frac{i}{2\lambda s}\exp(-i\pi 2s/\lambda)\exp(-i\pi(x^2+y^2)/(\lambda s)]\cdot\sqrt{\pi}\,w_o\exp\left[-\left(\frac{\pi w_o}{\lambda s}\right)^2 y^2\right]\cdot$$

$$\left\{\cdot\int_{d}^{\infty}\exp(-\xi^2/w_o^2)\exp(i2\pi x\xi/(\lambda s))d\xi - \int_{-\infty}^{d}\exp(-\xi^2/w_o^2)\exp(i2\pi x\xi/(\lambda s))d\xi\right\} \tag{3.4}$$

Eq. (3.4) is integrated with the use of A.S. 7.4.32 and A.S. 7.1.16. The result is given by:

$$V_g(x,y,z=s) = \frac{i}{2\lambda s}\exp(-iks)\exp[-i\pi(x^2+y^2)/(\lambda s)]\cdot$$
$$\cdot\ \pi w_o^2 \exp\left[-\left(\frac{\pi w_o}{\lambda s}\right)^2(x^2+y^2)\right]\left\{1 - \operatorname{erf}\left[\frac{d}{w_o} - \frac{i\pi x w_o}{\lambda s}\right]\right\} \tag{3.5}$$

where erf z is the conventional error function as defined by A.S. 7.1.1. The above expression is applicable for positive and negative values of d. As a consistency test of Eq. (3.5) letting $d \to -\infty$, i.e. no edge, we note that erf( ) $\to -1$; and Eq. (3.5) reduces to a well known result. Also, this expression is functionally similar to the result of Pearson et al. who studied the diffraction of Gaussian beam by a semi-infinite plane[1]. Specifically, Eq. 8 in Ref. 1 can be considered in the limit at $z \to \infty$, i.e., the transform or back focal plane distribution is a scaled far-zone radiation pattern.

For calculation purposes Eq. (3.5) can be rewritten in terms of the w-function defined by $w(z) = \exp(-z^2)(1 - \operatorname{erf}(-iz))$, as follows:

$$V_g(x,y,z=s) = \frac{i}{2\lambda s}\exp(-iks)\exp[-i\pi(x^2+y^2)/(\lambda s)]\exp[i\ 2\pi x d/(\lambda s)]\cdot$$
$$\pi w_o^2 \exp\left\{-[\pi w_o x/(\lambda s)]^2 - [d/w_o]^2\right\} w[\pi w_o x/(\lambda s) + id/w_o] \tag{3.6}$$

To demonstrate the 1/x dependence of the electric field (Eq. 3.6) we use the following approximation:

$$w(z) = iz\left(\frac{0.5124242}{z^2-0.2752551} + \frac{0.05176536}{z^2-2.724745}\right) \tag{3.7}$$

If we assume that $w_o = .5$ cm, $s = 20$ cm, $\lambda = 6328$ Å, then the above expression is valid for $x \geq .5$ mm by A.S. p. 328. Furthermore we notice that the contribution of the second term in Eq. (3.7) is less than 10% so that Eq. (3.6) can be written as:

$$V_g(x,y,z=s) = \frac{1}{\lambda s} \exp(-iks)\exp[-i\pi(x^2+y^2)/(\lambda s)]\exp[i\ 2\pi xd/(\lambda s)]\cdot$$

$$\pi w_o{}^2 \exp\left\{-[\pi w_o x/(\lambda s)]^2\right\}(d/w_o - 1)\left\{.256/[\pi w_o x/(\lambda s)]\right\} \tag{3.8}$$

Finally for an infinite slit, i.e., an aperture extending from $\xi = d_1$, to $\xi = d_2$ with $d_1 < d_2$, by Eq. (3.5), it is readily shown that the electric field V_{sg} is given by:

$$V_{sg}(x,y,z=s) = \frac{i}{2\lambda s} \exp(-iks)\exp[-i\pi(x^2+y^2)/(\lambda s)]\cdot$$

$$\pi w_o{}^2 \exp\left[-\left(\frac{\pi w_o}{\lambda s}\right)^2 (x^2+y^2)\right]\left\{\mathrm{erf}\left[\frac{d_2}{w_o} - \frac{i\pi x w_o}{\lambda s}\right] - \mathrm{erf}\left[\frac{d_1}{w_o} - \frac{i\pi x w_o}{\lambda s}\right]\right\} \tag{3.9}$$

3.3 Calculations

It can be seen from Eq. (3.6) that the back focal plane diffraction pattern for a Gaussian beam depends primarily on the behavior of the w function. Therefore, in this section, we first examine some interesting aspects of the w function (namely the isocontour diagram and the complex zeroes) and their physical consequences. Then we plot the intensity along the x axis, for $y = 0$, for various values of the displacement of the edge, and finally we present a three dimensional plot of the intensity as a function of the x and y coordinates.

In Fig. [3-1] the contour lines of the modulus and phase of the w function are presented. We note that for positive values of the real and imaginary argument the function has a monotonic behavior. However when the imaginary part becomes negative, zeroes are expected for certain values of the argument. These zeroes lie above the 45° ray and approach it asymptotically as $n \to \infty$. As it can be seen from Eq. (3.6) $\pi w_0 x/(\lambda s)$ sets the real part of the w function, while the displacement d/w_0 the imaginary. Thus as d/w_0 becomes negative, the edge is exposing more of the Gaussian wavefront and interesting nulls are to be expected at the zeroes of the w function. It is furthermore noted that the electric field can have at most one null for a given value of d/w_0 regardless of how large the $\pi w_0 x/(\lambda s)$ coordinate becomes. In Table [3-1] we show the first seven zeroes of the w function.

The calculation of the zeroes of the w function was made using the downhill method developed by J. A. Ward[2], and improved by H. Bach[3] in 1969. This method, theoretically, always converges toward a root; however because of the fact that $|w(z)| \to 0$ as $|z| \to \infty$ the search moves towards infinity and no roots are found. For this purpose we multiply the w function with $\exp(k|z|)$. This way the problem of the search moving towards infinity is eliminated but the valleys of the zeroes become infinitely narrow especially for large values of z. This necessitates the generation of a table so that expedient choices of starting points can be made. The computer programs for the above calculations are included in Appendix D.

d/w_o	$\pi w_o x/(\lambda s)$
-1.35481	1.99147
-2.17704	2.69115
-2.78439	3.23534
-3.28741	3.69731
-3.72595	4.10611
-4.11964	4.47681
-4.47982	4.81849

Table [3-1]

Nulls of the radiation pattern for a convergent Gaussian wave diffracted by an offset edge, Eq. (3.6)

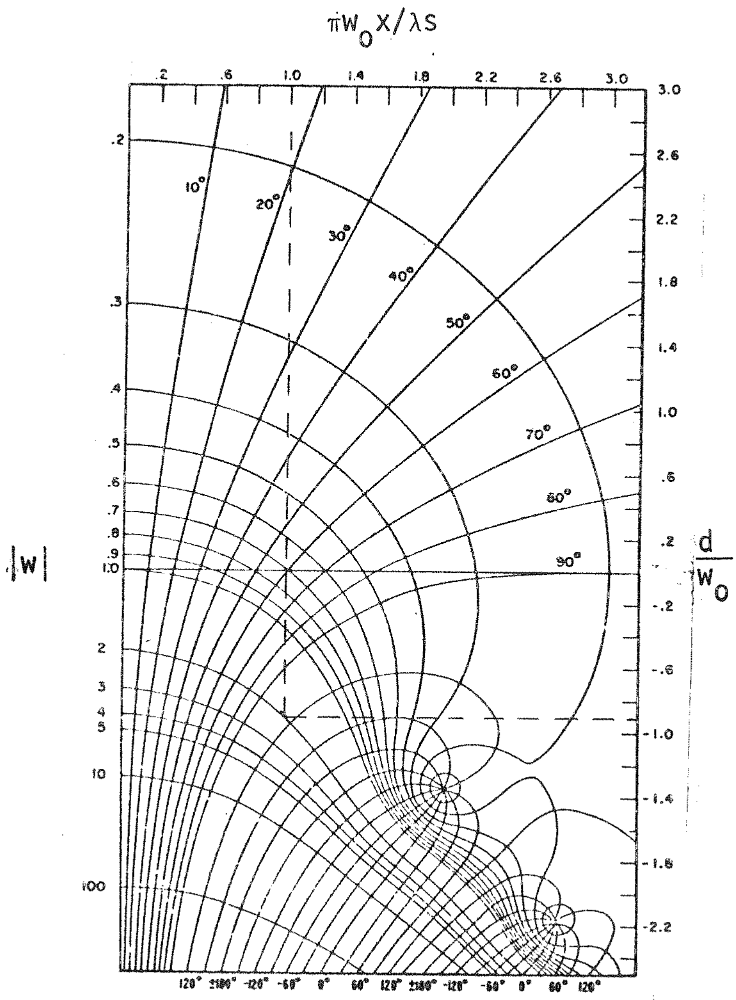

Fig. [3-1]*
Contour lines for the amplitude and phase of the w function. Dashed lines indicate that the choice of $\pi w_o x/\lambda s = 1.0$, and $d/w_o = -.95$ gives $|w| = 2.0$. From this to get $|V_g|$ we must multiply $|w|$ with $\exp\{-[\pi w_o x/(\lambda s)]^2 - (d/w_o)^2\}$.

*Reprinted from A.S. Fig. 7.3.

The variation in intensity versus normalized displacement along x, with $y = 0$ and for the parameter d/w_0, is shown in Fig. [3-2]. Plotted logarithmically is the intensity $V_g V_g^*(x = 2\pi w_0 x/(\lambda s), y = 0, z = s)$, for $d/w_0 = 0, \pm 0.25, \pm 0.50, \pm 0.71, \pm 1$ and -1.35, normalized to VV_0^* $(x = 2\pi w_0 x/(\lambda s), y = 0, z = s)$ with $d/w_0 = 0$. This type of normalization results in a straight line plot for the case of $d/w_0 = 0$. Values of negative d/w_0, exposing more aperture, are seen to have larger central intensity, peaking in the limit to a normalized value of the intensity equal to 4. Asymptotically, the curves for $\pm$ d/w_0 merge as $2\pi w_0 x/(\lambda s)$ exceeds 6.

Fig. [3-3] shows a three dimensional plot for the diffraction of a convergent wave by an edge symmetrically positioned. VV^* is calculated from Eq. (3.6) normalized by $[\pi w_0{}^2/2\lambda s]^2$ and plotted versus $2\pi w_0 x/(\lambda s)$ and $2\pi w_0 y/(\lambda s)$. The interval along the normalized x axis is $-80 \leq 2\pi w_0 x/\lambda s \leq +80$ and along the y from $-10 \leq 2\pi w_0 y/\lambda s < +10$.

In the above calculations of the electric field the w function was generated using the existing algorithm for the computation of the complimentary error function. These programs are included in Appendix C.

It is of academic interest to present an alternate way of calculating the w function with arbitrary precision using the backward recursion formula for the repeated integrals of the error function. W. Gautschi[4] has discussed the recursive computations of the repeated integrals of the error function. Using the method of backward recurrence discussed in his paper we have written a subroutine that calculates $i^n \mathrm{erf}\ cz$ for a given n and z where $i^n \mathrm{erf}\ cz$ is defined in

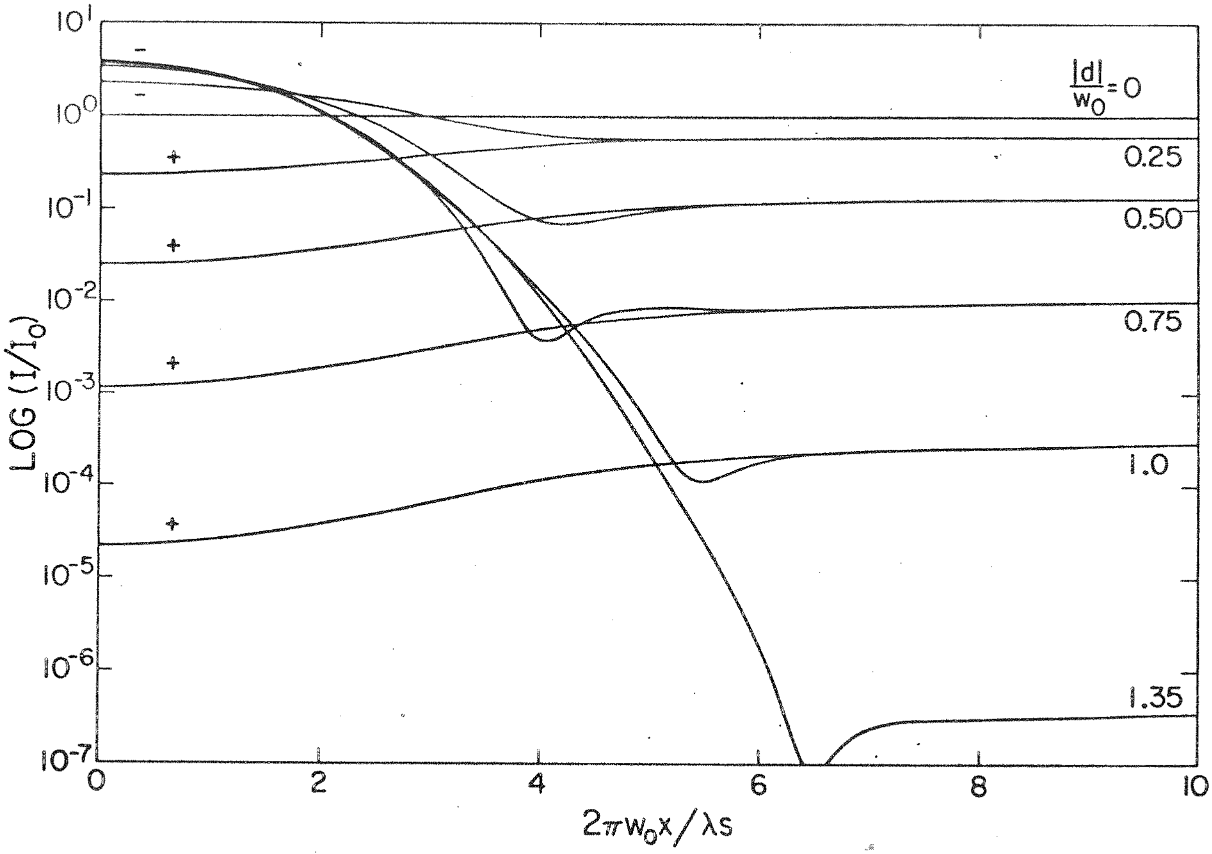

Fig. [3-2]. Transmitted irradiance I normalized to its $d/w_0 = 0$ value is plotted logarithmically vs $2\pi w_0 x/(\lambda s)$ for $y=0$. The curves whose normalized intensity at $2\pi w_0 x/(\lambda s) = 0$ is greater than one correspond to to negative values of $|d|/w_0$.

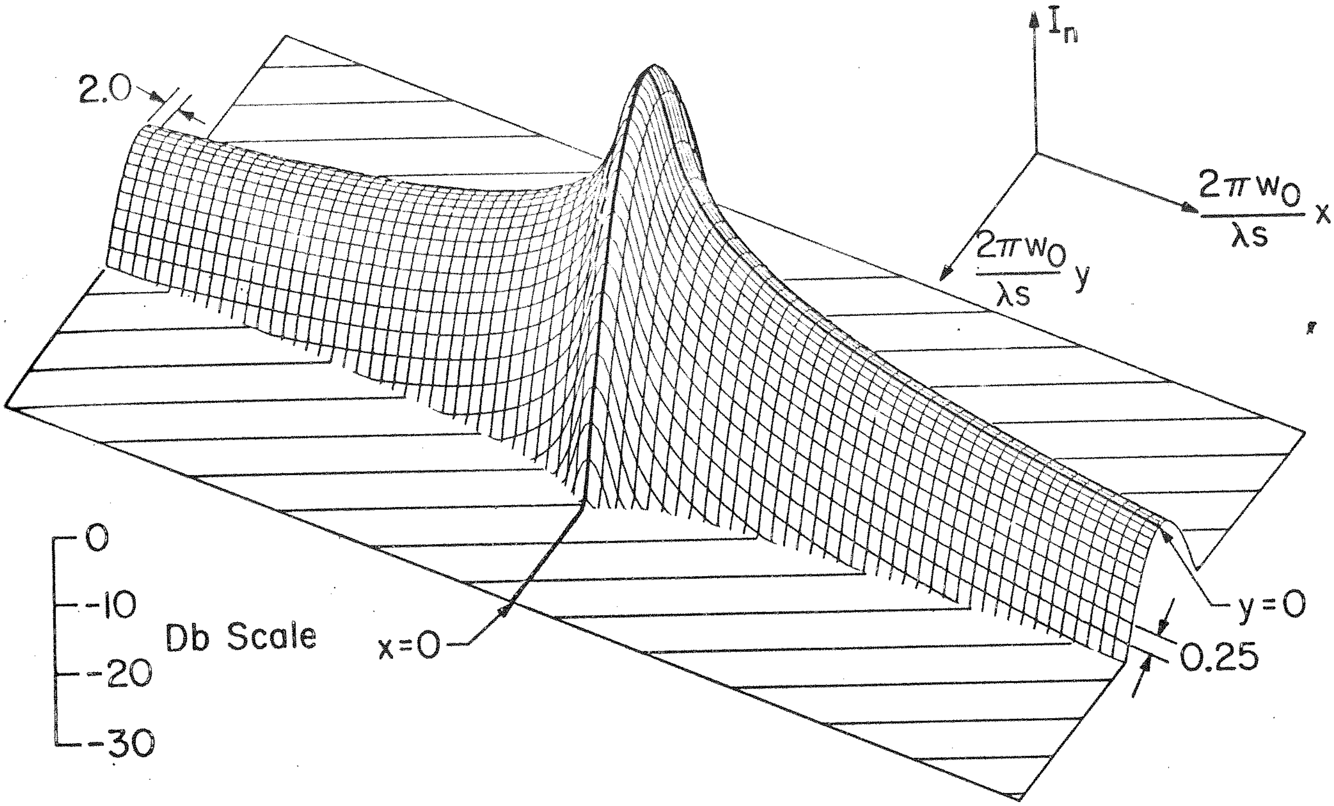

Fig. [3-3]. Normalized transmitted irradiance I_n is plotted logarithmically vs $2\pi w_o y/(\lambda s)$ and $2\pi w_o x/(\lambda s)$ with d=0, for an infinite edge illuminated with a convergent Gaussian wave. The maximum of I_n corresponds to a normalized irradiance of 1.0 while the horizontally ruled plane corresponds to an irradiance level of 10^{-5}. The interval along the normalized x axis is from $-80 - \frac{2\pi w_o x}{s} \leq +80$ and along y from $-10 - \frac{2\pi w_o y}{\lambda s} \leq +10$.

A.S. 7.2.3. Using the identities that

$$i^{-1}\,\text{erfc}z = \frac{2}{\sqrt{\pi}}\exp(-z^2) \tag{3.10}$$

and

$$i^{0}\,\text{erfc}z = w(iz)e^{-z^2} \tag{3.11}$$

w(z) can be determined within the desired accuracy. A copy of this function subroutine is included in Appendix E.

3.4 Summary and Conclusions

The optical transform pattern for a convergent Gaussian wave diffracted by an offset edge has been analyzed. The singularities which customarily occur in diffraction pattern problems without an aperture are absent in this case, as is to be expected with Gaussian beams. The general result for the focal plane electric field is given by Eq. (3.6) while that for an asymmetrical slit is presented in Eq. (3.9).

Characteristically the pattern produces a spike perpendicular to the edge and the intensity in the spike falls off with an inverse square distance dependence as can be seen from Eq. (3.8). In addition, with the Gaussian illumination, there is no ripple, although interesting nulls are predicted at large offsets of the edge as given in Table [3-1].

CHAPTER 3

REFERENCES

1. J. E. Pearson, T. C. McGill, S. Kurtin and A. Yariv, J. Opt. Soc. Am., 59, (1969), 1440.

2. J. A. Ward, J. ACM4, 2, (1957), p. 148-150.

3. H. Bach, Com. of ACM, 12, (1969), p. 675-677.

4. N. Gautschi, Math. Comp., 15, (1961), p. 227-232.

A.S. M. Abramowitz and I. A. Stegun, Handbook of Mathematical Functions, (Nat. Bureau of Standards, Washington, 1970).

CHAPTER 4

EXPERIMENT

4.1 Introduction

The purpose of this experiment was to demonstrate the diffraction patterns that were calculated in the previous chapters.

The Fourier transform patterns recorded for a semicircular aperture with uniform amplitude illumination, and for an infinite edge illuminated with a Gaussian wave, are presented here. The experimental set-up for taking the Fourier transforms is described, and some of its limitations are discussed.

4.2 Experimental Set-Up.

The total experimental layout is illustrated in Fig. [4-1]. An argon laser (SML) operated in the single mode fashion was the illuminating source. The mirror (M1) directed the laser beam through a shutter (S) that could be opened for time periods ranging from a few milliseconds to an hour. Consequently the beam passed through a series of glass neutral density filters (NDS), used for intensity modulation, and then redirected by mirror (M2) into a spatial filter comprised of an objective lens (MO) and a pinhole (P) located at the focal point of the objective. The collimating lens (CL), with the curvy side towards the film plate, was slightly misaligned such that instead of producing a collimated beam it focused the radiation with an effective focal length of 10.67 m. This was done so that the diffraction patterns could be directly recorded on a 10.16 x 12.7 cm

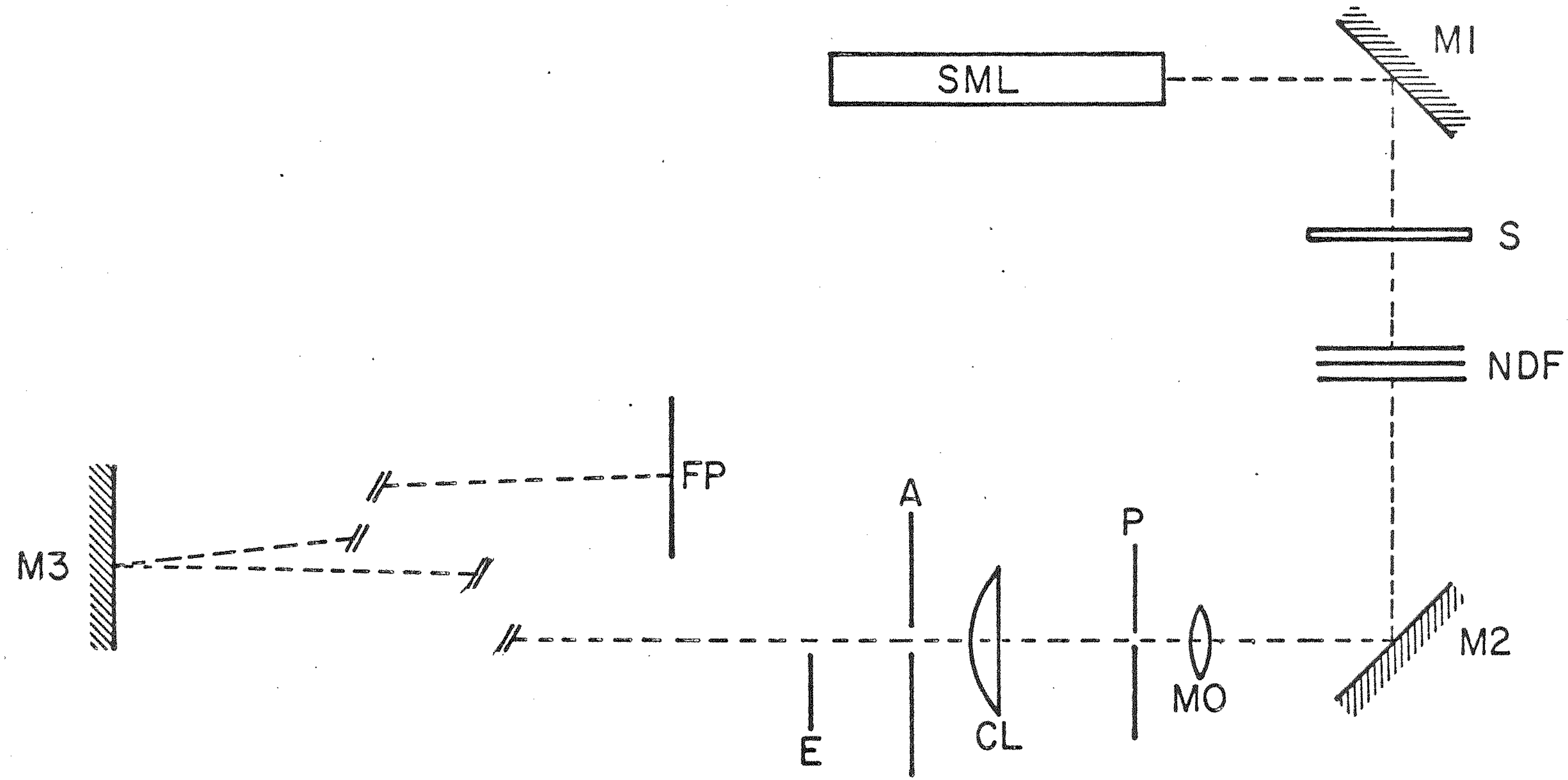

Fig. [4-1]

SML	Single Mode Laser	P	Pinhole
S	Shutter	CL	Collimating lens
NDF	Nuetral density filter	A	Circular aperture
M1,M2,M3	Mirrors	E	Edge
MO	Microscope objective	FP	Film plate

(4" x 5") film plate eliminating the use of a microscope with a camera attachment, thus sparing us the problem of ghost images and multiple reflections. Following the collimating lens a circular aperture (A) was located symmetrically in the beam and an edge (E) was mounted on a vertical micrometer translation stage so that a razor blade could be positioned accurately in the beam. Subsequently the diffracted beam traversed the length of the room and was reflected by a large rectangular mirror (M3) onto the film plate (FP). The angle of incidence of the diffracted beam and mirror M_3 was very close to 90° so that pattern distortion resulting from phase retardations would be minimized.

4.3 Photographs and Discussion

To generate the diffraction pattern of the uniform amplitude wave by the semicircular aperture, (Fig. [4-2]) a 40X Wild objective was used coupled with a 12 μm pinhole. This way the light incident onto the collimating lens was greatly overexpanded resulting in an amplitude variation not greater than 4% measured across the 1 cm aperture (A). To position the razor blade accurately in the center of the beam two micrometer readings were taken; one at the position of no light on the film, and another at the point where edge diffraction effects were totally absent from the Airy disc pattern. Then the edge was positioned at the half way setting. The distance between the diffracting edge and the film plate was 10.44 m. The value of the neutral density filters was 2.5, resulting in a power level, measured at the center of the pattern and averaged over a 1 cm

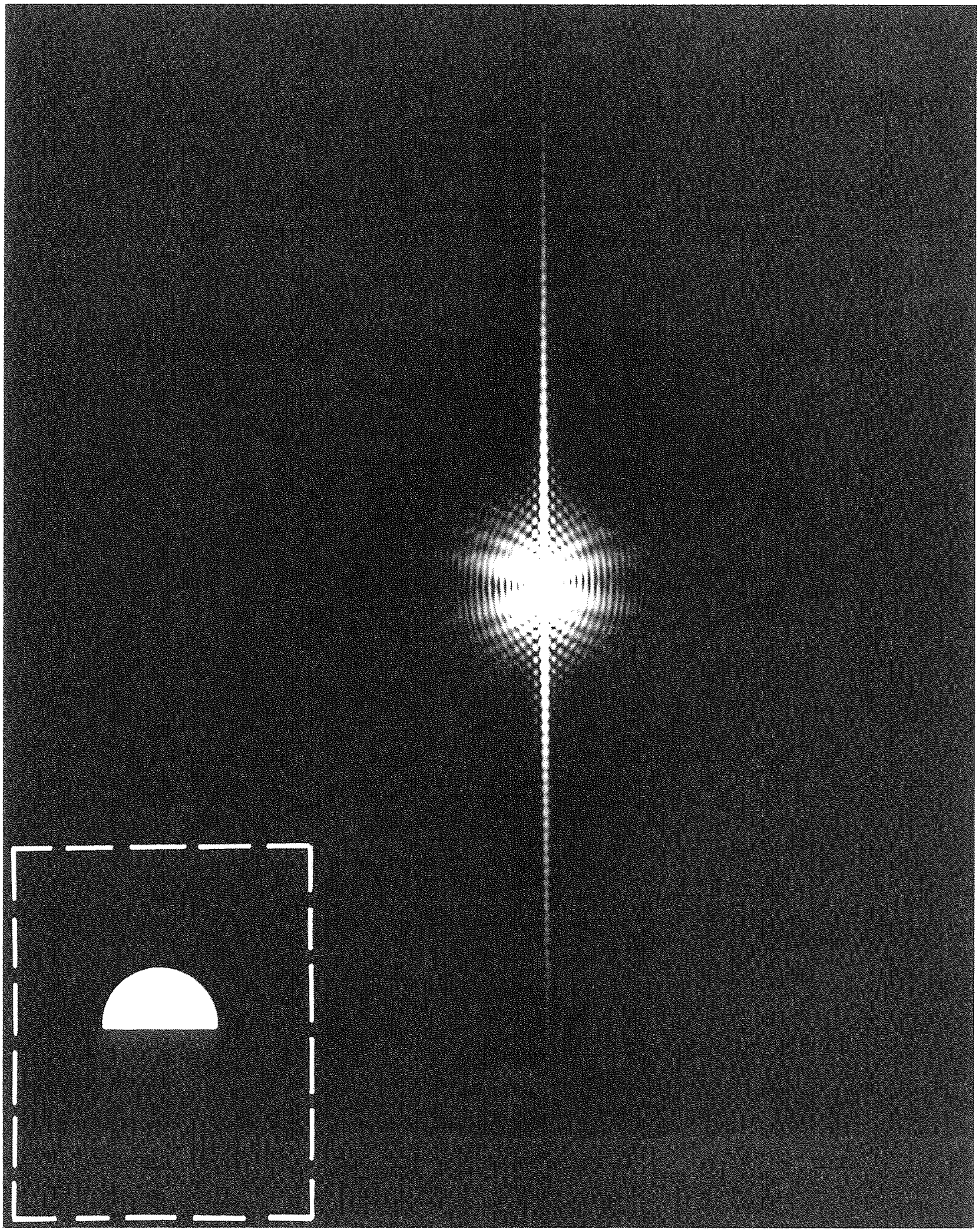

Fig. 4-2. Back focal plane radiation pattern of a convergent uniform amplitude wave diffracted by a semicircular aperture shown in the inset.

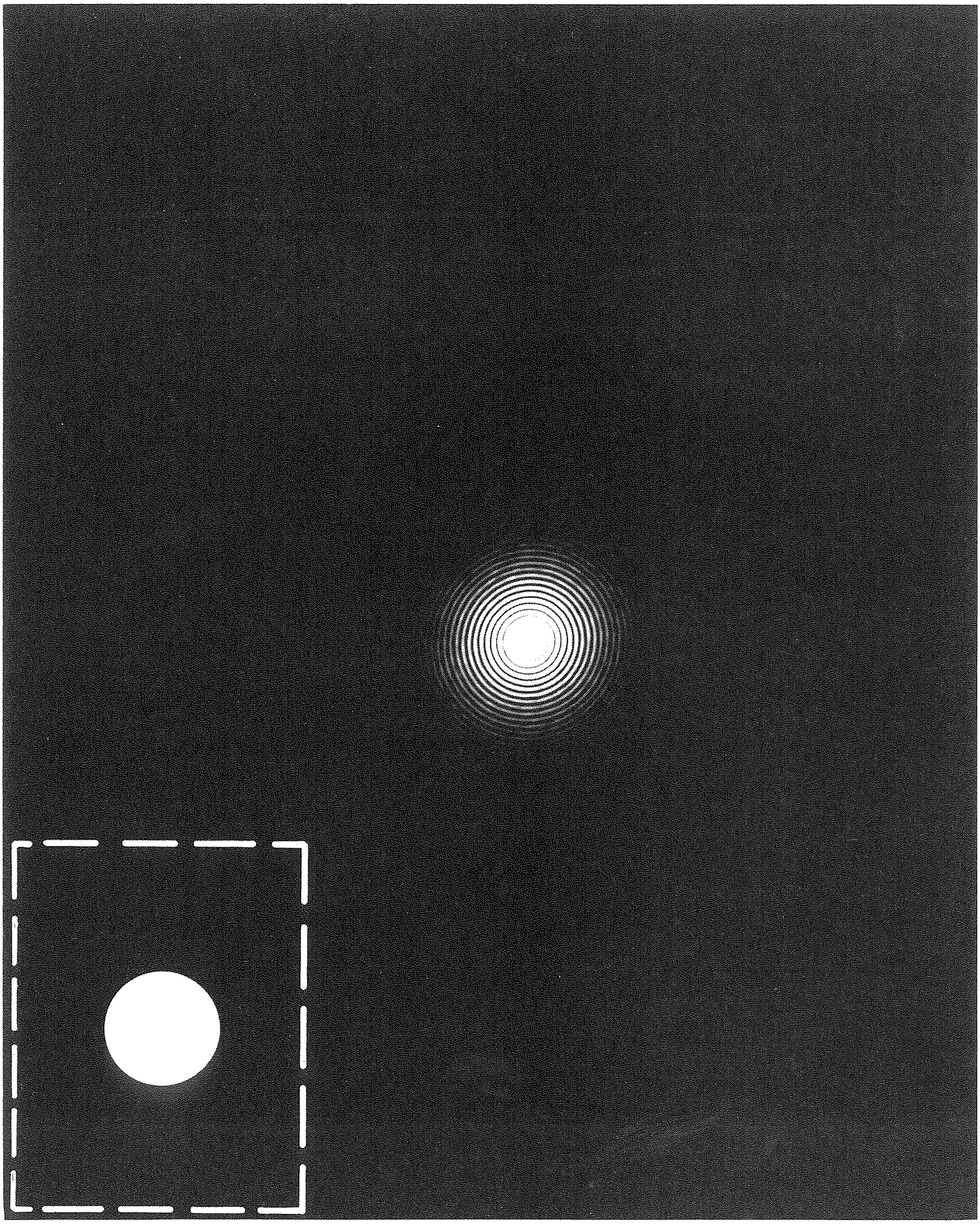

Fig. 4-3. Radiation pattern at the back focal plane of a lens illuminated by a wave of uniform amplitude and truncated by the circular aperture shown in the inset.

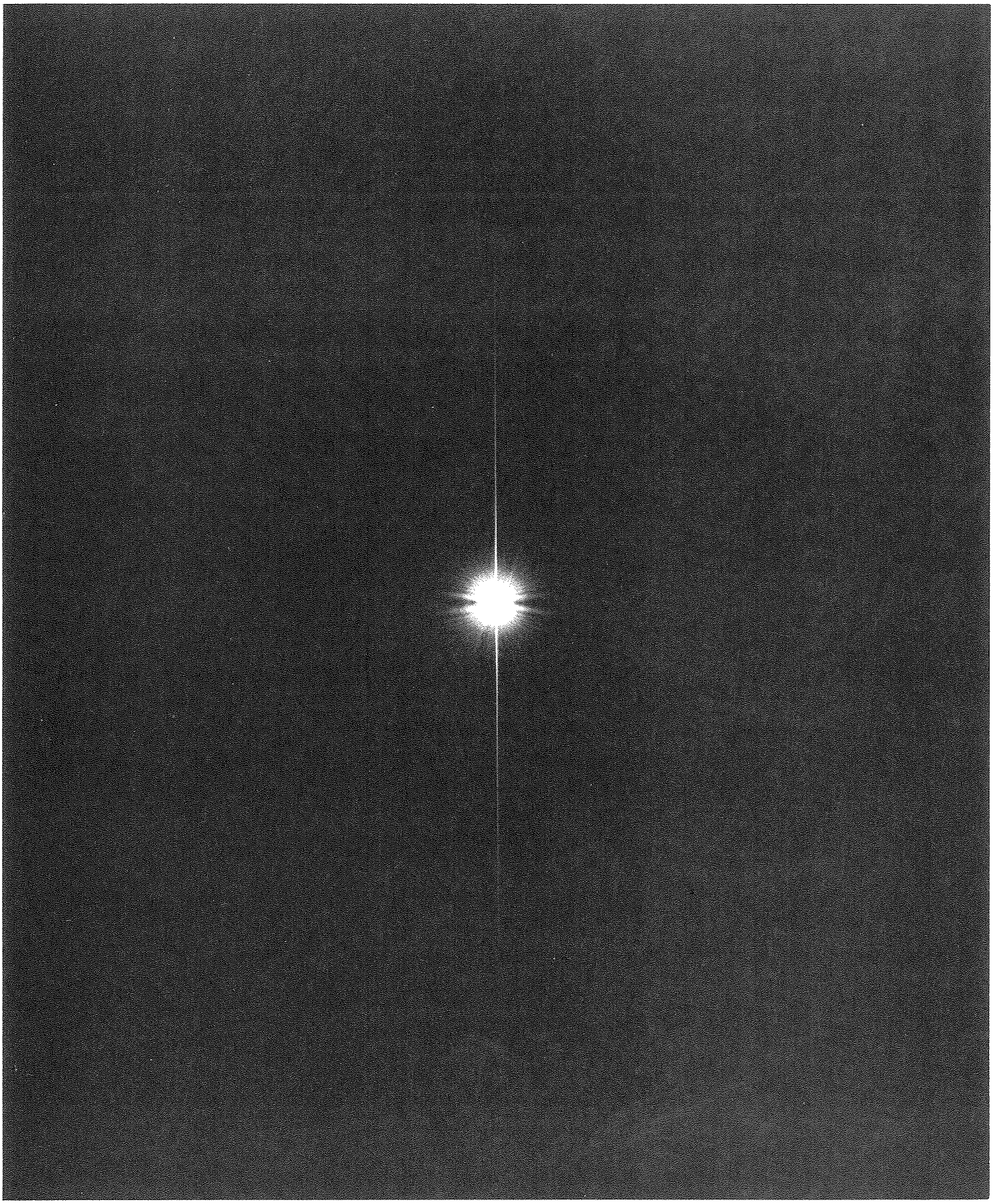

Fig. 4-4. Actual size back focal plane pattern of a lens with a semicircular aperture having a 1 m focal length and a .5 cm radius, illuminated by a uniform amplitude wave.

aperture, of .50 μW. The exposure time was 10 seconds and the film used was the Kodak Ektapan 4162 thick estar base. To get a qualitative feeling for the difference between this transform pattern and the one for a circular aperture we present Fig. [4-3]. This figure shows the Airy disk pattern and was made in the exact same configuration as for Fig. [4-2] except for the fact that the edge was removed from the system, and the exposure time cut by a factor of 2.

To get a recording of the overall pattern for the semicircular aperture case (Fig. 4-4) the focal length of the system was reduced to 1.27 m and the distance between the diffracting edge and the film plate was set at 1.04 m. At the same time the neutral density filter value was increased to 3 and the exposure time was kept the same.

To generate the focal plane patterns for a Gaussian beam diffracted by an edge [Fig. 4-6], a collimator was introduced, in the reverse order, between mirror (M2) and objective (MO). The objective was changed to a Lietz 2.5X, and the pinhole was enlarged to 1.6 mm so as to eliminate only the very high frequencies and not affect the Gaussian profile. The $1/e^2$ point was estimated from the beam profile curve to be 3.1 mm. To measure the amplitude distribution at the diffracting edge a 1.2 KHz chopper was introduced between the neutral density filters (NDF) and mirror (M2). The signal was read using a lock-in amplifier and the scanning aperture was 50 μm in diameter mounted on a U.D.T. PIN 10C detector. Fig. [4-5] shows the beam profile measured and the one calculated for w_o = 3.1 mm. To eliminate high frequency components all the mirror and lens surfaces were thoroughly cleaned. The exposure time for

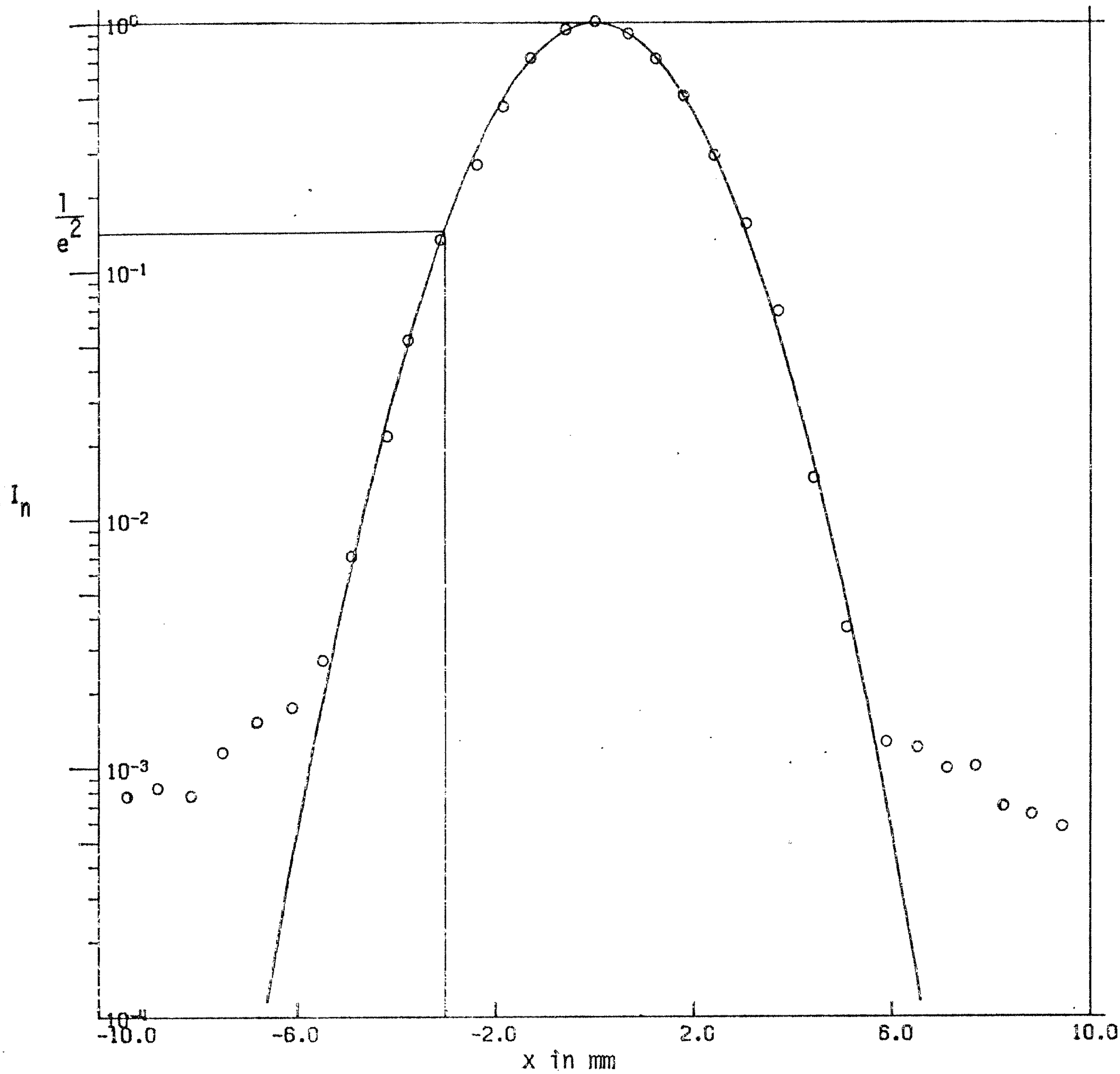

Fig. [4-5]. Normalized intensity versus displacement measured at the edge (E). Solid curve represents the theoretical Gaussian calculated for w_0 = 3.1 mm.

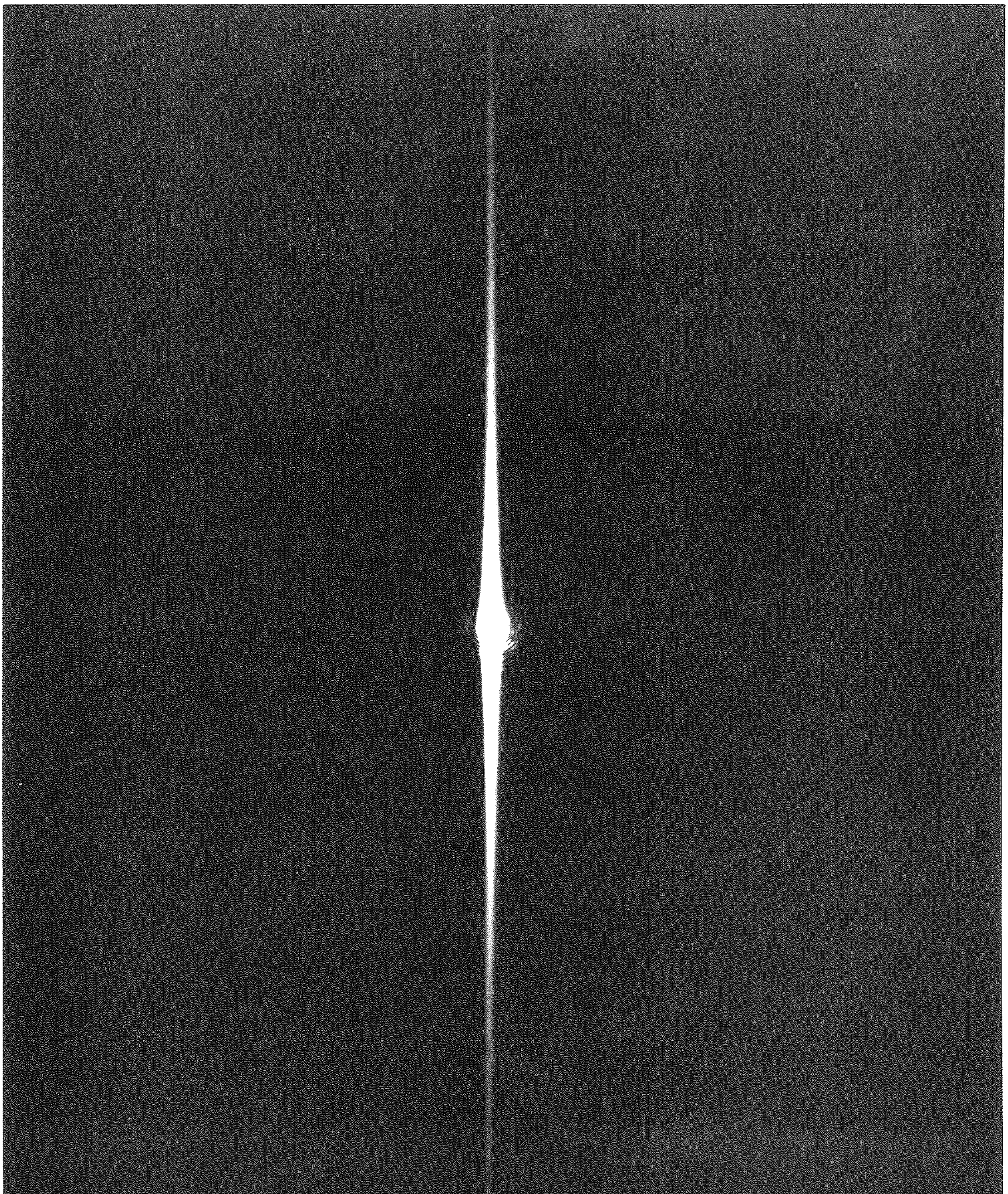

Fig. 4-6. Recorded intensity for a convergent wave of Gaussian amplitude truncated by an infinite edge.

the photographs was 10 sec with a neutral density filter value of 3.6, so that the average power on the center of the diffraction pattern was .5 μW.

CHAPTER 5

NEAR FOCUS DISTRIBUTION OF A CONVERGENT WAVE

5.1 Introduction

During the course of our experimental investigation an interesting way for finding the position of the back focal plane of a lens has been developed. Conventionally the intensity distribution, for unit amplitude and Gaussian waves, near the focal plane of a lens is symmetric about the optical axis[1,2]. Because of this symmetry the exact determination of the focal plane of the lens is difficult. However, if half of the lens is blocked, then the intensity patterns are symmetric only at the focal plane (as was shown in Ch. 2 and 3) and the above symmetry is very sensitive to the translation of the lens along the optical axis.

In this chapter we will calculate the intensity distribution, near the focal plane for a converging unit amplitude incident wave illuminating a semicircular aperture.

In the analysis that follows we use the approximate form of Sommerfeld diffraction theory integral that has been developed for the calculation of aberration-free diffraction images. The solution of this integral is expressed in terms of rapidly converging infinite series. Expressions for the on axis fields are also given.

The solution is evaluated numerically and isodensity contour plots are presented showing the lines of constant intensity for a number of planes including the meridional and back focal. The results agree with the experimental assertion that the back focal plane of a lens can be accurately determined by blocking half of the lens.

5.2 Theoretical Analysis

Consider a monochromatic unit amplitude plane polarized spherical wave with radius of convergence s incident on a semicircular aperture of radius a (see Fig. [5-1]. Defining

$$\xi = ar\sin\theta \qquad x = \rho\sin\theta$$
$$\eta = ar\cos\theta \qquad y = \rho\cos\theta \tag{5.1}$$

and

$$u = \frac{2\pi}{\lambda}\left(\frac{a}{s}\right)^2 z \quad , \qquad v = \frac{2\pi}{\lambda}\left(\frac{a}{s}\right)\rho = \alpha\rho \tag{5.2}$$

Sommerfeld's diffraction integral (Eq. 2.5) can be approximated for our particular case as follows:

$$V(v,\phi,u) = \frac{ia^2}{\lambda s}\exp[(-i(s/a)^2u]\cdot\int_0^1\int_{-\pi/2}^{\pi/2}\exp\{i[(vr\cos(\theta-\phi) + \frac{1}{2}ur^2]\}r\,dr\,d\theta \tag{5.3}$$

Eq. (5.3) can be obtained by using Eq. 8.81. (11) in Ref. 3 and setting $A/f = 1$, $f=s$, $\rho=r$, $\psi=\phi$, $i= -i$, and changing the limits of integration over θ so that the contribution from only half of the aperture is considered. Note that the above changes result in a $+i\omega t$ time dependence and unit amplitude incidence in agreement with our previous notation.

To solve Eq. (5.3) we first expand the exponent in terms of infinite series of Bessel functions using A.S. 9.1.44 and 9.1.45. Exchanging the order of integration and summation we get:

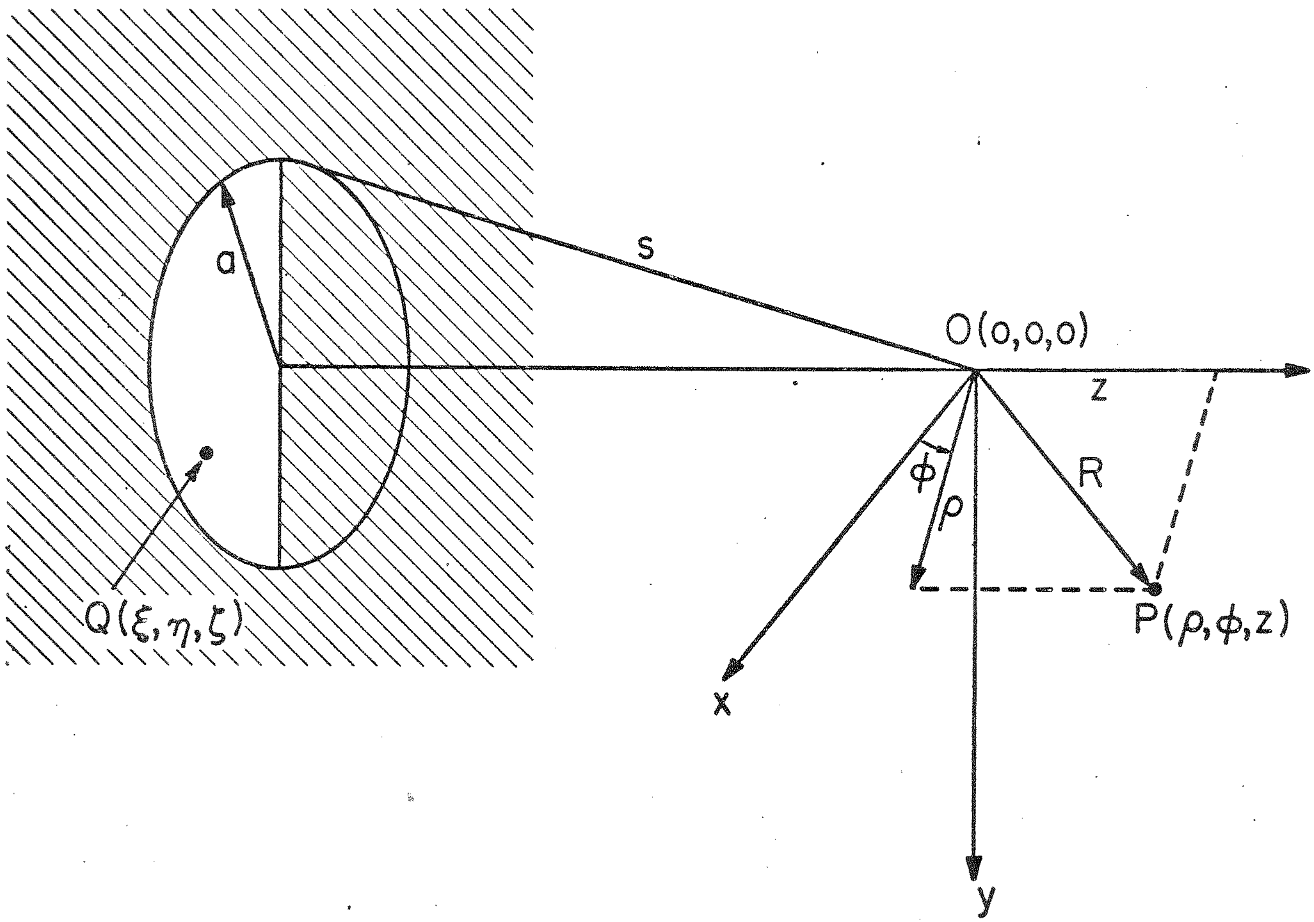

Fig. [5-1]. Geometry of relationships between semicircular aperture and near focus point $P(\rho,\phi,z)$.

$$V(v,\phi,u) = \frac{ia^2}{\lambda s}\exp[-i(s/a)^2u]\cdot\int_0^1\left\{J_o(vr)\int_{-\pi/2}^{\pi/2}d\theta + 2\sum_{k=1}^{\infty}(-1)^k J_{2k}(vr)\cdot\right.$$

$$\left.\cdot\int_{-\pi/2}^{\pi/2}\cos[2k(\phi-\theta)]d\theta + 2i\sum_{k=o}^{\infty}(-1)^k J_{2k+1}(vr)\cdot\int_{-\pi/2}^{\pi/2}\cos[(2k+1)(\phi-\theta)d\theta\right\}\exp(i\ \tfrac{u}{2}\ r^2)rdr \tag{5.4}$$

Integration with respect to θ gives the following result

$$V(v,\phi,u) = \frac{ia^2}{\lambda s}\exp[-i(s/a)^2u]\cdot\left\{\int_0^1\pi J_o(vr)\exp(i\ \tfrac{u}{2}\ r^2)rdr + \right.$$

$$\left. -4i\sum_{k=o}^{\infty}\frac{\cos(2k+1)\phi}{2k+1}\int_0^1 J_{2k+1}(vr)\exp(i\ \tfrac{u}{2}\ r^2)rdr\right\} \tag{5.5}$$

We note that the first term in Eq. (5.5) is similar to the integral analyzed by Lommel and expressed in terms of Lommel functions of two variables[4]. Since we do not wish to restrict our analysis to real u, we instead express the result of the first integral, $\mathcal{I}_1$, in terms of a single series by expanding the Bessel function using A.S. 9.1.10 and integrating term by term. This gives

$$\mathcal{I}_1 = \frac{\pi}{u}\exp(iu/2)\cdot\sum_{m=1}^{\infty}\left(\frac{-iu}{v}\right)^m J_m(v) \tag{5.6}$$

To evaluate the second integral, $\mathcal{I}_2$, we expand the exponential term into an infinite series and exchange the order of integration and summation. This gives the following expression for $\mathcal{I}_2$

$$\mathscr{I}_2 = -4i \sum_{k=o}^{\infty} \frac{\cos(2k+1)}{2k+1} \sum_{m=o}^{\infty} \frac{(\frac{iu}{2})^m}{m!} \int_0^1 r^{2m} J_{2k+1}(vr)\, r dr \qquad (5.7)$$

We note in Eq. (5.7) that the integration with respect to the Bessel function can be carried through and the result written in terms of Lommel's polynomials $S_{2m,2k}$ (5). However, series expansions for the above polynomials exist only when the sum or difference of the indices is an odd integer. For this reason, we prefer to expand again the Bessel function in terms of a power series using A.S. 9.1.10 and exchange the order of summation and integration. $\mathscr{I}_2$ can then be written in the form:

$$\mathscr{I}_2 = -2iv \sum_{k=o}^{\infty} \frac{\cos(2k+1)\phi}{2k+1} \sum_{m=o}^{\infty} \frac{(\frac{iu}{2})^m}{m!} \left(\frac{v}{2}\right)^{2k} \sum_{n=o}^{\infty} \frac{(\frac{-v^2}{4})^n}{n!(2k+n+1)!} \cdot \int_0^1 r^{2n} r^{2k+1} r^{2n} r dr \qquad (5.8)$$

Integrating and combining terms gives:

$$\mathscr{I}_2 = -2iv \sum_{m=o}^{\infty} \frac{(\frac{iu}{2})^m}{m!} \sum_{n=o}^{\infty} \frac{(\frac{-v^2}{4})^n}{n!} \sum_{k=o}^{\infty} \frac{(\frac{v^2}{4})^k \cos(2k+1)\phi}{(2k+1)(2k+n+1)!(2k+2m+2n+3)} \qquad (5.9)$$

The summations in Eq. (5.9) have been written in this order to indicate the convergence of the series.

Combining Eq. (5.9), (5.6), (5.5) gives the following general result for the electric field,

$$V(v,\phi,u) = \frac{ia^2}{\lambda s} \exp[-i(s/a)^2 u]\pi \cdot \left\{ \frac{\exp(iu/2)}{u} \cdot \sum_{m=1}^{\infty} \left(\frac{-iu}{v}\right)^m J_m(v) - \right.$$

$$\left. - \frac{2iv}{\pi} \sum_{m=o}^{\infty} \frac{\left(\frac{iu}{2}\right)^m}{m!} \sum_{n=o}^{\infty} \frac{\left(\frac{-v^2}{4}\right)^n}{n!} \sum_{k=o}^{\infty} \frac{\left(\frac{v^2}{4}\right)^k \cos(2k+1)\phi}{(2k+n+1)!(2k+1)(2k+2m+2n+3)} \right\} \tag{5.9}$$

For $u = 0$ i.e., focal plane calculation, the above expression reduces to:

$$V(v,\phi,0) = \frac{ia^2}{\lambda s} \pi \cdot \left\{ \frac{J_1(v)}{v} - \frac{2iv}{\pi} \sum_{n=o}^{\infty} \frac{\left(\frac{-v^2}{4}\right)^n}{n!} \sum_{k=o}^{\infty} \frac{\left(\frac{v^2}{4}\right)^k \cos(2k+1)\phi}{(2k+n+1)!(2k+1)(2k+2n+3)} \right\} \tag{5.10}$$

This result (except for a phase factor) is identical to the one presented in Chapter 2, Eq. (2.32).

The case of $v = 0$, that is on z axis calculation, can be reduced from Eq. (5.9) in the following way. We set the second part of Eq. (5.9) equal to zero and use the following limiting form for Bessel functions of small arguments (A.S. 9.1.7)

$$J_m(v) = \left(\frac{1}{2} v\right)^m / m! \tag{5.11}$$

Taking only the first term of the sum we write

$$V(0,\phi,u) = \frac{-a^2}{\lambda s} \exp[-i(s/a)^2 u]\pi \frac{1}{u} [1 - \exp(iu/2)] \tag{5.12}$$

We note that this result is independent of ϕ and in agreement with Eq. 8.8.2 (26) in Ref. 3, as expected.

Finally for $\phi = \pm\pi/2$, $\cos(2k+1)\phi = 0$ and Eq. (5.9) reduces to the form:

$$V(v,\pm\pi/2,u) = \frac{ia^2}{\lambda su} \exp[-i(s/a)^2u]\pi \cdot \exp(-iu/2) \sum_{m=1}^{\infty} \left(\frac{-iu}{v}\right)^m J_m(v) \qquad (5.13)$$

This last case is the near focus light distribution for a circular aperture with transmission of 0.5 across the full aperture.

5.3 Numerical Calculations

The representation of the intensity distribution as a function of coordinates for a fixed value of the third is presented in this section. The planes we have selected are the (x,y,z=0) (focal plane), (x,0,z) (meridional plane), (0,y,z) (plane parallel to the edge) and the plane $(\rho,\phi = \frac{\pi}{4}, \frac{5\pi}{4}, z)$. We use isodensity contours for various levels of intensity since conventional three dimensional plots are not suitable for plotting functions of oscillatory character over large regions.

The calculation of Eq. (5.9) was done in the following way. A double precision subroutine was generated to calculate the double sum over the n and k indices, as a function of m. Particular attention was paid in keeping terms of the same order together so as to eliminate precision and overflow problems common in calculations involving large factorials and powers. The sums were truncated for values of the index n and k of the same order as v with a few terms added for improved accuracy (last term of the order of 10^{-25}). The return from the subroutine was then used to generate an array of complex numbers which was consequently sorted and summed in double precision by a function subprogram.

The calculation of the first sum of Eq. (5.9) presented the problem that whenever $u \gg v$ the series would converge very slowly. The problem was solved with the use of the generating function for the Bessel series A.S. 9.1.41, namely that for $|t| > 1$ we use

$$\sum_{m=1}^{\infty} t^m J_m(v) = \exp[\tfrac{v}{2}(t - \tfrac{1}{t})] - J_o(v) - \sum_{m=1}^{\infty} (\tfrac{-1}{t})^m J_m(v) \qquad (5.14)$$

The computer program used for these calculations is included in Appendix F. To generate the contour plots, the program developed by Lawson and Block[6] (J.P.L.) was used.

Fig. [5-2] shows the intensity distribution of (x,y,z=0) i.e. the back focal plane, plotted as the normalized coordinates αx and αy defined by Eq. 5.2 and 5.1. The central maximum corresponds to point P_o in Fig. [2-1] and Fig. [2-2], the second maximum along the αx axis corresponds to P_2, and so on. The intensity VV^* from Eq. (5.10) normalized by $(\frac{\pi a^2}{\lambda s})^2$ is plotted linearly and the central maximum corresponds to an intensity of 0.25. The intensity values for the different contours is given by the legend accompanying the figure. The entire plot encompasses the region $-20 \leq \alpha x \leq 20$ and $-20 \leq \alpha y \leq +20$.

The intensity distribution in the meridional plane (x,0,z) is shown in Fig. [5-3]. This plot shows the change of the symmetry, that is characteristic of the focal plane pattern, as a function of the displacement along the normalized coordinate. Plotted is the intensity VV^* from Eq. 5.9 normalized to $(\frac{\pi a^2}{\lambda s})^2$ as a function of the normalized coordinate αx and the normalized z coordinate u.

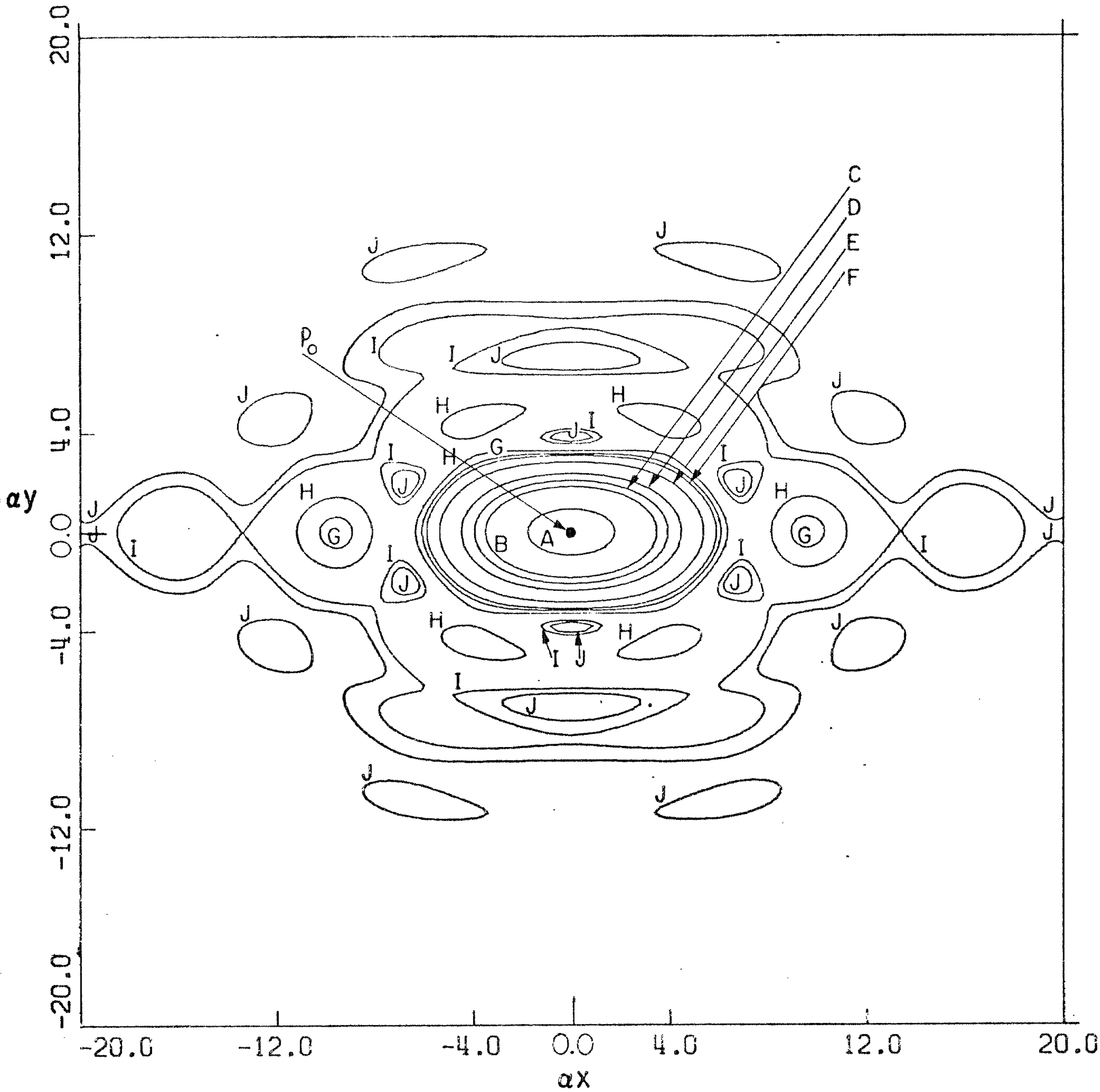

Fig. [5-2]. Focal plane (x,y,z=0) isophotes plotted vs. αx and αy. The center of the pattern P_o corresponds to a normalized intensity of 0.25.

A = 0.2000	F = 0.0100
B = 0.1000	G = 0.0075
C = 0.0750	H = 0.0050
D = 0.0500	I = 0.0010
E = 0.0200	J = 0.0005

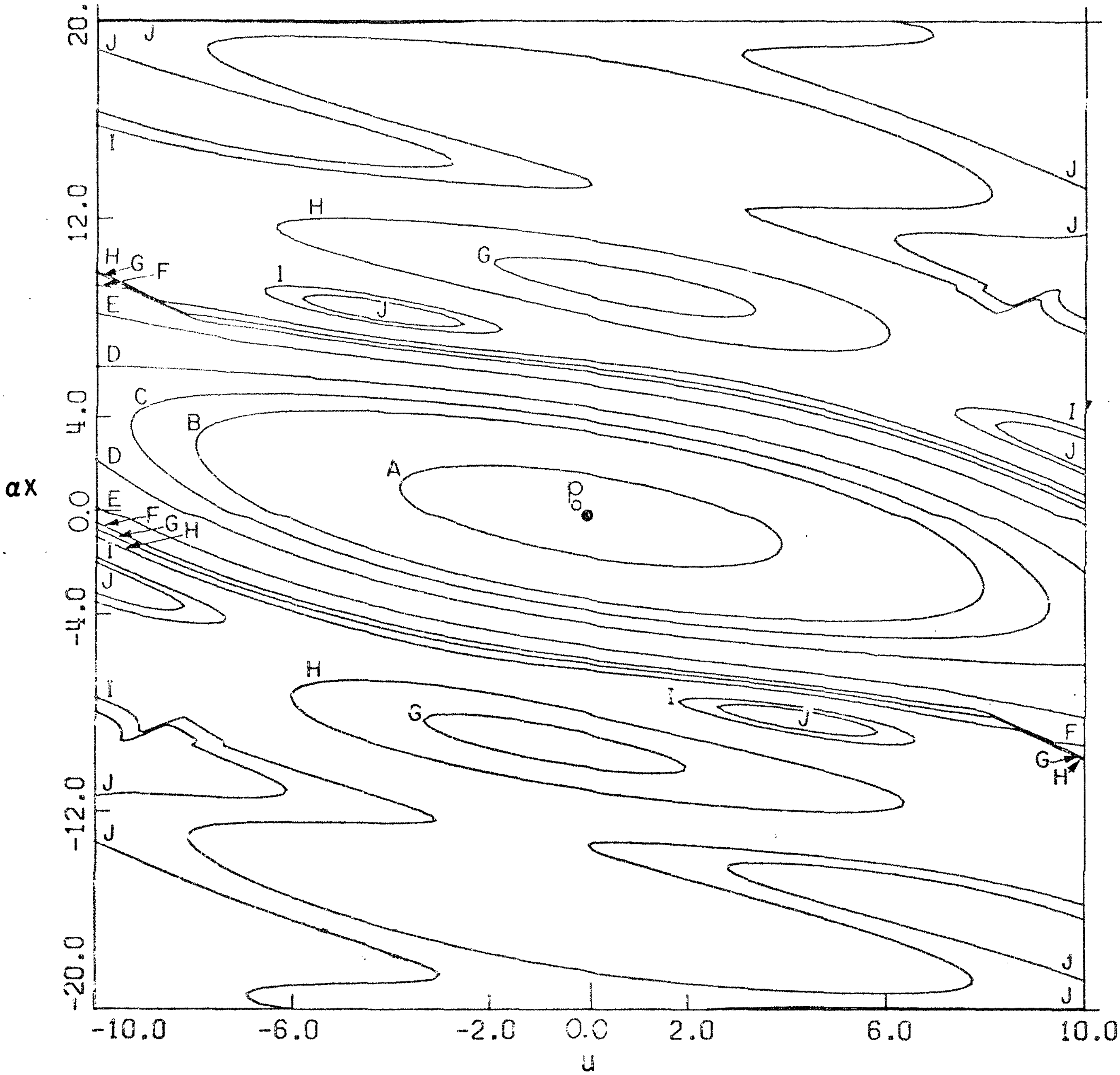

Fig. [5-3]. Contour lines in the meridional plane (x,o,z) of the normalized intensity plotted vs. αx and $2\pi/\lambda(a/s)^2z$.

A = 0.2000	F = 0.0100
B = 0.1000	G = 0.0075
C = 0.0750	H = 0.0050
D = 0.0500	I = 0.0010
E = 0.0200	J = 0.0005

The interval in αx is from $-20 \leq x \leq +20$ and in u from $-10 \leq u \leq 10$. We note that at the focal plane, the plane perpendicular to the line $u = 0$, the distribution is symmetric about the geometrical focus (0,0,0). However if we move either closer (in the -u direction) to the aperture, or further away from it, the distribution about the optical axis is changing asymmetrically. We note that the asymmetry for planes close to the focal plane is more pronounced for large values of αx. To get a more qualitative feeling assume that s = 35 cm a = 5 cm, λ = 6328 Å. Then each unit in u corresponds approximately to .05 mm. Furthermore from Eq. (8.2) we see that the degree of the asymmetry for a given z is proportional to the square of the ratio a to s.

Fig. [5-4] shows the intensity distribution contours of the plane parallel to the edge (0,y,z). We plot normalized intensity $VV^*/(\frac{\pi a^2}{\lambda s})^2$ from Eq. (5.13) versus u and αy. This plot is identical (except for a scaling factor, and choice of contour values) to the one presented in Ref. (3) page 440 describing the light distribution in the meridional plane for a full aperture. The plot is over the region $-20 \leq \alpha x \leq 20$ and $-10 \leq u \leq 10$. As expected the intensity is symmetric about the optical axis and the distribution on the $u = 0$ line is the Airy pattern.

To demonstrate the change from the (0,y,z) plane to the (x,0,z) Fig. [5-5] is presented. Plotted is the normalized intensity $VV^*/(\frac{\pi a^2}{\lambda s})$ for $\phi = \frac{\pi}{4}, \frac{5\pi}{4}$ versus u and v. The range in u and v is identical to the one in Figs. (5-2) and (5-3), namely $-10 \leq u \leq 10$

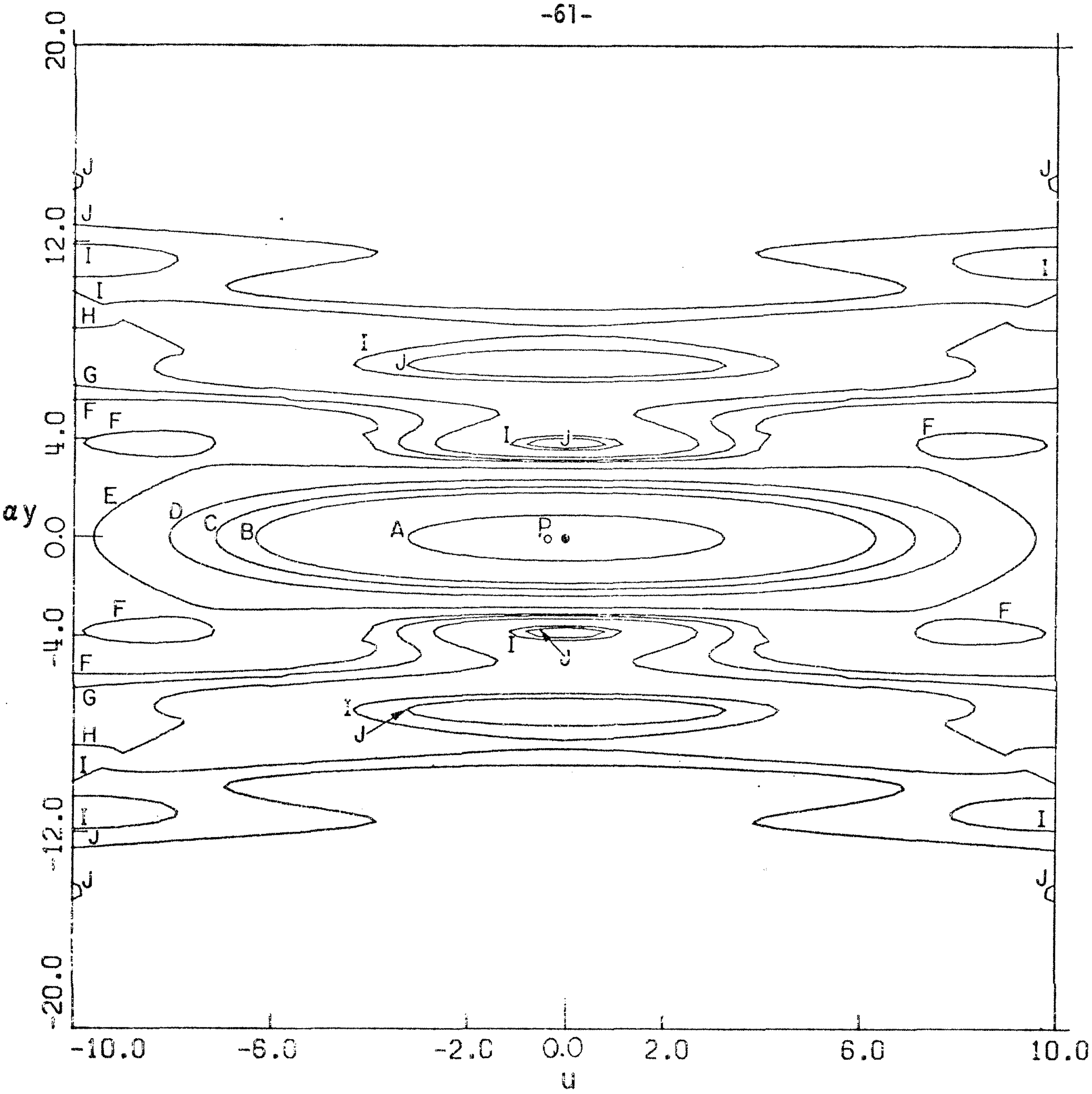

Fig. [5-4]. Isophotes at plane (0,y,z) plotted vs αy and u. This plane and the back focal (x,y,0) are the only ones that exhibit symmetry about the optical axis.

A = 0.2000
B = 0.1000
C = 0.0750
D = 0.0500
E = 0.0200

F = 0.0100
G = 0.0075
H = 0.0050
I = 0.0010
J = 0.0005

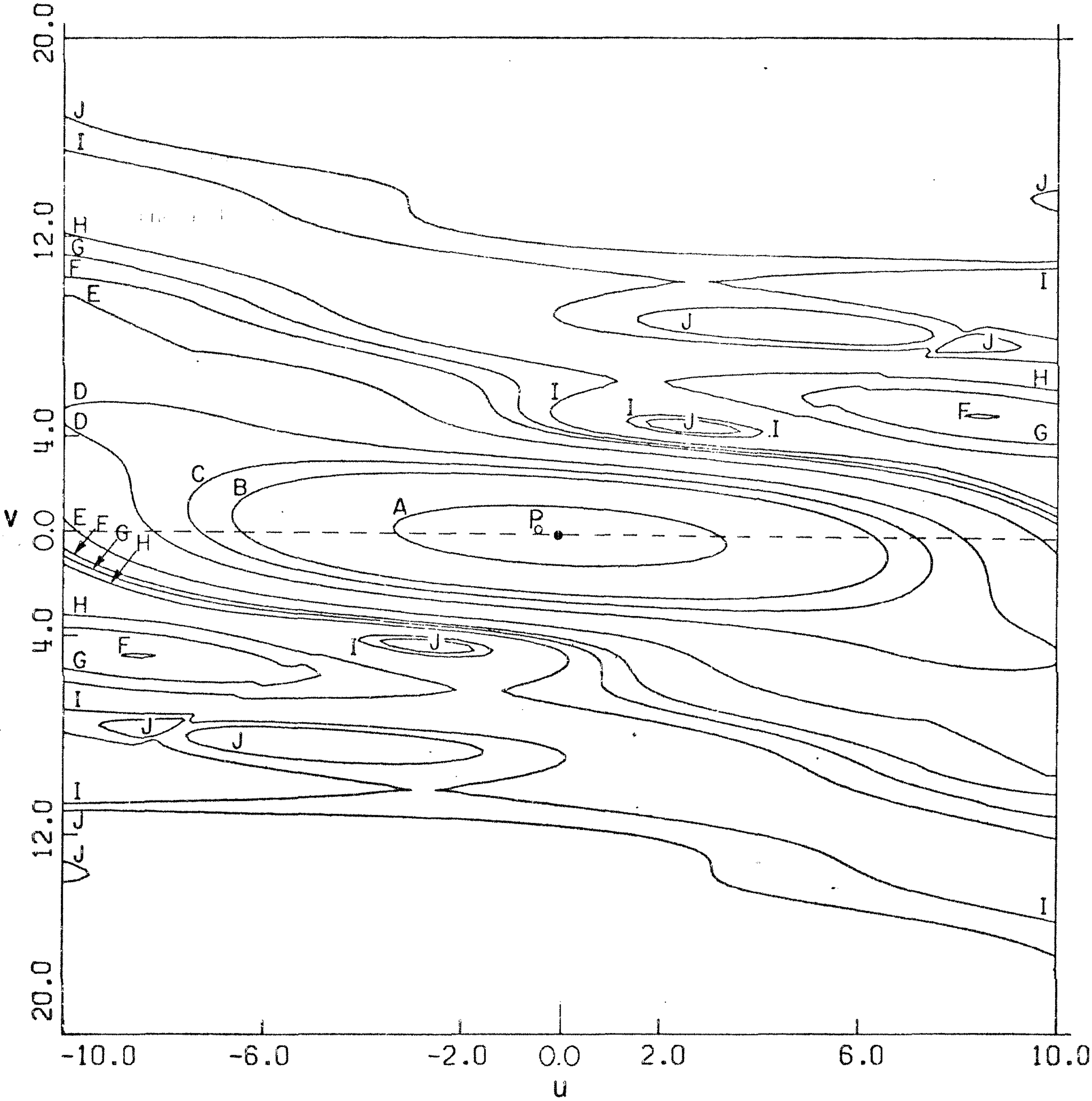

Fig. [5-5]. Intensity distribution in the $(v,\phi = \frac{\pi}{4},\frac{5\pi}{4}, z)$ plane plotted vs v and u. The plane above the dotted optical axis is the $(v,\phi = 5\pi/4,z)$ plane and the one below is the $(v,\phi = \pi/4,z)$ one.

A = 0.2000
B = 0.1000
C = 0.0750
D = 0.0500
E = 0.0200

F = 0.0100
G = 0.0075
H = 0.0050
I = 0.0010
J = 0.0005

and $-0 \leq v < 20$. The $(v, \frac{5\pi}{4}, u)$ plane lies above the dotted z axis and the $(v, \frac{\pi}{4}, u)$ below. We note the asymmetry of the pattern, with the intensity exhibiting a number of interesting minima for negative u and v.

5.4 Summary and Conclusions

The analysis of the near focus intensity distribution of a converging unit amplitude wave diffracted by a semicircular aperture has been presented. The general result for the electric field in the vicinity of the geometrical focus is given by Eq. (5.9). It is shown that the result for $z = 0$, i.e. back focal plane produces the intensity distribution evaluated in Chapter 2. The on z axis case Eq. (5.12) as well as the case of $\phi = \pm \pi/2$ (plane parallel to the edge) Eq. (5.13) are also given.

Although the analysis has been restricted to a unit amplitude case, the extension to a Gaussian amplitude one could be made as follows. In Eq. (5.3) an additional term $\exp(-a^2r^2/w_0^2)$ would be included in the integral. Since the solution is independent of whether u is real or imaginary, in Eq. (5.9) instead of u we use a new variable $t = (\frac{2\pi}{\lambda}(\frac{a}{s})^2 z + ia^2/w_0^2)$. The modification in the computer program is simple and straightforward.

The analysis shows that the intensity distribution, except for the focal plane and the plane parallel to the edge, is non-symmetric with respect to the optical axis. Furthermore the asymmetry of the pattern as we move away from the focal plane depends on the square of the ratio of the aperture radius to the radius of convergence.

CHAPTER 5

REFERENCES

1. M. Born and E. Wolf, Principles of Optics, (Pergamon Press, London, 1970), p. 440.
2. E. H. Linfoot, Recent Advances in Optics, (Clarendon Press, Oxford, 1955) p. 40.
3. M. Born and E. Wolf, ibid., p. 437.
4. G. N. Watson, A Treatise on the Theory of Bessel Functions, (Cambridge Univ. Press, Cambridge, 1966), p. 537.
5. G. N. Watson, ibid., p. 346.
6. Lauson, Block, J.P.L. Section 314 Report, 106, (1965).

A.S. M. Abramowitz and I. A. Stegun, Handbook of Mathematical Functions, (Nat. Bureau of Standards, Washington, 1970).

CHAPTER 6

SUMMARY AND CONCLUSIONS

In the work reported here several cases of edge diffraction of convergent spherical waves have been analyzed. We have presented solutions for the electric field at the focal plane as well as for arbitrary planes near the geometrical focus. The property that the focal diffraction patterns are symmetric was shown to be a very useful way of determining the location of the focal plane of an optical system.

For the case of an infinite edge, positioned off center in a circular aperture Eq. (2.20) gives the focal plane electric field for the uniform amplitude illumination. The corresponding result for a o-π radian phase mask can be written directly from Eq. (2.9) and (2.16). The above solution has been particularized to the semi-circular aperture and the electric field is given by Eq. (2.21). On axis calculations indicating the spatial frequency dependence of the patterns have been presented in Eq. (2.28) and (2.31). To illustrate these calculations we have shown 3-D plots of the intensity for a region near the origin and out along the spike. The intensity profile along the x and y axis has been presented, and an isophote diagram of the back focal plane is also included. The dominant feature of these patterns is the large spike of energy diffracted at right angles to the edge, having an intensity envelope falling off in proportion to the square of the inverse of the distance from the focal point; the fractional ripple of the spike is of the order of $|H_1^{(1)}(|\alpha x|)|^2$. The intensity along the x and y axes rings at an angular spacing consistent with the ratio of the wavelength and the corresponding dimension of the aperture. This analysis should be useful in problems of image quality enhancement as applied to photogrammetry, pattern recognition, and on-line inspection systems using optical transform methods.

The simpler case of the convergent wave with a Gaussian amplitude dependence diffracted by an offset edge has also been presented. Eq. (3.6) gives the general result for the focal plane electric field and Eq. (3.9) represents the light distribution resulting from an asymmetrical slit. The dominant feature of this pattern is again the large spike of energy perpendicular to the edge, with a $\frac{1}{x}$ intensity fall-off (x is the distance from the focal point). The basic difference between this optical transform and the one for the uniform amplitude illumination is the absence of the high frequency components and the extinction of the ripple. To illustrate the above points we have presented 3-D plots and line drawings showing the dependence of the intensity profile on the displacement of the edge. The tabulation of the zeroes of the w function and the methods employed for the calculation of the repeated integrals of the error function should be useful in the area of heat conduction and diffusion, where the w function most commonly appears.

In Chapter 4 we have presented photographs of the diffraction patterns for the uniform amplitude case as well as for the Gaussian one, and we have discussed a relatively simple set-up for obtaining magnified Fourier transforms of given aperture functions.

The near focus electric field for the convergent uniform amplitude illumination of a semicircular aperture is given by Eq. (5.9). This result was also shown to be applicable to Gaussian amplitude illumination with the redefinition of one of the variables. Solutions for the x-y plane (Eq. 5.10), y-z plane (Eq. 5.13), and on axis (Eq. 5.12) are also presented. To illustrate the change of symmetry as a function of displacement along the optical axis Fig. [5-3] and [5-5] are shown . The degree of distortion in the pattern is found to be directly proportional to the square of the ratio of the lens aperture to the focal length. The above analysis demonstrates a simple way of accurately determining the focal plane of a lens in the laboratory. By blocking half of the lens we translate a card along the optical axis until we find the location where the pattern is perfectly symmetric. Furthermore since the construction of a symmetry detector is not difficult this analysis should be useful in systems employing "self focusing" techniques.

APPENDIX A

```
C
C
      IMPLICIT REAL*8 (A-G,O-Z)
      REAL*8 L, LAMBDA
      REAL*4 SUMM, SUMK, ARGU, AIRY, COR, UU, XX, DD, UUU, XXN
      REAL*4 VAR, ASM
      DIMENSION UU(205), XX(205), UUU(500), XXN(500), DD(3), ASM(201)
      DIMENSION HXAS(201), HU(201)
      DIMENSION A(600), TAB(600), ATERM(600)
      DIMENSION B(5000), BTERM(5000)
      DATA DD/.0,.0,1./
      IMMX=200
      Z=20.D0
      L=1.D0
      LAMBDA=6328.D-8
      PI=3.14159265358979300
      ALPHA=PI*L/LAMBDA/Z
      X=.8D0
      H=X*ALPHA
      PP=PI
      WRITE (6,101) L, Z, ALPHA, X
  101 FORMAT(2X,'L=',F5.2,2X,'Z=',F6.2,3X,'ALPHA=',E13.6,3X,'X=',E13.6)
      WRITE (6,103)
  103 FORMAT(7X,'Y',11X,'ARGUMENT',7X,'INTEGRAL',6X,'AIRY DISC',6X,
     *'PERT. TERM',6X,'INTENSITY')
      Z2=ALPHA*X
      IF (X .EQ. 0.0) GO TO 109
      SUMK=.8D0*Z2-.5D0
      IKMAX=IFIX(SUMK+10.5)
      IKMAXP=Z2
      IORDK=2*IKMAX+2
      LDIMK=IKMAX+16+IKMAXP
      CALL BESJ(Z2, 0.D0, IORDK, B, 5000)
      DO 450 M=1,IMMX
      DO 400 K=1,IKMAX
      TERMK=1.D0/(2*(K+M)-1.D0)+1.D0/(2*(K+M)-3.D0)+1.D0/(2*(K-M)+1.D0)
     *+1.D0/(2*(K-M)-1.D0)
      TRMK=B(2*K)*TERMK
      BTERM(K)=TRMK
      IF (DABS(TRMK) .LT. 10.D-25) GO TO 410
  400 CONTINUE
      K=IKMAX
  410 TAB(M)=DSUM(BTERM,K)
  450 CONTINUE
  109 CONTINUE
      DO 100 N=1,201
      Y=(N-1)/2500.D0
      Z1=ALPHA*Y
      ARGU=ALPHA*DSQRT(X*X+Y*Y)
      IF (X .EQ. 0.0) GO TO 70
      IF (Y .EQ. 0.0) GO TO 40
      SUMM=.8D0*Z1-.5D0
      IMMAX=IFIX(SUMM+10.5)
      IORDM=2*IMMAX+2
      IMMAXP=Z1
      LDIMM=IMMAX+16+IMMAXP
      CALL BESJ(Z1, 0.D0, IORDM, A, 600)
      DO 550 M=1,IMMAX
      TRMM=A(2*M)*((-1)**(M-1))*TAB(M)
      ATERM(M)=TRMM
      IF (DABS(TRMM) .LT. 10.D-25) GO TO 560
  550 CONTINUE
      M=IMMAX
  560 DCOR=DSUM(ATERM,M)
      HCOR=2.D0/(PI*ALPHA*Y)*DCOR
      GO TO 50
   70 DCOR=0.0
      HCOR=0.0
      GO TO 50
   40 DCOR=TAB(1)/2.D0
      HCOR=TAB(1)/PI
   50 COR=DCOR
      IF (X .EQ. 0.0 .AND. Y .EQ. 0.0) GO TO 90
      AIRY=BESJ1(ARGU)/ARGU
      GO TO 80
   90 AIRY =.5
   80 VAR=AIRY**2+HCOR**2
      UU(N)=ALOG10(VAR)
      HU(N)=VAR
      XX(N)=Y
      WRITE (6,102)  Y, ARGU, COR, AIRY, HCOR, VAR
  102 FORMAT(6(2X,E13.6))
  100 CONTINUE
      ASM(1)=UU(1)
      I=2
      NI=2
      GO TO 620
  630 I=I+1
  620 IF (UU(I) .GT. UU(I-1) .AND. UU(I) .GT. UU(I+1)) GO TO 610
      I=I+1
      IF (I .LE. 200) GO TO 620
      GO TO 605
  610 ASM(NI)=UU(I)
      HXAS(NI)=XX(I)
      NI=NI+1
      IF (I .LT. 200) GO TO 630
  605 NIMAX=NI-1
      WRITE (6,104) (ASM(NI), NI=1,NIMAX)
  104 FORMAT ((8(2X,E13.6)))
      DO 300 NN=1,401
      YN=(NN-1)/5000.D0
      ARGU=ALPHA*DSQRT(X*X+YN*YN)
      IF (X .EQ. 0.0 .AND. YN .EQ. 0.0) GO TO 310
      HAIRY=BESJ1(ARGU)/ARGU
      GO TO 320
  310 HAIRY=.5
  320 HVAR=HAIRY**2
      UUU(NN)=ALOG10(HVAR)
      XXN(NN)=YN
  300 CONTINUE
      CALL LABEL(0., 0., XX(1), XX(201), 15., 10, 'Y', 1,0)
      CALL LOGAXS(0., 0., 10., 1,10, 0, 0, 'LOG(I/I0)', 9, 3)
      CALL XYPLOT(N, XX, UU, XX(1), XX(201),-10., 0., DD, 0)
      CALL XYPLOT(NN, XXN,   UUU, XXN(1), XXN(401),-10., 0., DD, 0)
       CALL XYPLT(NN, XXN,   UUU, XXN(1), XXN(401),-10., 0., DD,1,4)
      CALL LABEL(0., 0., XX(1), XX(201), 15., 10, 'Y', 1,0)
      CALL LOGAXS(0., 0., 10., 1,10, 0, 0, 'LOG(I/I0)', 9, 3)
      CALL INTPLT(NIMAX,200,1,2,HXAS,ASM,XX(1),XX(201),-10., 0.,1)
  600 CONTINUE
      STOP
      END
```

```
C
      SUBROUTINE BESJ(X,V,N,A,LDIMA)
      IMPLICIT REAL*8 (A-H,O-Z)
      REAL*8 X,A,V
C
C     ENTRY BESJ OF SUBROUTINE CALCULATES THE J-BESSEL
C     FUNCTION OF X FOR ORDERS V,1+V,2+V,...,N+V
C          R(K) IS STORED IN A(K+2) (TEMPORARILY)
C          J(V+K) IS STORED INTO A(K+1)
C          X>0
C          C<=V<1.DO
C          N>=0
C     DIMENSION OF ARRAY A MUST BE AT LEAST MAX(X,N)+16
C     LDIMA IS THE DIMENSION OF A SUPPLIED BY THE
C     USER.
C
C     ****************************************************************
C                E R R O R   R E T U R N S
C     FOR X, V, OR N OUT OF RANGE OR IF DIMENSION
C           OF ARRAY FURNISHED IS TOO SMALL.
C
C     ERROR RETURN INFORMATION INCLUDES
C          X, V, N, MU, AND LDIMA WHERE MU IS THE
C          SIZE-2 OF THE ARRAY A NEEDED (MU IS
C          MEANINGLESS IF ANOTHER PARAMETER IS
C          OUT OF RANGE, E.G.,X=-5.)
C
      DIMENSION A(1)
      DIMENSION GA(8),GB(7)
      DATA PI/3.14159265358979320D/
      DATA GA/5.5636964340807375D-1,-1.5497028047270494D1,
     X-3.6268398299612859D0,-1.1271046203309880D1,
     X8.7016417889220691D0,-2.6919115854447927D0,
     X1.3413198732411108D-1,-6.2606299618306871D0/
      DATA GB/1.1373935737962844D1,4.7985452207286753D1,
     X6.0876455111305554D0,1.0555979154972231D2,
     X-3.6235080158088192D0,6.4632210255382896D0,
     X4.8169233955859386D-1   /
      DATA PI2/1.5707963267948966D0/
      EQUIVALENCE (GU,GOLRGV,GOSMLV)
      DATA THRSHV/.789D-3/
      DATA EC       /Z4093C467E37D80C8/
      DATA S2/1.6449340668482264/,
     1      S2O2SQ/Z40AD28F5A5CE72C3/,
     2      S5/1.0369277551433700/,
     3      S33/.4005856343865314/,
     4      S4/1.0823232337111381900/
      DATA PI4D72/Z4115A57E8579CE55/
      DATA THSJ/.12D0/
      DIMENSION GOVSMC(4)
      ASSIGN 510 TO JY1
      ASSIGN 110 TO JY4
   80 CONTINUE
      IF(X.LE.0.OR.V.LT.0.OR.V.GE.1.0.OR.N.LT.0) GO TO 995
C
C     SET OVERFLOW INDICATOR OFF
C
C  87 CALL OVERFL(MU)
      VP1=V+1.0D0
      IX=IFIX(SNGL(X))
      LMB=IX+1
      MU=LMB
      GO TO JY4,(110,120)
  110 CONTINUE
      IF(LMB.LT.N) MU=N
  120 CONTINUE
C
C     LMB IS THE VALUE OF I FOR WHICH WE ARE ASSURED
C          THAT J(V+I,X) IS ON THE TAIL OF THE FUNCTION,
C          I.E.,LMB=IFIX(X+1)
C     LET LL=MAX(LMB,N)...
C          DEFINE MU TO BE THE POINT FROM WHICH WE
C          MUST RECUR TO ASSURE THAT J(V+LL,X)
C          IS ACCURATELY DETERMINED
C
C     FOR I=LL,LL+1,...,MU
C          WE STORE R(I)=J(I+1,X)/J(I,X) INTO A(I+2).
C          THIS AVOIDS THE PROBLEM OF OVERFLOW
C          INHERENT IN THE GROWTH OF THE J-FUNCTION
C          WHEN RECURRING BACKWARD ON ITS TAIL
C     NOTE THAT R(I-1)=X/(2*(V+I)-X*R(I))
      TWODX=2.0D0/X
      DR=TWODX*(V+DFLOAT(MU))
      FKP1=1.D0
      FK=0.D0
  180 CONTINUE
C
C     ITERATE UNTIL FKP1 IS GREATER THAN REGISTER ACCURACY
C
      MU=1+MU
      DR=DR+TWODX
      FKM1=FK
      FK=FKP1
      FKP1=DR*FK-FKM1
      IF ((FKP1+1.D0).NE.FKP1) GO TO 180
C
C     THE VALUE OF MU IS NOW WELL DETERMINED
C
      MU=MU+1
      M=MU
      IF((M+2).GT.LDIMA) GO TO 995
      A(M+2)=0.D0
  200 CONTINUE
      IF (M.EQ.LMB) GO TO 250
      DR=2*(M+V)
      M=M-1
      A(M+2)=X/(DR-X*A(M+3))
      GO TO 200
C
C      STORE JBAR(I) INTO A(I+1) FOR I=0,1,2,...,LMB+1
C
  250 CONTINUE
      A( M +1)=1.0D0/A( M +2)
      A( M +2)=1.0D0
C
C     RECUR BACKWARD TO GET JBAR'S
C
  280 CONTINUE
      DR=2*(M+V)/X
      A(M)=DR*A(M+1)-A(M+2)
      M=M-1
```

```
      IF (M.GT.0) GO TO 280
C
C     CLEAR R'S   UNDERFLOW MAY OCCUR HERE
C
      LMB=LMB+1
      DO 290 M=LMB,MU
      A(M+2)=A(M+2)*A(M+1)
C
C 287 CALL OVERFL(I)
C 288 IF (I.EQ.3) A(M+2)=0.D0
  290 CONTINUE
C
C     NORMALIZE SEQUENCE OF JBARS BY SUMMATION
C
      IF (V.EQ.0.D0) GO TO 305
      VX=V+2.0D0
      BGAM=GA(1)+GB(1)/(VX+
     X     GA(2)+GB(2)/(VX+
     X     GA(3)+GB(3)/(VX+
     X     GA(4)+GB(4)/(VX+
     X     GA(5)+GB(5)/(VX+
     X     GA(6)+GB(6)/(VX+
     X     GA(7)+GB(7)/(VX+GA(8)))))))
      BGAM=BGAM/VP1
      BGAMSQ=BGAM*BGAM
      Q2DXPV=(2.0D0/X)**V
  305 CONTINUE
C
C     SUMMATION
      ALPHA=A(1)
      PHI=2.0D0
      IF (V.EQ.0.0D0) GO TO 320
      D1=1.0D0
      D2=V
      EN2=V
      EN1=V+2.0D0
      PHI=Q2DXPV*BGAM
      ALPHA=PHI*ALPHA
  320 CONTINUE
      DO 350 M=1, MU,2
      IF (V.EQ.0.D0) GO TO 330
      PHI=PHI*(EN2/D2)*(EN1/D1)
      D2=D2+2.0D0
      EN1=EN1+2.0D0
      D1=1.0D0+D1
      EN2=EN2+1.0D0
  330 CONTINUE
      ALPHA=ALPHA+PHI*A(M+2)
  350 CONTINUE
C     A(1),A(2),....,A(LMB+2) CONTAIN JBAR(0),JBAR(1),....,JBAR(LMB+1)
C     A(LMB+3),....,A(MU+2) CONTAIN R(LMB+1),....,R(MU)
C
C     NORMALIZE JBARS
C
      M=MU+2
      DO 460 I=1,M
  457 A(I)=A(I)/ALPHA
  460 CONTINUE
  500 CONTINUE
      GO TO JY1,(510,1100)
  510 CONTINUE
      RETURN
  995 PRINT 1,X,V,N,MU,LDIMA
      RETURN
    1 FORMAT('0ERROR IN BESL X=',E14.5,'V=',E14.5,'N=',I5,'MU=',I5,
     X',LDIMA=',I5)
      RETURN
      ENTRY BESY(X,V,N,A,LDIMA)
      ASSIGN 1100 TO JY1
      ASSIGN 120 TO JY4
      GO TO 80
 1100 CONTINUE
      VX=V
      TJ=DABS(A(1))-THSJ
C
C      COMPUTE G0 AND G1
      IF (V.LT.THRSHV) GO TO 1200
      VX=V-1.0D0
      IF ((VX+THRSHV).GT.0.D0) GO TO 1190
      VX=V
      G0LRGV=DCOTAN(V*PI)-(Q2DXPV**2/PI)*BGAMSQ/V
      GO TO 1220
 1190 CONTINUE
C
C     FUNCTIONS OF V USED IN COMPUTING G0 AND G1
C     MUST BE TRANSFORMED TO FUNCTIONS OF VX=1-V
C
      Q2DXPV=Q2DXPV/TWODX
      BGAMSQ=BGAMSQ/V**2
 1200 CONTINUE
C
C     COMPUTE G0 USING EXPANSION
      Z=EC+DLOG(X/2.0D0)
      G0= Z/PI2
      IF (V.NE.0.0D0) GO TO 1210
      G1=2.0D0/PI2
      BGAMSC=1.0D0
      Q2DXPV=BGAMSQ
      GO TO 1230
 1210 CONTINUE
      ASQ=Z*Z
      ACUB=Z*ASQ
      AFORTH=Z*ACUB
      AFIFTH=AFORTH*Z/15.D0
      G1=-VX
      G0SMLV=
     X     (((((2.0D0*(AFIFTH+ACUB*S2/3.D0+ASQ*S33+Z*S2D2SQ)
     X      +Z*S4/2.D0+S2*S33+S5)*G1+
     X              2.0D0*Z*S33+S2D2SQ+ASQ*S2
     X     +AFORTH/3.0D0+PI4D72)*G1+
     X          S33+Z*S2+ACUB/1.5D0 )*G1+
     X            1.5D0*S2+ASQ  )*G1+Z)/PI2
 1220 CONTINUE
C     COMPUTE G1
      G1=(Q2DXPV**2/PI2)*BGAMSQ*(2.0D0+VX)/(1.0D0-VX)
 1230 CONTINUE
C     COMPUTE Y0 FROM SUM(J'S) FORM
C
      EN3=VX+1.0D0
      EN2=VX+EN3
      EN1=VX+4.0D0
      D1=2.0D0
      D2=D1-VX
      D3=D1+VX
```

```
      TJE =0
       IF(TJ.GE.0.D0.AND.VX.GE.0.D0) GO TO 1232
      TJE=1
C
C     Y(VX+1,X) MUST ALSO BE COMPUTED BY A SUM
C
      THVDX=3.0D0*VX/X
      PSIZ=-8GAMSQ*Q2DXPV**2/(PI2*X)
      PSI1=G0-.5D0*G1
 1232 CONTINUE
      IF (VX.LT.0.D0) GO TO 1233
      M=3
      YV=GC*A(1)
      IF (TJ.GE.0) GO TO 1238
      YVP1=PSIZ*A(1)+PSI1*A(2)
      GO TO 1238
 1233 CONTINUE
      Z=TWODX*V*A(1)-A(2)
      YV=G0*Z
      M=2
      YVP1=PSIZ*Z+PSI1*A(1)
 1238 CONTINUE
      DO 1250 I=M,MU,2
      YV=G1*A(I)+YV
      G=G1
      G1=-G1*(EN1/D1)*(EN2/D2)*(EN3/D3)
      EN1=EN1+2.0D0
      EN2=EN2+1.0D0
      EN3=EN3+1.0D0
      D1=D1+1.0D0
      D2=1.0D0+D2
      D3=D3+2.0D0
      IF (TJE) 1240,1250,1240
 1240 CONTINUE
      YVP1=YVP1+THVDX*G*A(I)+.5*(G-G1)*A(I+1)
 1250 CONTINUE
      IF (VX.GE.0.D0) GO TO 1260
      Z=YVP1
      YVP1=V*Z*TWODX-YV
      YV=Z
      GO TO 1400
 1260 CONTINUE
      IF (TJ.LT.0.D0) GO TO 1400
 1270 CONTINUE
C
C     NOW COMPUTE Y(V+1)
C     WRONSKIAN PROVIDED NOT NEAR A ZERO OF J
C
      YVP1=(YV*A(2)-1.0D0/(X*PI2))/A(1)
 1400 CONTINUE
C
C     RECUR FORWARD TO GET Y'S (WISE)
C
      A(1)=YV
      A(2)=YVP1
      G=V*TWODX
      DO 1500 I=2,N
C
      G=G+TWODX
C     OVERFLOW MAY OCCUR HERE
      A(I+1)=G*A(I)-A(I-1)
C1487 CALL OVERFL(LMB)
C1488 IF (LMB.EQ.1) A(I+1)=1.D78
 1500 CONTINUE
      RETURN
      END
C
C
C
C
      DOUBLE PRECISION FUNCTION DSUM(X,N)
      EQUIVALENCE (IEQ,W)
      REAL*8 R(43),S8,X(1)
      DO 10 I=1,43
   10 R(I)=0.0D0
      DO 20 I=1,N
      W=DABS(X(I))
      IEXP=IEQ/50331648+1
   20 R(IEXP)=R(IEXP)+X(I)
      S8=0.0D0
      DO 30 I=1,43
   30 S8=S8+R(44-I)
      DSUM=S8
      RETURN
      END
```

APPENDIX B

```
      COMMON/XYZLEN/XLONG,YLONG,ZLONG,XOFF,YOFF,SIDEZ
      LOGICAL NOAXIS,NOLABL
      DIMENSION UU(81,161)
      DIMENSION DD(6)
    1 FORMAT (6A4)
      READ (5,1)DD
      READ (10) UU
      CALL MAXMIN(UU, 13041, AMAX, AMIN)
      NOAXIS=.TRUE.
      NOLABL=.TRUE.
      XLONG=12.
      YLONG=12.
      SIDEZ=5.
      ZLONG=5.
      XOFF=4.
      YOFF=6.5
      CALL CPLT3D(UU, AMAX, AMIN, 81, 161, 1, 1, 81, 1, 2, 161, 3, 45.,C
     * 30., DD, NOAXIS, NOLABL)
      WRITE (6,100) AMAX, AMIN
  100 FORMAT (2X, 'AMAX=', E14.7,5X,'AMIN=', E14.7)
      STOP
      END
C
C
      SUBROUTINE CPLT3D(A,AMAX,AMIN,IDIM,JDIM,ISTART,IDELTA,ISTOP,JSTART
     1,JDELTA,JSTOP,MODE,THEDEG,PHIDEG,DD,NOAXIS,NOLABL)
      DIMENSION A(IDIM,JDIM),BCDW(22),DD(1)
      COMMON/XYZLEN/XLONG,YLONG,ZLONG,XOFF,YOFF,SIDEZ
      INTEGER RTIME
      LOGICAL OPAQUE,BLOCK,ARRAY,NOAXIS,NOLABL
      BMAX=AMAX
      ARRAY=IDIM.NE.1
      BLOCK=MODE.EQ.2.OR.MODE.EQ.4
      OPAQUE=MODE.EQ.3.OR.MODE.EQ.4
      THETA=(3.1416/180.)*THEDEG
      PHI=(3.1416/180.)*PHIDEG
      SIDEX=ISTOP-ISTART
      SIDEY=JSTOP-JSTART
      IF(SIDEX.GE.SIDEY) GO TO 5
      SIDEX=XLONG*SIDEX/SIDEY
      SIDEY=YLONG
      GO TO 6
    5 SIDEY=YLONG*SIDEY/SIDEX
      SIDEX=XLONG
    6 XH=SIDEX*SIN(PHI)
      YH=SIDEY*COS(PHI)
      XV=SIDEX*COS(PHI)*COS(THETA)
      YV=SIDEY*SIN(PHI)*COS(THETA)
      TX=(XH-YH)/2.+3.
      TY=(XV+YV)/2.+4.5
      JMAX=JSTOP
      JMIN=JSTART
      IF(NOLABL) GO TO 34
C     WRITE DESCRIPTIVE INFORMATION USING STANDARD CALCOMP ROUTINES
      CALL SYSSYM(11.,9.5,0.2,DD,24,0)
      CALL SYSSYM(C,1.8,0.15,'PLOT OF LOGI VRS X AND Y', 24,0)
      CALL SYSSYM(0.,1.4,.2,13HVIEWING ANGLE ,13,0.)
      CALL SYSSYM(0,1.1,0.2,7HTHETA =,7,0)
      CALL CUTCOR (BCDW,NWRD)
      WRITE (6,22) THEDEG
   22 FORMAT(F6.2)
      CALL SYSSYM(1.2,1.1,0.2,BCDW,6,0)
      CALL OUTCOR
      CALL SYSSYM(0,0.8,0.2,5HPHI =,5,0)
      CALL CUTCOR (BCDW,NWRD)
      WRITE (6,24) PHIDEG
   24 FORMAT(F6.2)
      CALL SYSSYM(1.2,0.8,0.2,BCDW,6,0)
      CALL OUTCOR
      CALL SYSSYM(0,0.4,0.1,6HMODE =,6,0)
      CALL CUTCOR (BCDW,NWRD)
      WRITE (6,26) MODE
   26 FORMAT(I4)
      CALL SYSSYM(0.6,0.4,0.1,BCDW,4,0)
      CALL CUTCOR
   34 CONTINUE
      TM=ZLONG*SIN(THETA)
C     MOVE TO CENTER OF PAPER
      CALL SYSPLT(XOFF,YOFF,3)
      IF(NOAXIS) GO TO 35
C     DRAW X Y Z AXIS
      CALL SYSPLT(XOFF,TM+YOFF,2)
      CALL SYSPLT(YH+XOFF,-YV+YOFF,3)
      CALL SYSPLT(XOFF,YOFF,2)
      CALL SYSPLT(-XH+XOFF,-XV+YOFF,2)
   35 CONTINUE
      NOW=RTIME(KKK)
C     CALL SUBROUTINE PTT3D WHICH CALCULATES AND WRITES
C     THE PERSPECTIVE TRANSFORMATION
      CALL CPTT3D (A,BMAX,AMIN,IDIM,JDIM,ISTART,IDELTA,ISTOP,JSTART,
     *JDELTA,JSTOP,THETA,PHI,OPAQUE,BLOCK,ARRAY,SIDEX,SIDEY,SIDEZ)
      LATER=RTIME(KKK)
      TM=FLOAT(NOW-LATER)/3600.
C     ADVANCE PAPER FOR NEXT PICTURE
      CALL SYSEND(1,1)
      RETURN
      END
C
```

```
C
      SUBROUTINE CPTT3D (A,AMAX,DISC,MAXDMX,MAXDMY,STARTX,SKIPX,DIMX,
     *STARTY,SKIPY,DIMY,THETA,PHI,OPAQUE,BLOCK,ARRAY,SCALEX,SCALEY,
     *SCALEZ)
      CONTINUE
      DIMENSION A(MAXDMX,MAXDMY),SV(260),SH(260),DDD(3)
      INTEGER STARTX,SKIPX,DIMX,STARTY,SKIPY,DIMY
      LOGICAL SEE,SAW,OPAQUE,BLOCK,ARRAY,SCANX
      DATA DDD/3*0./
      EQUIVALENCE (M1,J1)
      EQUIVALENCE (M12,J12)
      EQUIVALENCE (J13,M13)
      EQUIVALENCE ( M2,J2)
      EQUIVALENCE (MC,JC)
      EQUIVALENCE (MP,JP)
      JCMIN=STARTY
      JCMAX=DIMY
      MCMIN=STARTX
      MCMAX=DIMX
      TDIMX=DIMX-STARTX
      TDIMY=DIMY-STARTY
      TSTRTX=STARTX-1
      TSTRTY=STARTY-1
      XH=SCALEX*SIN(PHI)
      YH=SCALEY*COS(PHI)
      XV=SCALEX*COS(PHI)*COS(THETA)
      YV=SCALEY*SIN(PHI)*COS(THETA)
      DH=TDIMY/YH
      DV=AMAX/(SCALEZ*SIN(THETA))
      IF(ABS(YH).LT..01) DH=500.*AMAX
      IF(THETA.LT..01) DV=500.*AMAX
      DELY=ABS(XH*TDIMY/YH/TDIMX)
      DELX=ABS(YH*TDIMX/XH/TDIMY)
      SCANX=TDIMX/ABS(XV).LT.TDIMY/ABS(YV)
      STO3=DV*XV/TDIMX
      STO4=DV*YV/TDIMY
      STO7=DH*XH/TDIMX
      STO9=DH*YH/TDIMY
      DO 500 M=STARTX,DIMX,SKIPX
      TM=M-STARTX
      STO2=TM+TSTRTX+1.5
      STO5=TM/TDIMX*XH*DH
       SEE = .TRUE.
      SAW=.FALSE.
      J1=0
C     DO 700 MC=STARTX,DIMX
      DO 200 JC=JCMIN,JCMAX
      J=JC
      POINT=0.
      POINT=A(M,J)
      TJ=J-STARTY
      STO1=TJ+TSTRTY+1.5
      STO8=DV*(XV*TM/TDIMX+YV*TJ/TDIMY)
      IF(.NOT.OPAQUE) GO TO 150
      IF(.NOT.SCANX) GO TO 70
      DM=-1.
      N1=STARTX
      N2=M
      IF(-YH)50,50,60
   50 N1=M
      N2=DIMX
      DM=1.
   60 DJ=DELY
      IF(YV.LT.0.) DJ=-DJ
      GO TO 100
   70 DJ=-1.
      N1=STARTY
      N2=J
      IF(-XH)80,80,90
   80 N1=J
      N2=DIMY
      DJ=1.
   90 DM=DELX
      IF(XV.LT.0.) DM=-DM
  100 TI=0.
      DO 125 I=N1,N2
      TI=TI+1.
      JIP=DJ*TI+STO1
      MIP=DM*TI+STO2
      IF(JIP.GT.DIMY.OR.JIP.LT.STARTY.OR.MIP.GT.DIMX.OR.MIP.LT.STARTX)
     *GO TO 125
      POINTP=0.
      POINTP=A(MIP,JIP)
      SEE=POINTP-ABS(DM*TI*STO3)-ABS(DJ*TI*STO4).LE.POINT
      IF(.NOT.SEE) GO TO 130
  125 CONTINUE
  130 IF(SEE) GO TO 150
      IF(.NOT.SAW) GO TO 200
  135 J=J-1
  140 IF(J1.LT.2) J1=0
      IF(J1.EQ.0) GO TO 200
      J2=J-J1+1
      IF(BLOCK) J2=J-J1/2+1
      L=1
      DO 141 JP=J2,J
      TJP=JP-STARTY
      SH(L)=TJP-STO5
      IF(.NOT.BLOCK) GO TO 141
      L=L+1
      SH(L)=SH(L-1)+1.
  141 L=L+1
      CALL CLNPLT(J1,SH,SV,DH,DV)
      IF(.NOT.BLOCK) GO TO 145
      DO 142 I=1,J1
      SV(I)=SV(I)-STO3
  142 SH(I)=SH(I)-STO7
      CALL CLNPLT(J1,SH,SV,DH,DV)
  145 J1=0
      IF(JC.EQ.DIMY) GO TO 500
      SAW=.FALSE.
      GO TO 200
  150 IF(POINT.LT.DISC.OR.POINT.GT.AMAX) GO TO 135
      J1=J1+1
      SV(J1)=POINT-STO8
      SAW=SEE
      IF(.NOT.BLOCK) GO TO 175
      J1=J1+1
      SV(J1)=SV(J1-1)-STO4
  175 IF(JC.EQ.DIMY) GO TO 140
  200 CONTINUE
  500 CONTINUE
      DO 1000 J=STARTY,DIMY,SKIPY
      TJ=J-STARTY
      STO1=TJ+TSTRTY+1.5
```

```
       SEE = .TRUE.
       SAW=.FALSE.
       M1=0
C      DO 200 JC=STARTY,DIMY
       DO 700 MC=MCMIN,MCMAX
       M=MC
       POINT=0.
       POINT=A(M,J)
       TM=M-STARTX
       STO2=TM+TSTRTX+1.5
       STO8=DV*(XV*TM/TDIMX+YV*TJ/TDIMY)
       IF(.NOT.OPAQUE) GO TO 650
       IF(.NOT.SCANX) GO TO 570
       DM=-1.
       N1=STARTX
       N2=M
       IF(-YH)550,550,560
   550 N1=M
       N2=DIMX
       DM=1.
   560 DJ=DELY
       IF(YV.LT.0.) DJ=-DJ
       GO TO 600
   570 DJ=-1.
       N1=STARTY
       N2=J
       IF(-XH)580,580,590
   580 N1=J
       N2=DIMY
       DJ=1.
   590 DM=DELX
       IF(XV.LT.0.) DM=-DM
   600 TI=0.
       DO 625 I=N1,N2
       TI=TI+1.
       JIP=DJ*TI+STO1
       MIP=DM*TI+STO2
       IF(JIP.GT.DIMY.OR.JIP.LT.STARTY.OR.MIP.GT.DIMX.OR.MIP.LT.STARTX)
      1GO TO 625
       POINTP=0.
       POINTP=A(MIP,JIP)
       SEE=POINTP-ABS(DM*TI*STO3)-ABS(DJ*TI*STO4).LE.POINT
       IF(.NOT.SEE) GO TO 630
   625 CONTINUE
   630 IF(SEE) GO TO 650
       IF(.NOT.SAW) GO TO 700
   635 M=M-1
   640 IF(M1.LT.2) M1=0
       IF(M1.EQ.0) GO TO 700
       M2=M-M1+1
       IF(BLOCK) M2=M-M1/2+1
       L=1
       DO 641 MP=M2,M
       TMP=MP-STARTX
       SH(L)=TJ-TMP*STO7
       IF(.NOT.BLOCK) GO TO 641
       L=L+1
       SH(L)=SH(L-1)-STO7
   641 L=L+1
       CALL CLNPLT(M1,SH,SV,DH,DV)
       IF (.NOT.BLOCK) GO TO 645
       DO 642 I=1,M1
       SV(I)=SV(I)-STO4
   642 SH(I)=SH(I)+STO9
       CALL CLNPLT(M1,SH,SV,DH,DV)
   645 M1=0
       IF(MC.EQ.DIMX) GO TO 1000
       SAW=.FALSE.
       GO TO 700
   650 IF(POINT.LT.DISC.OR.POINT.GT.AMAX) GO TO 635
       M1=M1+1
       SV(M1)=POINT-STO8
       SAW=SEE
       IF(.NOT.BLOCK) GO TO 675
       M1=M1+1
       SV(M1)=SV(M1-1)-STO3
   675 IF(MC.EQ.DIMX) GO TO 640
   700 CONTINUE
  1000 CONTINUE
       RETURN
       END
C
C
       SUBROUTINE CLNPLT(N,X,Y,DX,DY)
       DIMENSION X(1),Y(1)
       DATA IFG/1/
       COMMON/XYZLEN/XLONG,YLONG,ZLONG,XOFF,YOFF,SIDEZ
       IPEN = 3
       IF(IFG .LT. 0) GO TO 22
       DO 20 I = 1,N
       CALL SYSPLT(X(I)/DX+XOFF,Y(I)/DY+YOFF,IPEN)
    20 IPEN = 2
       GO TO 32
    22 NP1 = N + 1
       DO 30 I = 1,N
       K = NP1 - I
       CALL SYSPLT(X(K)/DX+XOFF,Y(K)/DY+YOFF,IPEN)
    30 IPEN = 2
    32 IFG = -IFG
       RETURN
       END
C
C
//SYSPLTON    DD SYSOUT=N
//DATA   DD    *
DIFRACTION OF SEMICIRCLE
C
C
```

APPENDIX C

```
C
C
      COMPLEX FUNCTION CW(ZP)
      REAL LAMBDA
      COMPLEX CW,ZP,AI,Z,ZA,CERF
      LOGICAL B
      DATA AI/(0.0,1.0)/
      ZP=-ZP*(0.0,1.0)
      Z=AI*ZP
      X=REAL(Z)
      Y=AIMAG(Z)
      IQ=1
      IF (X .LT. 0.0) IQ=2
      IF (Y .LT. 0.0) IQ=3
      IF (Y .LT. 0.0 .AND. X  .GE. 0.0) IQ=4
      X=ABS(X)
      Y=ABS(Y)
      ZA=CMPLX(X,Y)
      IF (Y .LT. 4.29 .AND.X .LT. 5.33) GO TO 10
      GO TO 15
   10 S=(1.0-Y/4.29)* SQRT(1.0-X*X/28.41)
      H = 1.6*S
      H2=2.0*H
      K= 6+ 23*S
      LAMBDA=H2**K
      NU=9+ 21*S
      GO TO 20
   15 H=0.0
      K=0
      NU=8
   20 CONTINUE
      B=.FALSE.
      IF(H.EQ. 0.0 .OR. LAMBDA .EQ. 0.0) B=.TRUE.
      R1=0.0
      R2=0.0
      S1=0.0
      S2=0.0
      N=NU+1
   30 N=N-1
      IF(N .LT. 0) GO TO 50
      NP1=N+1
      T1=Y+H+NP1*R1
      T2= X-NP1*R2
      C= .5/(T1*T1+T2*T2)
      R1=C*T1
      R2=C*T2
      IF(H.LE.0.0 .OR.  N .GT. K) GO TO 30
      T1=LAMBDA+S1
      S1=R1* T1-R2*S2
      S2=R2*T1+R1*S2
      LAMBDA=LAMBDA/H2
      GO TO 30
   50 CONTINUE
      IF (Y .NE. 0.0) GO TO 60
      RE=EXP(-X*X)/1.1283791671
      GO TO 70
   60 RE=S1
      IF (B) RE=R1
   70 AIM=S2
      IF (B) AIM=R2
      CERF=1.12837916709551* CMPLX(RE,AIM)
      IF (IQ .EQ. 1) GO TO 90
      IF (IQ .NE. 2) GO TO 80
      CERF=CONJG(CERF)
      GO TO 90
   80 CERF=2.0*CEXP(-ZA*ZA)-CERF
      IF (IQ .EQ. 3) GO TO 90
      CERF=CONJG(CERF)
   90 CW=CERF
      RETURN
      END
C
       COMPLEX ZE, ANS, CW, ZETA
       REAL LAMBDA, K, IZETA
       DIMENSION ANN(302), XX(302), DD(3)
       DIMENSION X1(14), AN(14,201)
       DATA X1/0.,-1.35,-1.,-.75,-.5,-.25,.25,.5,.75,1./
       DATA DD/0., 0., 1./
       DATA LAMBDA/.6328E-4/
       DATA PI/3.1416/
       Z=20.
       K=2.*PI/LAMBDA
       W0=.5
       BETA=PI*W0/(LAMBDA*Z)
       DO 201 LL=1,10
       X0=X1(LL)
       WRITE (6,200) W0, BETA,X0
 200   FORMAT (1X,'W0=',E13.6,2X,'BETA=', E13.6,'X0=',E13.6)
       DO 100 I=1,201
       ALPHA=(I-1)/20.
       X=ALPHA/2./BETA
       ZETA=X*BETA+(0.0,1.0)*X0/W0
       RZETA=REAL(ZETA)
       IZETA=AIMAG(ZETA)
       ZE=ZETA
       IF (RZETA .GE. 3.9 .AND. RZETA .LE. 6.0) GO TO 12
       IF (IZETA .GE. 3.0 .AND. IZETA .LE. 6.0) GO TO 12
       IF (RZETA .GE. 6.0 .OR. IZETA .GE. 6.0) GO TO 10
       ANS=CW(ZE)
       GO TO 11
 12   ANS=(0.0,1.0)*ZETA*(0.4613135/(ZETA*ZETA-0.1901635)
     * +0.09999216/(ZETA*ZETA-1.7844927)+0.002883894/(ZETA*ZETA-
     * 5.5253437))
       GO TO 11
 10    ANS=(0.0,1.0)*ZETA*(0.5124242/(ZETA*ZETA-0.2752551)+
     * 0.05176536/(ZETA*ZETA-2.724745))
 11    U=CABS(ANS)
       AN(LL,I)=(U*EXP(-(X0/W0)**2))**2
       AN1=ALOG10(AN(LL,I)/AN(1,I))
C      WRITE (6,250) X, ZETA, ANS, U, AN1
 250   FORMAT (1X,'X=',E13.6,2X,'ZETA=',2E13.6,2X,'ANS=',2E13.6,
     * 2X,'U=',E13.6,2X,'AN1=',E13.6)
       ANN(I)=AN1
       XX(I)=ALPHA
 100   CONTINUE
       IF (LL .GT. 1) GO TO 112
       CALL LABEL(0., 0., XX(1), XX(201), 15., 15, '2*PI*W0/(LAMDA*S)',
     * 17, 0)
       CALL LOGAXS(0., 0., 10., 1, 8, 1, 0, 'LOG(I/I0)', 9, 3)
 112  CALL XYPLOT(201, XX, ANN, XX(1), XX(201), -7., 1., DD, 0)
       CALL XYPLT(201, XX, ANN, XX(1), XX(201), -7., 1., DD, 0, LL)
 201   CONTINUE
       STOP
       END
```

APPENDIX D

```
      DIMENSION W(100,100)
      EXTERNAL CW
      COMPLEX CW, ZETA
      DO 1 J=1,100
      Y=J/50.+4.
      DO 2 I=1,100
      X=I/50.+4.
      ZETA=X-(0.0,1.0)*Y
  2   W(I,J)=CABS(CW(ZETA))
  1   CONTINUE
      WRITE (6,100) ((W(I,J),I=1,100),J=1,100)
 100  FORMAT(10(1X,E11.4))
      STOP
      END
C
C
      COMPLEX ZS, ZE, FUN, ZI(5)
      EXTERNAL FUN
      DATA ZI/(4.48,-4.12),(4.82,-4.48),(5.14,-4.82),(5.44,-5.12),
     * (5.72,-5.42)/
      M1=10
      DO 2 M=6,M1
      ZS=ZI(M-5)
  1   CALL CRF(ZS, 1.E-5, 1.E-6, 1.E-5, FUN, DS, ZE, HE, DE, N)
      WRITE (6,100) DS, ZE, HE, DE, N, M
 100  FORMAT(2X,'DS=',E13.6,2X,'ZE=',2(1X,E13.6),2X,'HE=',E13.6,2X,
     * 'DE=',E13.6,2X,'N=',I5,2X,'M=',I2)
  2   CONTINUE
      STOP
      END
      COMPLEX FUNCTION FUN(ZP)
      REAL IZETA
      COMPLEX ZETA, ANS, CW, FUN, ZP
      ZETA=ZP
      ANS=CW(ZETA)
 11   FUN=ANS*CABS(ZETA)
      RETURN
      END
C
C
      SUBROUTINE CRF(ZS,HS,HM,DM,FUNC,DS,ZE,HE,DE,N)
C
C     THE SUBROUTINE DETERMINES A ROOT OF A TRANSCEN-
C     DENTAL COMPLEX EQUATION F(Z)=0 BY STEP-WISE ITE-
C     RATION.(THE DOWN HILL METHOD)
C
C     INPUT-PARAMETERS.
C
C     ZS = START VALUE OF Z.(COMPLEX)
C     HS = LENGTH OF STEP AT START.
C     HM = MINIMUM LENGTH OF STEP.
C     DM = MINIMUM DEVIATION.
C
C     SUBPROGRAM.
C
C     FUNC(Z), A COMPLEX FUNCTION SUBPROGRAM FOR THE
C     CALCULATION OF THE VALUE OF F(Z) FOR A COMPLEX
C     ARGUMENT Z.
C
C     OUTPUT-PARAMETERS.
C
C     DS = CABS(FUNC(ZS))=DEVIATION AT START.
C     ZE = END VALUE OF Z.(COMPLEX)
C     HE = LENGTH OF STEP AT END.

C     DE = CABS(FUNC(ZE))=DEVIATION AT END.
C     N = NUMBER OF ITERATIONS.
C
C     RESTRICTIONS.
C
C     THE FUNCTION W=F(Z) MUST BE ANALYTICAL IN THE
C     REGION WHERE ROOTS ARE SOUGHT.
C
      REAL W(3)
      COMPLEX ZO,ZS,ZE,ZD,ZZ,Z(3),CW,A,V,U(7),FUNC
      DATA U/(1.0,0.0),(0.8660254,0.5),(0.0,1.0),(0.9659258,0.2588190),
     1(0.7071068,0.7071068),(0.2588190,0.9659258),(-0.2588190,.9659258)/
C     U(1)=(1.,0.)
C     U(2)=(0.8660254,0.5000000)
C     U(3)=(0.0000000,1.0000000)
C     U(4)=(0.9659258,0.2588190)
C     U(5)=(0.7071068,0.7071068)
C     U(6)=(0.2588190,0.9659258)
C     U(7)=(-0.2588190,0.9659258)
      H=HS
      ZO=ZS
      N=0
C
C     CALCULATION OF DS.
C
      CW=FUNC(ZO)
      WO=ABS(REAL(CW))+ABS(AIMAG(CW))
      DS=WO
      IF(WO-DM) 18,18,1
    1 K=1
      I=0
    2 V=(-1.,0.)
C
C     EQUILATERAL TRIANGULAR WALK PATTERN.
C
    3 A=(-0.5,0.866)
C
C     CALCULATION OF DEVIATIONS W IN THE NEW TEST POINTS.
C
    4 Z(1)=ZO+H*V*A
      CW=FUNC(Z(1))
      W(1)=ABS(REAL(CW))+ABS(AIMAG(CW))
      Z(2)=ZO+H*V
      CW=FUNC(Z(2))
      W(2)=ABS(REAL(CW))+ABS(AIMAG(CW))
      Z(3)=ZO+H*CONJG(A)*V
      CW=FUNC(Z(3))
      W(3)=ABS(REAL(CW))+ABS(AIMAG(CW))
      N=N+1
```

```
C
C     DETERMINATION OF W(NR), THE SMALLEST OF W(I).
C
      IF(W(1)-W(3)) 5,5,6
    5 IF(W(1)-W(2)) 7,8,8
    6 IF(W(2)-W(3)) 8,8,9
    7 NR=1
      GOTO 10
    8 NR=2
      GOTO 10
    9 NR=3
   10 IF(WO-W(NR)) 11,12,12
   11 GOTO (13,14,15),K
   12 K=1
      I=0
C
C     FORWARD DIRECTED WALK PATTERN.
C
      A=(0.707,0.707)
      V=(Z(NR)-ZO)/H
      WO=W(NR)
      ZO=Z(NR)
      IF(WO-DM) 18,18,4
   13 K=2
C     REDUCTION OF STEP LENGTH.
C
      IF(H.LT.HM) GOTO 18
      H=H*0.25
      GOTO 3
   14 K=3
C
C     RESTORATION OF STEP LENGTH.
C
      H=H*4.
      GOTO 2
   15 I=I+1
C
C     ROTATION OF WALK PATTERN.
C
      IF(I-7) 16,16,17
   16 V=U(I)
      GOTO 3
C
C     REDUCTION OF STEP LENGTH.
C
   17 IF(H.LT.HM) GOTO 18
      H=H*0.25
      I=0
      GOTO 2
   18 ZE=ZO
      HE=H
      DE=WO
      RETURN
      END
```

APPENDIX E

```
C
C
      IMPLICIT REAL*8(A-G,O-Z)
       DIMENSION Y(5000)
       N=8
       P=6.D0
       N2=N+2
      DO 10 I=2,11
       X=I-1
      CALL RINERF(X,N,P,Y)
       WRITE (6,100) (Y(J),J=1,N2)
  100 FORMAT(10(1X,E11.4))
   10 CONTINUE
      STOP
      END
C
C
       SUBROUTINE RINERF(X,N,P,Y)
       IMPLICIT REAL*8(A-G,O-Z)
       DIMENSION Y(5000), W(5000)
       DATA PI/3.14159265358979D0/
       A=1.D-10
       XMN=2.D0*DSQRT(2.D0*N)*X+P*DLOG(10.D0)+DLOG(2.D0)
       XMD=2.D0*DSQRT(2.D0)*X
       M=(XMN*XMN/(XMD*XMD))
       M2=M+2
       M3=M+3
       M4=M3+1
       M5=M4+1
       N2=N+2
       W(M4)=0.D0
       GO TO 2
  1    A=A/100.D0
  2    W(M3)=A
       DO 10 J=1,M2
       W(M3-J)=2.D0*(M3-J)*W(M5-J)+2.D0*X*W(M4-J)
       IF (W(M3-J) .GT. 1.D60) GO TO 1
  10   CONTINUE
       WT1=2.D0*DEXP(-X*X)/DSQRT(PI)
       C=WT1/W(1)
       DO 20 K=1,N2
  20   Y(K)=C*W(K)
       RETURN
       END
C
C
```

APPENDIX F

```
C
C
      IMPLICIT REAL*8(A-G,O-Z)
      COMPLEX*16 TERMM1,TERMM2
      COMPLEX ANS1,PART1,ANS2,PART2,CSUM,PART1N,PART2N
      REAL*4 DD
      DIMENSION TERMM1(100),TERMM2(35)
C     DIMENSION OF G DEPENDS ON M
C     DIMENSION OF BJ DEPENDS ON MAX(V+IORDM+16)
      DIMENSION G(35),BJ(100)
      DIMENSION DD(3)
      DIMENSION HI(101,101)
      DATA PI/3.14159265358979300/
      HPI=PI
C     PHI=90.D0
C     PHI=0.D0
      PHI=45.D0
      FI=PHI*PI/180.D0
C     M IS DETERMINED FROM MAX(U) BY ADDING 25
C     V IS THE NORMALIZED RO COORDINATE
      M=35
      DO 200 J=1,101
      V=(J-1)/5.D0
      HV=V
      IF (V .EQ. 0.D0) GO TO 110
      CALL DGSUM(V,FI,M,G)
      WRITE (6,210) (G(IM),IM=1,M)
      IMMAX=.8D0*V+10.5D0
      IORDM=IMMAX+1
      CALL BESJ(V,0.D0,IORDM,BJ,100)
      HBJ=BJ(1)
C     U IS THE NORMALIZED Z COORDINATE
  110 DO 100 I=51,101
      U=(I-51)/5.D0
      HU=U
      IF (U .EQ. 0.D0 .AND. V .EQ. 0.D0) GO TO 130
      IF (V .EQ. 0.D0) GO TO 120
      IF (U .EQ. 0.D0) GO TO 140
      INFM2=DABS(U)+25.D0
      TERMM2(1)=G(1)
      FAC=1.D0
      DO 10 MI=2,INFM2
      TERMM2(MI)=((0.0,1.0)*U/2.D0)**(MI-1)*G(MI)/FAC
      FAC=FAC*MI
      IF (CDABS(TERMM2(MI)) .LT. 1.D-25) GO TO 20
   10 CONTINUE
      MI=INFM2
   20 ANS2=CSUM(TERMM2,MI)
      PART2=ANS2*HV/HPI*2.0
      RATIO=U/V
      IF (DABS(RATIO) .GT. 1.D0) RATIO=V/U
      DO 30 MF=1,IMMAX
      TERMM1(MF)=((0.0,-1.0)*RATIO)**MF*BJ(MF+1)
      IF (CDABS(TERMM1(MF)) .LT. 1.D-25) GO TO 40
   30 CONTINUE
      MF=IMMAX
   40 ANS1=CSUM(TERMM1,MF)
      IF (DABS(U/V) .LE. 1.D0) GO TO 50
      ANS1=CEXP((HV*HV+HU*HU)/(2.*HU)*(0.0,-1.0))-HBJ-ANS1
   50 PART1=CEXP((0.0,1.0)*HU/2.)/HU*ANS1
      GO TO 150
  130 PART1=0.5
      PART2=0.0
      GO TO 150
  120 PART2=0.0
      PART1=(1.-CEXP((0.0,1.0)*HU/2.))/HU
      GO TO 150
  140 HBJ2=BJ(2)
      PART1=HBJ2/HV
      PART2=2.D0*(0.0,1.0)*V/PI*G(1)
  150 HS1=CABS(PART1)
      HS2=CABS(PART2)
      HSS=(CABS(PART1+PART2))**2
      PART1N=-CONJG(PART1)
      PART2N=CONJG(PART2)
      HSSN=(CABS(PART1N+PART2N))**2
      WRITE (6,220) HV,HU,HS1,HS2,HSS,HSSN
  210 FORMAT ((8(2X,E13.6)))
  220 FORMAT(6(3X,E13.6))
      HI(J,I)=HSS
      HI(J,102-I)=HSSN
  100 CONTINUE
  200 CONTINUE
      WRITE (10) HI
      WRITE (6,230) HI
  230 FORMAT ((10(1X,E11.4)))
      STOP
       END

C
      COMPLEX FUNCTION CSUM(X,N)
      EQUIVALENCE (IEQ,W)
      REAL*8 R(43),S8,DBLE,X(1)
      DO 40 K=1,2
      DO 10 I=1,43
   10 R(I)=0.0D0
      DO 20 I=K,N,2
      W=CABS(X(I))
      IEXP=IEQ/50331648+1
   20 R(IEXP)=R(IEXP)+X(I)
      S8=0.0D0
      DO 30 I=1,43
   30 S8=S8+R(44-I)
      GO TO (11,12),K
   11 REA=S8
      GO TO 40
   12 AIM=S8
   40 CONTINUE
      CSUM=CMPLX(REA,AIM)
      RETURN
       END
```

```
C
C
      SUBROUTINE DGSUM(V,F,L,G)
      IMPLICIT REAL*8(A-H,O-Z)
      DIMENSION G(1)
      IF (F .EQ. 0.D0) GO TO 6
      VSQ4=V*V*0.25D0
      SINPO=DSIN(F)
      DO 5 M=1,L
      TWOM3=2*M+1
      K=0
      TWOKP1=1.D0
      SINP=SINPO
      C2=TWOM3
      AOK=SINP/C2
      SUMPOS=AOK
      SUMNEG=0
      TWOK=0.0
      GO TO 30
   10 K=K+1
      TWOK=TWOK+2.D0
      TWOKM1=TWOKP1
      SINM=SINP
      C1=C2
      TWOKP1=TWOK+1.D0
      SINP=DSIN(TWOKP1*F)
      C2=C2+2.D00
      FAC=(TWOKM1+1.D00)*TWOKP1
      EPSK=VSQ4/FAC
      AOK= AOK*EPSK*SINP/SINM*TWOKM1/TWOKP1*C1/C2
      KO2=K/2
      KGO=1+K-KO2*2
      GO TO (11,12),KGO
   11 SUMPOS=SUMPOS+AOK
      GO TO 13
   12 SUMNEG=SUMNEG+AOK
   13 DCSUM=SUMPOS-SUMNEG
      IF(DABS(AOK/DCSUM).LT.1.OD-16) GO TO 5
   30 N=0
      ANK=AOK
      D2=C2
   40 N=N+1
      EPSN=VSQ4/((TWOKP1+N)*N)
      D1=D2
      D2=D1+2.D00
      ANK= ANK*EPSN*D1/D2
      KNO2=(K+N)/2
      KGO=1+K+N-KNO2*2
      GO TO (21,22),KGO
   21 SUMPOS=SUMPOS+ANK
      GO TO 23
   22 SUMNEG=SUMNEG+ANK
   23 DCSUM=SUMPOS-SUMNEG
      IF(DABS(ANK/DCSUM).LT.1.OD-16) GO TO 10
      GO TO 40
    5 G(M)=DCSUM
      RETURN
    6 DO 7 MI=1,L
    7 G(MI)=0.D0
      RETURN
      END
C
```

```
C
      SUBROUTINE DGSUM(V,F,L,G)
      IMPLICIT REAL*8(A-H,O-Z)
      DIMENSION G(1),TERMK(25),PTERMN(500),TERMN(500)
      IF (F .EQ. 0.D0) GO TO 6
      VSQ4=V*V*0.25D0
      KMAX=V+15.D0
      NMAX=KMAX
      DO 5 M=1,L
      TWOMP3=2*M+1
      DNFACU=1.D0
      DO 10 N=1,NMAX
      DN=N-1
      FACTK=1.D0
      DO 20 K=1,KMAX
      TWOKP1=2*K-1
      TERMK(K)=DSIN(TWOKP1*F)/TWOKP1/(TWOMP3+2.D0*DN+TWOKP1-1.D0)*FACTK
      IF (DABS(TERMK(K)) .LT. 1.D-25) GO TO 21
      FACTK=-VSQ4/(DN+TWOKP1+1.D0)/(DN+TWOKP1+2.D0)*FACTK
   20 CONTINUE
      K=KMAX
   21 PTERMN(N)=DSUM(TERMK,K)
      TERMN(N)=PTERMN(N)*DNFACU
      IF (DABS(TERMN(N)) .LT. 1.D-25) GO TO 5
      DNFACU=-VSQ4/(DN+1.D0)*DNFACU/(DN+2.D0)
   10 CONTINUE
      N=NMAX
    5 G(M)=DSUM(TERMN,N)
      RETURN
    6 DO 7 MI=1,L
    7 G(MI)=0.D0
      RETURN
      END
C
C
```

APPENDIX G

```
      DIMENSION HI(101,101)
      COMMON/CONCOM/KFLAG1,KFLAG2,FUN,NF,UMIN,UMAX,VMIN,VMAX,NDIM,NU,
     * NV,U,V,EXCLUD
      COMMON/BUFA/A(2000)/BUFB/B(2000)/BUFC/C(2000)/BUFZ/Z(103)
      DIMENSION CX(4),CTRVAL(10),TITLE(18),AA(10)
      DATA CTRVAL/0.2,0.1,0.075,0.05,0.02,0.01,0.0075,0.005,0.001,
     * 0.0005/
      READ (10) HI
      DO 17 IKK=1,2
      NF=10
      UMIN=-10.
      UMAX=10.
      VMIN=-20.
      VMAX=20.
      NDIM=2000
      NU=10.
      NV=201
      EXCLUD=0.
      DO 4 I=1,NF
      AA(I)=CTRVAL(I)
    4 A(I)=AA(I)
      CALL LEGEND(AA,TITLE,NF,UMIN,UMAX,VMIN,VMAX,CX)
      KFLAG1=1
   11 CONTINUE
      CALL CONTUR
      GO TO (21,22,22,24),KFLAG2
   21 I=5.*U+51.5
      J=5.*ABS(V)+1.5
      IF (V) 30,31,31
   30 FUN=HI(J,102-I)
      GO TO 11
   31 FUN=HI(J,I)
      GO TO 11
   22 CONTINUE
      CALL PLTCTR
      GO TO (99,11,99),KFLAG2
   24 WRITE (6,200)
  200 FORMAT(31H0CONTUR NEEDS MORE BUFFER SPACE)
   99 CONTINUE
   17 CONTINUE
      STOP
       END
C
      SUBROUTINE LEGEND(BUFA,TITLE,NF,XMIN,XMAX,YMIN,YMAX,C)
      COMMON/CPLOT2/DX,DY,XL,YL
       COMMON/LBLCOM/ITEST,SLBL,STTL,SSCL
       DIMENSION FMT(2)
       DIMENSION BUFA(1)
      DIMENSION LINE(22),LABELC(6), ALPHA(26), C(4), TITLE(12)
C     DATA LABELC/6HARC LA, 3HBEL, 1H , 6H CONTO, 5HUR VAL, 2HUE/
      DATA ALPHA /1HA,1HB,1HC,1HD,1HE,1HF,1HG,1HH,1HI,1HJ,1HK,1HL,1HM,
     11HN,1HO,1HP,1HQ,1HR,1HS,1HT,1HU,1HV,1HW,1HX,1HY,1HZ/
       DATA FMT/' (F5','.1) '/
C GENERATE LEGEND
      DO 11 J = 1, NF
      L = 1 + MOD(J-1,26)
      WRITE (6,105) ALPHA(L), BUFA(J)
  105 FORMAT(24X,A1,17X,F15.6)
   11 CONTINUE
C SET UP GRID FOR PLOTTING CONTOURS
      CALL SCALE (XMAX,XMIN,XU,XL,30,K)
      CALL SCALE(YMAX,YMIN,YU,YL,20,K)
      DX = (XU-XL)/15.0
      DY = (YU-YL)/10.
       ITEST=1
       SLBL=0.18
       STTL=0.24
       SSCL=0.10
       CALL VLABEL(2.5,0.,-20.,20.,10., 5,'V',0,1,FMT,5)
       CALL VLABEL(2.5,0.0,-10.,10.,10.,5,'U',0,0,FMT,5)
       CALL LABEL(12.5,0.,0.,20.,10.,-1,'V',0,1)
       CALL LABEL(2.5,10.,-10.,10.,10.,-1,'V',0,0)
      RETURN
      END
C
      SUBROUTINE PLTCTR
      COMMON/CONCOM/KFLAG1,KFLAG2,FUNCTN,NF,XMIN,XMAX,YMIN,YMAX,NDIM,
     1 NX,NY,XX,YY,EXCLUD
      COMMON /SCOM/KSTART,KGO,HLABEL,TLABEL,IZ,  Z,IARC,X,Y
      COMMON/CPLOT2/DX,DY,XL,YL
      DIMENSION ALPHA(26)
      DATA ALPHA/1H ,1H ,1H ,1H ,1H ,1H ,1H ,1H ,1H ,1H ,1H ,1H ,
     * 1H ,1H ,1H ,1H ,1H ,1H ,1H ,1H ,1H ,1H ,1H ,1H ,1H ,1H /
      DATA IPEN/3/
      LOGICAL FIRST,HLABEL,TLABEL,TLSAVE
      KSTART = 1
      FIRST = .TRUE.
   10 CALL CSCAN
      X = (X-XL)/DX
      Y = (Y-YL)/DY
      GO TO (12,24,15,32,20),KGO
   12 IF(.NOT.FIRST) GO TO 24
      FIRST = .FALSE.
      GO TO 28
   15 CONTINUE
      CALL SYSPLT(X,Y,3)
      GO TO 32
   20 IF(FIRST) GO TO 40
   24 CONTINUE
      CALL SYSPLT(XX,YY,3)
      IF(TLSAVE) CALL SYSSYM(XX,YY,.1,ALPHA(IALPHA),1,0)
C     CALL SYSPLT(X,Y,3)
       CALL SYSPLT(XX,YY,3)
      GO TO (28,30,99,99,36),KGO
   28 CONTINUE
      IALPHA = 1 + MOD(IZ-1,26)
   30 TLSAVE = TLABEL
      CALL SYSPLT(X,Y,3)
      IF(HLABEL) CALL SYSSYM(X,Y,.1,ALPHA(IALPHA),1,0)
      CALL SYSPLT(        X,Y,3)
   32 CONTINUE
      CALL SYSPLT(X,Y,IPEN)
   33 CONTINUE
      XX = X
      YY = Y
      IPEN = 2
      GO TO 10
   36 CONTINUE
      IF(KFLAG2.EQ.2) RETURN
   99 CONTINUE
   40 CONTINUE
      CALL SYSEND  (1,1)
      RETURN
      END
```

PART II

DIFFRACTION OF LAGUERRE GAUSSIAN BEAMS BY A CIRCULAR APERTURE

CHAPTER 1

INTRODUCTION

The diffraction of an electromagnetic wave with a Gaussian amplitude profile by a circular aperture has been an important problem in optics because the $TEM_{o,o}$ mode of laser resonators produces a beam whose variation in the transverse direction is Gaussian.
In addition to the general diffraction theory references of Part I p. 7, selected references pertinent to Gaussian resonator modes are given(1-4).

F. Kauffman(5) and A. L. Buck(6) first calculated the far zone diffraction patterns, resulting from the truncation of a Gaussian beam by a circular aperture, by solving numerically Kirchhoff's integral. The near zone patterns were calculated by Campbell and De Shazer(7) using digital techniques. F. O. Olaofe(8), R. G. Schell and G. Tyras(9) were the first ones to evaluate the diffraction integral analytically in the near and far zone region, their solution expressed in terms of infinite sums of Bessel functions.

In the work reported here we have extended these analyses to include any higher order Gaussian beams using the associated Laguerre polynomial to describe the radial distribution of the electric field. This type of representation of the electric field corresponds to the general $TEM_{p,\ell}$ mode of an optical resonator(10),(2-4). In addition we present calculations of the loss of power as a function of aperture size and mode index showing that the conventional rule of thumb in selecting apertures by "going out a few times w_o" is not accurate for large mode indices.

Specifically in Chapter 2 we analyze the diffraction of a high order Laguerre Gaussian beam ($TEM_{p,\ell}$) by a circular aperture, and discuss the behavior of the general solution, the case of restricted radial dependence ($TEM_{0,\ell}$ mode), and we present some interesting aspects of the minima of the lowest index mode ($TEM_{0,0}$).

In Chapter 3 we study the loss of power as a function of the aperture size and mode index for Laguerre and Hermite Gaussian beams, and in Chapter 4 we present a summary of the important solutions and the conclusions thereof .

CHAPTER 1

REFERENCES

1. G. D. Boyd and J. P. Gordon, Bell System Tech. J., 40 (1961), p. 489.
2. A. G. Fox and T. Li, Bell System Tech. J., 40, (1961), p. 453.
3. G. D. Boyd and H. Kogelnik, Bell System Tech. J., 41, (1962), p. 1341.
4. J. E. Pearson, T. C. McGill, S. Kurtin, and A. Yariv, J. Opt. Soc. Am. 59, (1969), p. 1440.
5. J. F. Kauffman, IEEE Trans. Antennas and Propagation (Commun.), AP-13, (1965), p. 473.
6. A. L. Buck, Proc. IEEE (Proc. Letters), (1967), p. 448.
7. J. P. Campbell and L. G. DeShazer, J. Opt. Soc. Am., 59, (1969), p. 1427.
8. J. O. Olaofe, J. Opt. Soc. Am., 60, (1970), p. 1654.
9. R. G. Schell and G. Tyras, J. Opt. Soc. Am., 61, (1971), p. 31.
10. A. E. Siegman, An Introduction to Lasers and Masers, (McGraw-Hill, New York, 1971), p. 330.

CHAPTER 2

DIFFRACTION OF LAGUERRE GAUSSIAN BEAMS BY A CIRCULAR APERTURE

2.1 Introduction

In this chapter we present the calculation of the Fresnel region diffraction patterns of a high order Laguerre Gaussian beam truncated by a circular aperture.

In the analysis that follows circular polar coordinates are used and the incident field has a cosine or sine angular dependence while its radial distribution is given by the associated Laguerre polynomial multiplied by a weighting factor. Sommerfeld's diffraction integral is solved with the Fresnel approximation, and the diffracted field is expressed in terms of converging power series and series involving the incomplete gamma function. Some special cases are considered resulting from the restriction of the radial or angular dependence, and corresponding expressions for the electric field are given. It is shown that for the high order modes, the irradiance on the z axis is zero when the mode index associated with the radial dependence, ℓ, is different than zero. On the other hand when ℓ is zero the central lobe is always a maximum.

2.2 Analysis

Consider a circular aperture of radius a, located in the plane $z = 0$, having a transmittance function $T(\rho',\phi')$ given by

$$T(\rho',\phi') = \mathrm{circ}(\rho') = 1 \qquad (\rho' \le a) \qquad (2.1)$$

$$= 0 \qquad \text{otherwise.}$$

The wave incident on the aperture is monochromatic and plane polarized. The following scalar function $U_{p\ell}(\rho',\phi')$ is taken to describe the transverse component of the illumination at $z = 0$[(1)*]

$$U_{p\ell}(\rho',\phi') = \frac{2}{(1+\delta_{0\ell})^{1/2}} \left[\frac{p!}{\pi(\ell+p)!}\right]^{1/2}$$

$$\frac{1}{w_0}\left(\frac{\sqrt{2}}{w_0}\right)^{\ell} \rho'^{\ell} L_p^{\ell}\left(\frac{2\rho'^2}{w_0^{\,2}}\right) \cdot \begin{pmatrix} \cos\ell\phi' \\ \sin\ell\phi' \end{pmatrix} \exp(-\rho'^2/w_0^{\,2}) \qquad (2.2)$$

where the Kronecker delta $\delta_{0\ell} = 1$ for $\ell = 0$ and zero for $\ell \neq 0$, L_p^{ℓ} is the associated Laguerre polynomial, and w_0 = spot size of Gaussian wave at plane $z = 0$. We have chosen this type of representation of the electric field because we are concerned with special filtering (truncation at the focal plane). In this case it can be shown, for example with the use of the Collins chart[(2)], that Eq. 8-4 (7) in Ref. 1, which describes the field at an arbitrary point $(\rho'\phi',z)$ reduces to the form of Eq. (2.2). Furthermore, the generalization of the analysis to include truncation for expanding and converging waves can be easily made by changing w_0 to $w(z)$, including a spherical wavefront in the Gaussian amplitude term, and multiplying with a phase factor that is a function of z.

To calculate the scalar component of the electric field amplitude at $(\rho,\phi,z > 0)$, see Fig. [2-1]. We use the usual Fresnel-zone approximation of Sommerfeld's formula[(3)],

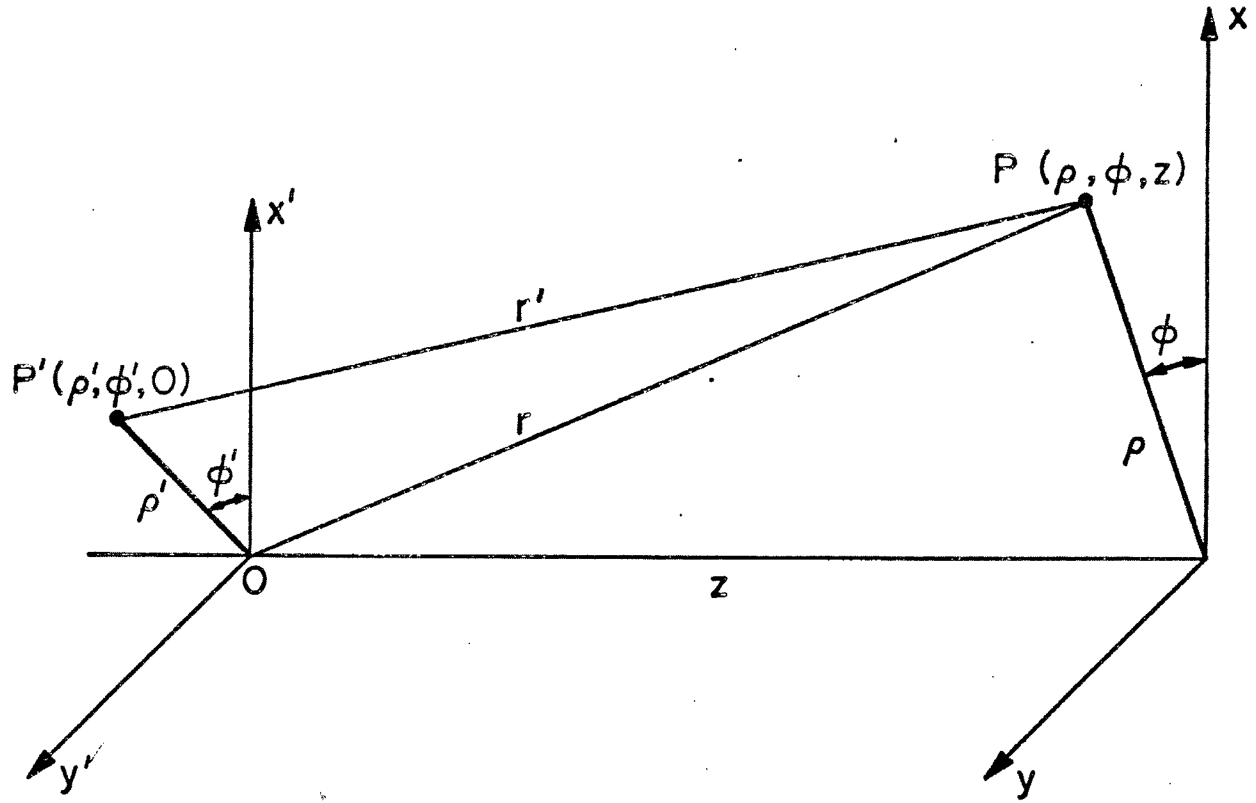

Fig. [2-1]. Geometry of relationships between aperture and observation plane.

$$V(\rho,r) = \frac{iz}{\lambda r} e^{-ikr} \iint_S U(\rho',\phi')\exp[-ik(\rho'^2/2r - \frac{\rho\rho'\cos(\phi'-\phi)}{r}]\rho' d\rho' d\phi' \quad . \tag{2.3}$$

Combining Eqs. 2.1, 2.2, and 2.3 gives

$$V_{p\ell}(\rho,r) = \frac{iz}{\lambda r} \exp(-ikr)\frac{2}{(1+\delta_{o\ell})^{1/2}}\left[\frac{p!}{\pi(\ell+p)!}\right]^{1/2}\frac{1}{w_o}\left(\frac{\sqrt{2}}{w_o}\right)^{\ell} \cdot$$

$$\cdot \int_0^{2\pi}\int_0^{a} L_p^{\ell}\left(\frac{2\rho'^2}{w_o^2}\right)\exp(-\rho'^2/w_o^2)\exp(\frac{-ik\rho'^2}{2r})\begin{pmatrix}\cos\ell\phi' \\ \sin\ell\phi'\end{pmatrix}\exp\frac{ik\rho\rho'\cos(\phi-\phi')}{r} \cdot$$

$$\cdot \rho'^{2\ell+1} d\rho' d\phi' \tag{2.4}$$

Using the relation[4]

$$\exp[in(\pi/2-\phi)]J_n(\frac{k\rho\rho'}{r}) = \frac{1}{2\pi}\int_0^{2\pi}\exp[ik(\rho\rho'/r)\cos(\phi-\phi')- in\phi']d\phi' \tag{2.5}$$

and integrating (2.4) with respect to ϕ' we get

$$V_{p\ell}(\rho,r) = \frac{iz\exp(-ikr)}{\lambda r^2}\exp(\frac{i\ell\pi}{2})\begin{pmatrix}\cos\ell\phi \\ \sin\ell\phi\end{pmatrix}\frac{4\sqrt{\pi}}{(1+\delta_{o\ell})^{1/2}}\frac{p!}{(\ell+p)!}\frac{1}{w_o}\left(\frac{\sqrt{2}}{w_o}\right)^{\ell}.$$

$$\cdot \int_0^a \rho'^{\ell+1}J_\ell(\frac{k\rho\rho'}{r})L_p^{\ell}(\frac{2\rho'^2}{w_o^2})\exp[-\rho'^2(\frac{1}{w_o^2} + \frac{ik}{2r})]d\rho' \tag{2.6}$$

The integral with respect to ρ', which we call I_ρ, can be evaluated as follows. We first substitute $\rho' = \frac{x}{a}$ and then expand the Bessel function and the Laguerre polynomial in terms of power series A.S. 9.1.10 and G.R. 8.970 and exchange the order of summation and integration, getting

$$I_\rho = a^2\left(\frac{k\rho a}{2r}\right)^\ell \sum_{n=o}^{n=p}(-1)^n \binom{p+\ell}{p-n} \frac{\left(\frac{2a^2}{w_o^2}\right)^n}{n!} \cdot \sum_{m=o}^{\infty} \frac{\left(\frac{-k^2\rho^2a^2}{4r^2}\right)^m}{m!(m+\ell)!}$$

$$\cdot \int_o^1 x^{2n+2m+2\ell+1} \exp\left[-x^2\left(\frac{a^2}{w_o^2} + \frac{ika^2}{2r}\right)\right] dx \qquad (2.7)$$

The integral in Eq. (2.7) can be evaluated by A.S. 6.5.2 in terms of the incomplete gamma function with the substitution $u = x^2\left(\frac{a^2}{w_o^2} + \frac{ika^2}{2r}\right)$, giving

$$I_\rho = \frac{a^2}{2}\left(\frac{k\rho a}{2r}\right)^\ell \frac{1}{\alpha^{\ell+1}} \sum_{n=o}^{n=p} \frac{(-1)^n(p+\ell)!\left(\frac{2a^2}{w_o^2\alpha}\right)^n}{(\ell+n)!(p-n)!n!} \cdot \sum_{m=o}^{\infty} \frac{\left(\frac{-k^2\rho^2a^2}{4r^2}\right)^m}{m!(m+\ell)!} \gamma(m+\ell+n+1,\alpha)$$

$$(2.8)$$

$$\text{where } \alpha = \frac{a^2}{w_o^2} + \frac{i\pi a^2}{\lambda r} \,. \qquad (2.9)$$

Defining

$$b = \frac{k\rho a}{r}, \quad \xi = \frac{2a^2}{w_o^2\alpha}, \quad g = \frac{-b^2}{4\alpha}, \quad h = \frac{ab}{\sqrt{2}w_o} \qquad (2.10)$$

and combining Eqs. (2.10), (2.9), (2.8), (2.6) we get the following general result for the electric field:

$$V_{p\ell}(\rho,r) = i\,\frac{2\sqrt{\pi}}{\lambda}\frac{a^2z}{r^2}\,\frac{1}{w_o}\left[\frac{p!(\ell+p)!}{1+\delta_{o\ell}}\right]^{1/2} h^\ell \exp(-ikr)\exp\left(\frac{i\ell\pi}{2}\right)\binom{\cos\ell\phi}{\sin\ell\phi}\frac{1}{\alpha^{\ell+1}} \,\cdot$$

$$\cdot \sum_{n=o}^{n=p} \frac{\xi^k}{(\ell+n)!(p-n)!n!} \cdot \sum_{m=o}^{\infty} \frac{g^m \gamma(\ell+m+n+1,\alpha)}{m!(m+\ell)!} \qquad (2.11)$$

Restricting the radial dependence to $\rho'^{\ell}\exp(-\rho'^2/w_o^2)$ by setting $p = 0$ one gets

$$V_{o,\ell}(\rho,r) = i\,\frac{2\sqrt{\pi}}{\lambda}\,\frac{a^2 z}{r^2}\,\frac{1}{w_o}\left[\frac{1}{\ell!\,(1+\delta_{o\ell})}\right]^{1/2} h^{\ell}\exp(-ikr)\exp\left(\frac{i\ell\pi}{2}\right)\begin{pmatrix}\cos\ell\phi\\ \sin\ell\phi\end{pmatrix}\frac{1}{\alpha^{\ell+1}}$$

$$\cdot \sum_{m=o}^{\infty} \frac{g^m{}_{\gamma}(\ell+m+1,\alpha)}{m!\,(m+\ell)!} \tag{2.12}$$

Using A.S. 6.5.4 and 6.5.29 Eq. (2.12) can be written

$$V_{o,\ell}(\rho,r) = i\,\frac{2\sqrt{\pi}}{\lambda}\,\frac{a^2 z}{r^2}\,\frac{1}{w_o}\left[\frac{1}{\ell!\,(1+\delta_{o\ell})}\right]^{1/2} h^{\ell}\exp(-ikr)\exp\left(\frac{i\ell\pi}{2}\right)\begin{pmatrix}\cos\ell\phi\\ \cos\ell\phi\end{pmatrix}$$

$$e^{-\alpha}\sum_{m=o}^{\infty}\frac{\left(\frac{g}{\alpha}\right)^m}{m!}\sum_{n=o}^{\infty}\frac{\alpha^n}{\Gamma(\ell+m+1+n+1)} \tag{2.13}$$

Now exchanging the order of summation and using A.S. 9.1.10 one can show that

$$V_{o\ell}(\rho,r) = \frac{2i\sqrt{\pi}}{\lambda}\,\frac{a^2 z}{r^2}\,\frac{1}{w_o}\left[\frac{1}{\ell!\,(1+\delta_{o\ell})}\right]^{1/2}\beta^{\ell}\,\exp(-ikr)\exp\left(\frac{i\ell\pi}{2}\right)\begin{pmatrix}\cos\ell\phi\\ \sin\ell\phi\end{pmatrix}$$

$$\cdot\,\frac{e^{-\alpha}}{\alpha}\sum_{m=1}^{\infty}\frac{J_{\ell+m}(b)}{d^m} \tag{2.14}$$

where $d = b/2\alpha$, $\beta = \sqrt{2}\,a/w_o$.

Finally setting $\ell = 0$, $p = 0$ we get the following result for the lowest order Gaussian beam:

$$V_{oo}(\rho,r) = \frac{(2\pi)^{1/2}}{\lambda} \; \frac{a^2 z}{r^2} \frac{1}{w_o} \frac{e^{-\alpha}}{\alpha} \exp(-ikr) \sum_{m=1}^{\infty} \frac{J_m(b)}{d^m} \tag{2.15}$$

We note that this result is equivalent with the ones in Ref. 3 and 5.

2.3 Numerical Calculations

In this section we will discuss the numerical evaluation of Eq. (2.11) and present graphs of the important cases discussed in the previous analysis. Specifically we will show the variation of intensity for a $TEM_{5,6}$ mode as a function of the aperture size, demonstrate the lobe structure and high frequency components for the diffraction of a $TEM_{0,4}$ wave, and finally we will display the variation of the minima of the $TEM_{o,o}$ mode as a function of the truncation parameter.

The numerical evaluation of Eq. (2.11) involved basically the calculation of the double sum of the incomplete gamma function of complex argument with the appropriate powers and factorials. To avoid the repeated computation of the incomplete gamma function a double precision table was generated using the A.S. 6.5.29 series for each calculation. Subsequently,the values of the table were used in combination with the binomial coefficients and the appropriate powers to produce double precision complex arrays which were consequently sorted and summed. As is the case with problems involving factorials and powers particular care was exercised in grouping and operating with terms of equal magnitude. The criterion for truncation was that the last term be of the order of 10^{-60} compared with the total sum. This type of truncation was considered necessary because of the highly oscillatory nature of the result. The programs for these calculations are included in Appendix A.

An illustration of the radiation patterns for the high-order modes is shown in Fig. [2-2]. We plot $V_{5,6}V^*_{5,6}$ from Eq. (2.11) normalized to I_{oo} vs. x(i.e. ϕ=0) for a/w_o = 1.0 and 0.8. I_{oo} is the irradiance of the TEM_{oo} mode at point (o,z), in the absence of the aperture and is given by:

$$I_{oo} = 2\pi w_o{}^2/(\pi^2 w^4+\lambda^2 z^2) \tag{2.16}$$

For a/w_o = 1.0 only about 12% of the total power is transmitted through the aperture. By way of contrast we note that with same aperture size 86% of the power is coupled for the $TEM_{o,o}$ mode. For a/w_o = 0.8 as shown in Fig. [2-2], we see that the power transmitted in the $TEM_{5,6}$ mode drops sharply to a mere 2.5% of the incident power.

In Fig. [2-3] we plot lines of constant intensity $V_{0,4}V^*_{0,4}$ from Eq. (2.14) normalized to I_{oo} given by Eq. (2.16) versus normalized coordinates $\frac{2\pi a}{\lambda z}$ x and $\frac{2\pi a}{\lambda z}$ y. The center of the pattern has zero intensity and this fact can be seen from Eq. (2.14) by taking the limit of $b \to 0$. In addition the intensity has zeroes along the lines of ϕ where $\cos^2 4\phi$ is equal to zero. In the absence of the diffracting aperture the irradiance would have had only the eight central lobes (compare this figure with Ref. 1 page 332). The introduction of the circular aperture causes the higher spatial frequency ringing limited in the sectors where $\cos^2 4\phi \neq 0$. For this configuration a/w_o was taken to be equal to 1.0. The intensity values for the different contours is given by the legend accompanying the figure. To calculate Eq. (2.14) and draw the isophotes we employed the same techniques and programs that were discussed in

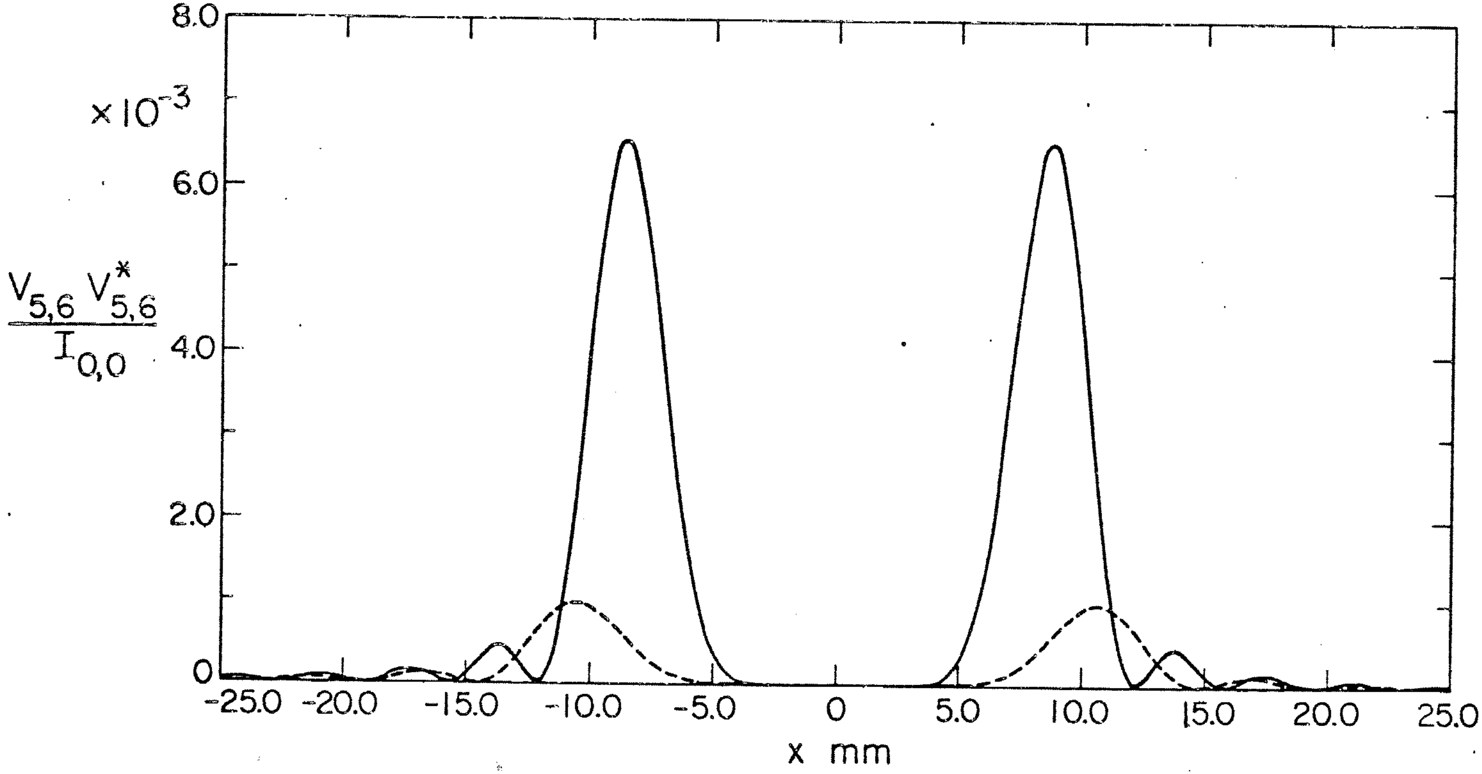

Fig. [2-2]. Normalized transmitted irradiance $V_{5,6}V^*_{5,6}/I_{00}$ vs x; a/w_o = 0.8, 1.0 are dashed and solid curves respectively, for λ = 0.6328 μm, z = 0.1 m, ϕ = 0, and w_o = 10 μm.

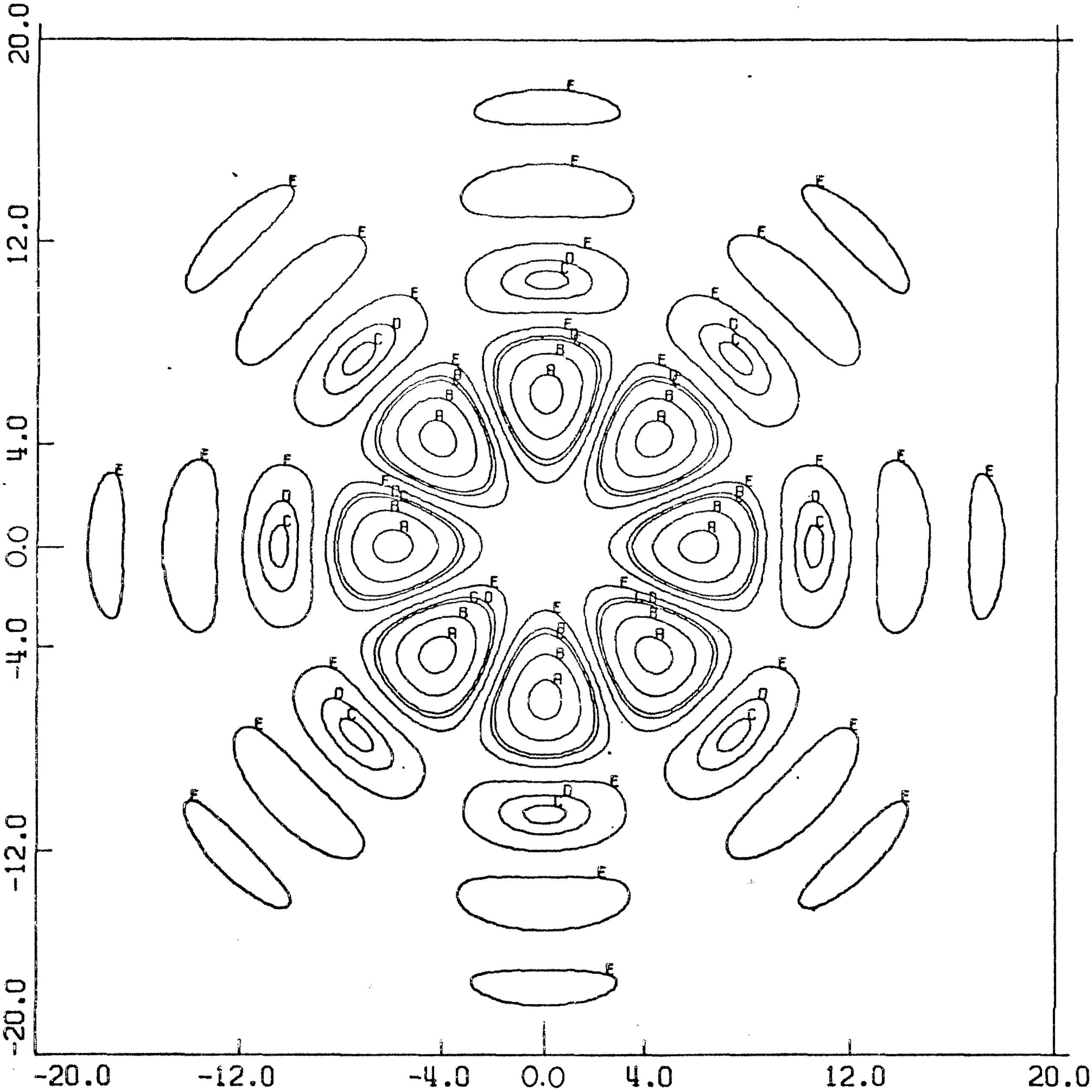

Fig. [2-3]. Isophotes of the diffracted $TEM_{0,4}$ mode plotted vs $\frac{2\pi a}{\lambda z}$ x and $\frac{2\pi a}{\lambda z}$ y, for $\frac{a}{w_o}$ = 1.0 and w_o = 10 μm.

A = 0.000500
B = 0.000230
C = 0.000074
D = 0.000050
E = 0.000010

Part 1, Section 5.1.

To illustrate the minima of the radiation pattern for the $TEM_{o,o}$ mode we present Fig. [2-4]. The solid curves represent the minima of the function

$$\left| \frac{\exp(-\alpha)}{\alpha} \sum_{m=1}^{\infty} \frac{J_m(b)}{(\frac{b}{\alpha})^m} \right|^2 \qquad (2.17)$$

while the dashed ones the zeroes of the $J_1(b)$ function denoted by $j_{1,1}$ for the first zero, $j_{1,2}$ the second and so on. The locus of the zeroes of $J_1(b)$ do not depend on the parameter α and are therefore straight lines. The minima of Eq. (2.17) do depend on α and their deviation from $j_{1,n}$ (n=1,6) can be determined from this figure. In these calculations α was taken to be real since from Eq. (2.9) it can be seen that for aperture values of $a \sim 10$ µm the imaginary part of this expression is of the order of 5×10^{-4}, for z = 100 cm, $\lambda = .6328$ µm. Then Eq. (2.17) has exactly the same minima as the expression for the intensity of the $TEM_{o,o}$ mode so long as $(a/w_o)^2 >> \frac{\pi a^2}{\lambda z}$. The range in α is $0 < \alpha \leq 4$ and in b $0 \leq b \leq 20$. This plot indicates that for spatial filtering applications ($a/w_o \sim 2$) the minima of the radiation pattern are within a few percent of the zeroes of the $J_1(b)$ i.e., plane wave illumination. Furthermore, for moderate values of α, the minima of Eq. (2.17) as b goes to infinity approach asymptotically $j_{1,n}$ $n \to \infty$. However as α goes to infinity, i.e. Gaussian wave, then the zeroes of Eq. (2.17) merge asymptotically at very large values of b.

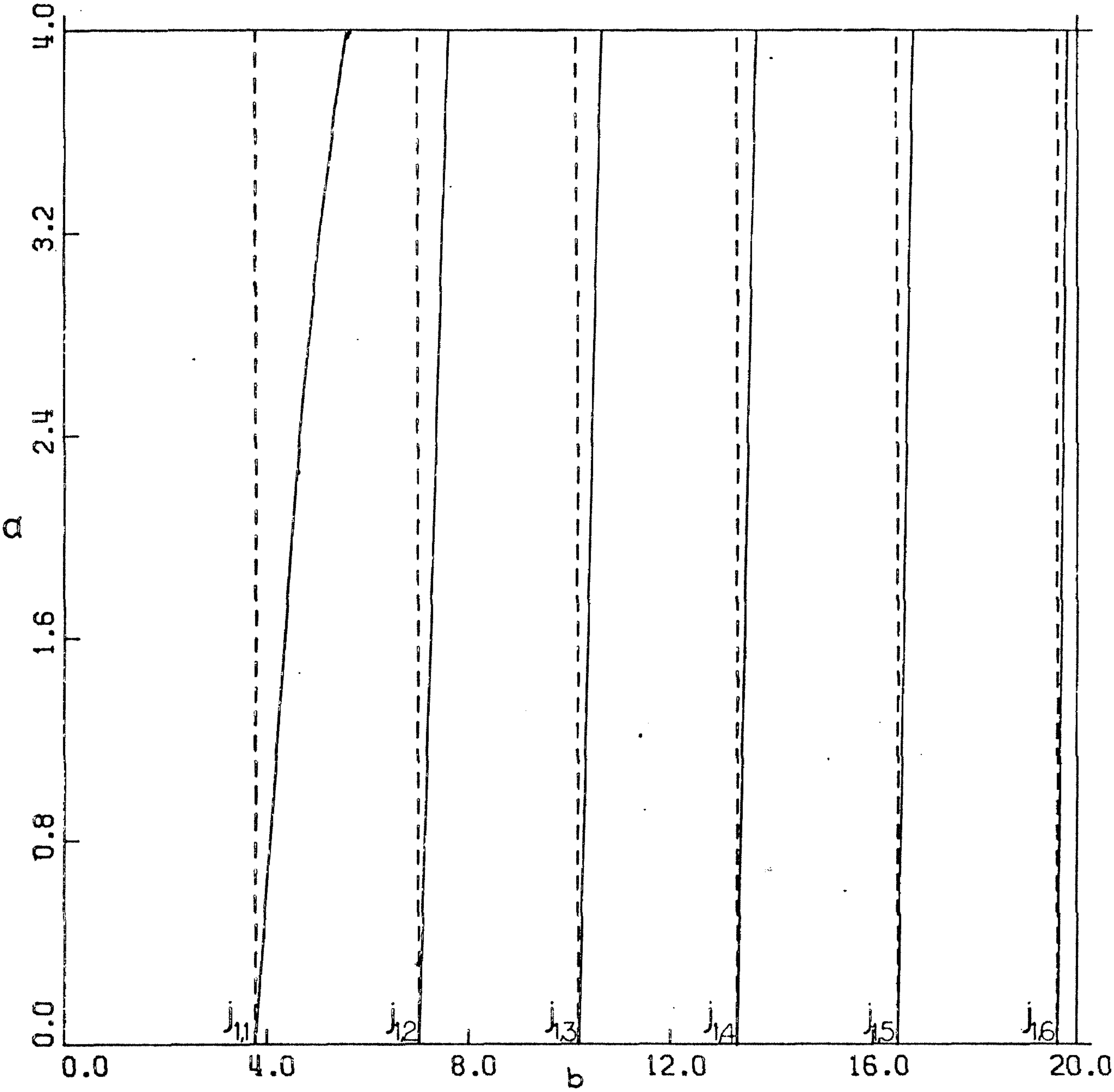

Fig. [2-4]. Intensity minima for the $TEM_{0,0}$ mode, solid curves, and the zeroes of the $J_1(b)/b$ pattern, dashed curves plotted vs α and b.

To generate Fig. [2-4] a table of the $\log_{10}$ of Eq. (2.17) was constructed. Subsequently a contour diagram was made for function values ranging from -6 to -9. This established the valleys of the minima. The actual determination of the minima was made using bivariate linear interpolation between the two closest contours of the same value.

In summary from Eq. (2.11) it can be seen that if ℓ=o, $V_{p,\ell}(o,r) = 0$, (ρ=o $\Longrightarrow$ h $\to$ 0 $\longrightarrow$ $h^{\ell} \to 0$), so the irradiance is zero on the z axis. The only case that this does not happen is when ℓ=o and then the pattern has a maximum at ρ=o. In addition for the simple case of the $TEM_{o,o}$ mode the minima of the intensity distribution have approximately the same spatial distribution as the minima of the Airy pattern.

CHAPTER 2

REFERENCES

1. A. E. Siegman, <u>An Introduction to Lasers and Masers</u>, (McGraw-Hill, New York, 1971), p. 330.
2. A. E. Siegman, <u>ibid</u>., p. 318.
3. R. G. Schell and G. Tyras, J. Opt. Soc. Am., <u>61</u>, (1971), p. 31.
4. A. G.Fox and T. Li, Bell System Tech. J., <u>40</u>, (1961), p. 487.
5. G. O. Olaofe, J. Opt. Soc. Am., <u>60</u>, (1970), p. 1654.

A.S. M. Abramowitz and I. A. Stegun, <u>Handbook of Mathematical Functions</u>, (Nat. Bureau of Standards, Washington, 1970).

G.R. I. S. Gradshteyn and I. M. Ryzhik, <u>Table of Integrals</u>, <u>Series and Products</u>, (Academic Press, New York, 1965).

*Note: A square root has been incorporated in the term $\frac{p!}{\pi(\ell+p)!}$ so that the eigenfunctions would be normalized to 1.

CHAPTER 3

APERTURE MATCHING FOR HIGH ORDER MODES

3.1 Introduction

In this chapter we calculate the loss of power as a function of the aperture ratio a/w_0, for high order modes. The input electric field is written, for the first case examined, in the form of Eq. (2.2) i.e. in the Laguerre-Gaussian representation resulting from the solution of the resonator integral equation in cylindrical coordinates. We compute the ratio of the transmitted to the incident power and plot it as a function of a/w_0. In the second case the input field is written in terms of the Hermite-Gaussian representation appropriate for a solution of the resonator equation in Cartesian coordinates. Again the dependence of the ratio of the transmitted to the incident power is calculated and the results are plotted as a function of the rectangular aperture size a'/w_0. The results indicate that relative aperture sizes greater than five are required in order to achieve transmittion efficiencies greater than 90% for high order modes.

3.2 Laguerre Gaussian Matching

To study the loss of power as a function of the aperture ratio for the Laguerre Gaussian incident field we must evaluate

$$\frac{P_{tr}}{P_{in}} = \frac{\int_0^{2\pi}\int_0^{a} |U_{p\ell}|^2 \rho' d\rho' d\phi'}{\int_0^{2\pi}\int_0^{\infty} |U_{p\ell}|^2 \rho' d\rho' d\phi'} \tag{3.1}$$

where the incident and transmitted powers are denoted by P_{in} and P_{tr} respectively and where $U_{p\ell}$ is given by Eq. (2.2).

We note that the denominator in Eq. (3.1) is equal to 1 by virtue of the fact that the eigenfunction solutions $U_{p\ell}$ have been normalized to 1, or by directly calculating the integral using G.R. 7.414.3. Combining Eq. (2.2) and (3.1) and using the above property we get the following result:

$$\frac{P_{tr}}{P_{in}} = \frac{4}{1+\delta_{o\ell}} \frac{p!}{\pi(\ell+p)!} \left(\frac{1}{w_o^2}\right)\left(\frac{2}{w_o^2}\right)^{\ell} \int_0^{2\pi} \begin{pmatrix} \cos^2\ell\phi' \\ \sin^2\ell\phi' \end{pmatrix} d\phi' \quad \cdot$$

$$\cdot \int_0^{a} \rho'^{2\ell} \left| L_p^{\ell}\left(\frac{2\rho'^2}{w_o^2}\right)\right|^2 \exp(-2\rho'^2/w_o^2)\rho' d\rho' \tag{3.2}$$

In Eq. (3.2) the integration with respect to ϕ' gives π, and the substitution of $u = 2\rho'^2/w_o^2$ gives:

$$\frac{P_{tr}}{P_{in}} = \frac{1}{(1+\delta_{o\ell})} \cdot \frac{p!}{(\ell+p)!} \cdot \int_0^{2a^2/w_o^2} u^{\ell} |L_p^{\ell}(u)|^2 e^{-u} du \tag{3.3}$$

Eq. (3.3) was solved numerically in the following fashion. A function subprogram calculated the associated Laguerre polynomial for a given p, ℓ, and x using the forward recursion formula G.R. 8.971.4.

This process is sufficiently accurate for indices not exceeding 25. Subsequently the integrand was formed and integrated using the Simson approximation, for a given initial guess of the upper limit of integration. The returned value multiplied by the weighting factor was compared with the desired value of P_{tr}/P_{in}. If the difference was not within one percent the limit of integration would be modified accordingly and the process repeated until the desired accuracy was achieved. The computer program for this calculation is included in Appendix B.

Fig. [3-1] shows dashed lines of constant efficiency, P_{tr}/P_{in} for values of 0.5, 0.7 and 0.9 with ℓ=5 plotted versus p and a/w_0. Range bars are shown on each curve to permit interpolation for mode indices from ℓ=0 to ℓ=10. As an example, to get a transmission efficiency of 0.7 for the $TEM_{7,9}$ mode the aperture ratio is calculated from the graph to be 4.8.

3.3 Hermite Gaussian Matching

The determination of the transmission efficiencies for a rectangular aperture of dimension 2a' x 2a' involves the solution of an equation similar to the one presented in Section 3.2, namely

$$\frac{P_{tr}}{P_{in}} = \frac{\int_{-a'}^{a'}\int_{-a'}^{a'} |U_{m,n}|^2 dx'dy'}{\int_{-\infty}^{+\infty}\int_{-\infty}^{+\infty} |U_{m,n}|^2 dx'dy'} \qquad (3.4)$$

where $U_{m,n}$ is defined by(1):*

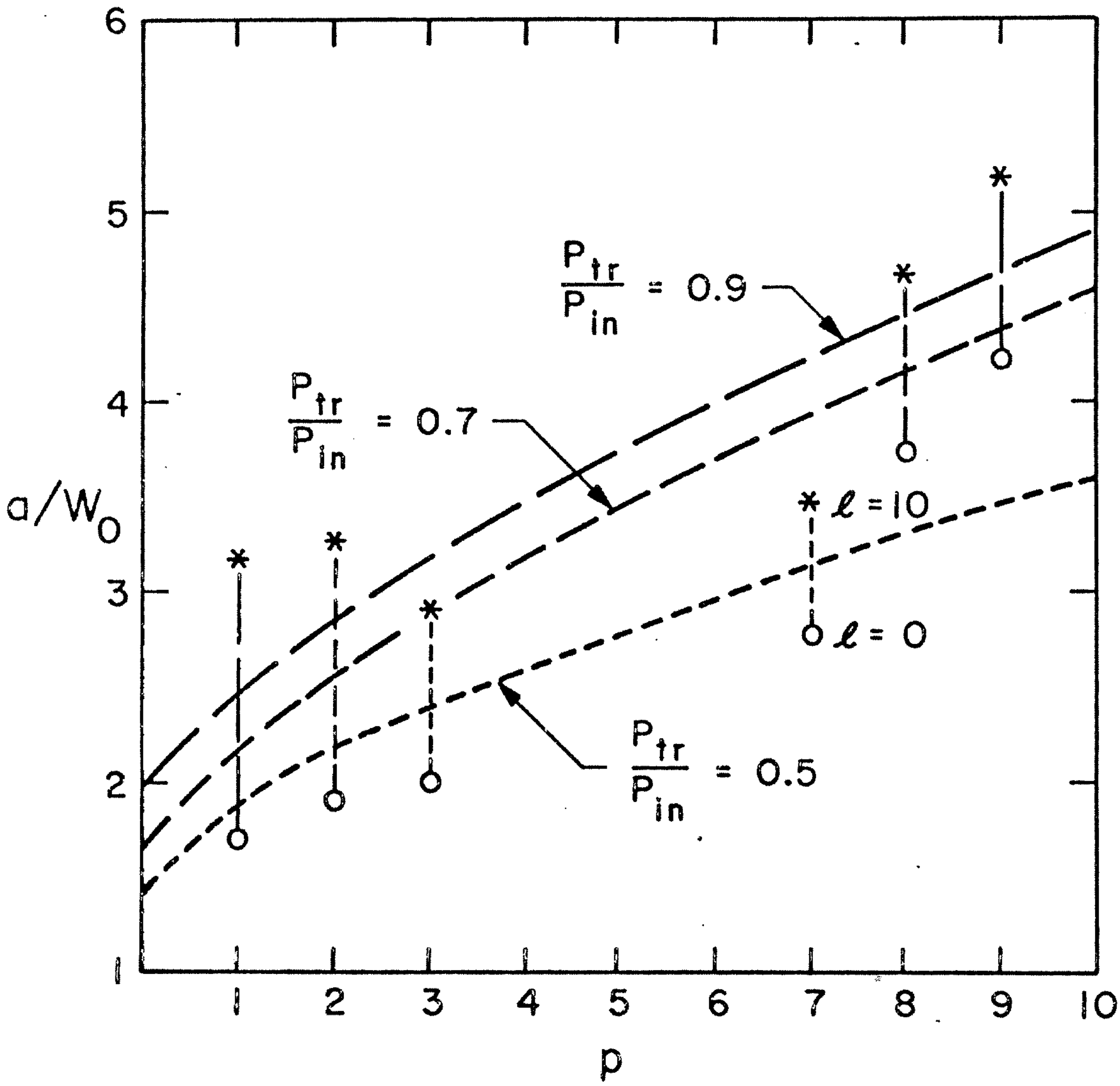

Fig. [3-1]. Transmittance P_{tr}/P_{in} as a function of relative aperture size and mode index p. The dashed curves are for ℓ=5; range bars are shown on each curve to permit interpolation for mode indices from ℓ=0 (0) to ℓ= 10(*).

$$U_{m,n}(x',y',z=0) = \left[\frac{1}{2^{m+n}m!n!}\right]^{\frac{1}{2}} \frac{\sqrt{2/\pi}}{w_o} H_m\left(\frac{\sqrt{2}x'}{w_o}\right) H_n\left(\frac{\sqrt{2}y'}{w_o}\right) \exp[-(x'^2+y'^2)/w_o^2] \tag{3.5}$$

H_m and H_n are the Hermite polynomials of order m and n respectively.

Using the same arguments as in section 3.2 P_{in} can be set to 1 and upon substitution of Eq. (3.5) in (3.4) we get

$$\frac{P_{tr}}{P_{in}} = \frac{1}{2^{m+n-1}m!n!} \; \frac{1}{\pi w_o^2} \int_{-a}^{+a} \left| H_m \left(\frac{\sqrt{2}x^2}{w_o}\right)\right|^2 \exp\left(-\frac{x'^2}{w_o^2}\right)dx' \cdot$$

$$\cdot \int_{-a}^{+a} \left| H_m \left(\frac{\sqrt{2}y'}{w_o}\right) \right. \exp\left(\frac{-y'^2}{w_o^2}\right)dy' \tag{3.6}$$

Using the property that $|H_m(-x)| = |H_m(x)|$ and substituting $u = \frac{\sqrt{2}x'}{w_o}$ and $v = \frac{\sqrt{2}y'}{w_o}$ Eq. (3.6) can be rewritten

$$\frac{P_{tr}}{P_{in}} = \frac{1}{\pi 2^{m+n-2}m!n!} \int_0^{\frac{\sqrt{2}a}{w_o}} |H_m(u)|^2 \exp(-u^2)du \cdot \int_0^{\frac{\sqrt{2}a}{w_o}} |H_n(v)|^2 \exp(-v^2)dv \tag{3.7}$$

Eq. (3.7) was evaluated numerically for given values of P_{tr}/P_{in} in a similar way as Eq. (3.3) was. A function subprogram generated the Hermite polynomials for a given index and argument, using the forward recursion relationship; then the integrand was formed and a special subroutine controlled the upper limit of integration until the solution was achieved within the desired accuracy.

In Fig. [3-2] lines of constant efficiency are drawn as a function of n and a'/w_o with $m=5$. The P_{tr}/P_{in} values are 0.5, 0.7 and 0.9 for comparison with Fig. [3-1]. Again range bars are drawn to permit interpolation between mode indices $m=0$ and $m=10$.

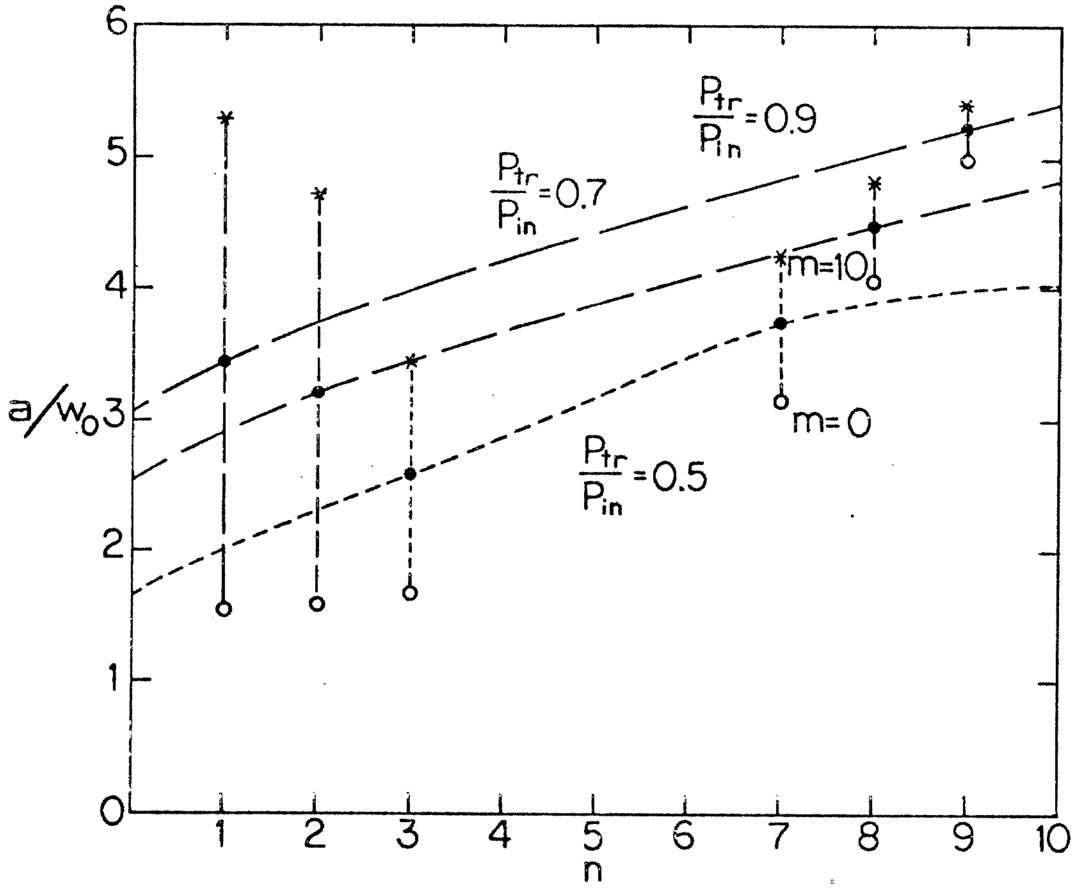

Fig. [3-2]. Transmission efficiency P_{tr}/P_{in} as a function of relative aperture size and mode index n, for m=5. Range bars to be used for interpolation between indices m=0 (0) and m=10(*).

CHAPTER 3

REFERENCES

1. A. E. Siegman, An Introduction to Lasers and Masers, (McGraw-Hill, New York, 1971), p. 330.

G.R. I. S. Gradshteyn and I. M. Ryzhik, Table of Integrals, Series and Products, (Academic Press, New York, 1965).

*Note: A factor of $\sqrt{2/\pi}$ has been incorporated in the expression for $U_{m,n}$ so that these eigenfunctions would be normalized to 1.

CHAPTER 4

SUMMARY AND CONCLUSIONS

In this part of our work we have examined the diffraction of a Laguerre Gaussian beam by a circular aperture, and we have studied the transmission efficiency as a function of mode indices and relative aperture size for Laguerre as well as Hermite Gaussian beams.

The general result for the electric field for a diffracted $TEM_{p,\ell}$ mode is given by Eq. (2.11). If the radial dependence is restricted to $\rho'^{\ell}\exp(-\rho'^2/w_o^2)$ the corresponding result for the $TEM_{o,\ell}$ mode is Eq. (2.14). The electric field for the fundamental mode is given by Eq. (2.15). To illustrate the variation of the intensity distribution for a $TEM_{5,6}$ mode as a function of the distance from the z axis and relative aperture size we have presented Fig. [2-2]. The two-dimensional lobe structure and the high spatial frequencies of the distribution for a $TEM_{o,\ell}$ mode are shown in Fig. [2-3]. The calculation of the deviations of the minima of the $TEM_{o,o}$ mode from the zeroes of the Airy pattern can be made using Fig. [2-4]. We note from the above analysis that in general the diffraction pattern for a $TEM_{p,\ell}$ mode is always zero on the z axis for values of $\ell \neq 0$. When $\ell=0$ then the central lobe is a maximum. In addition the intensity drop for a small change of relative aperture size is much larger in the case of the higher order modes. Finally the zeroes of the fundamental $TEM_{o,o}$ mode for practical values of a/w_o are in close proximity to the zeroes of the Airy pattern and the greatest deviations occur near the first zero $j_{1,1}$.

The evaluation of the transmission efficiency for Laguerre and Hermite Gaussian beams was done numerically and the results are shown in Fig. [3-1] and Fig. [3-2] respectively. We have plotted constant values of the ratio of transmitted to incident power, as a function of relative aperture size and mode indices. These plots can be effectively used to calculate the necessary aperture size for a given transmission efficiency and set of mode indices. In general the results indicate that higher order modes require aperture sizes, much larger than what was thought necessary, in order to achieve efficient mode coupling.

```
      COMPLEX TERM
      COMPLEX *16 ALPHA,CSUM
      COMMON/MISVA/RZ,A
     REAL  LAMBDA
      DATA LAMBDA/.6328E-3/
     DIMENSION R(500)
     DIMENSION DD(3)
     DATA DD/0.,0.,1.0/
      DIMENSION HH(5), ZZ(3), UU(500)
     DATA  ZZ/50.,100.,1000./
     DATA  PI/3.141593/
      DATA HH/1., .8, .4, .2, .1/
     INTEGER P
      P=5
      L=6
     WRITE (6,560) P,L
 560 FORMAT(1H1 'P = ',I5, 2X'L=',I5)
     DEL = 1.
     TT = 1.
     IF(L.EQ. 0) GO TO 8
     DEL = 0.
     DO 5 I = 1,L
     TT = TT/(P+I)
   5 CONTINUE
   8 CONTINUE
     KK = 0
      N=51
     KK = KK+1
     IF(KK.GT.3) STOP
     Z = ZZ(KK)
     Z = 100.
     W0 = 1.E-2
      CM=2.*PI*W0*W0/(PI*PI*W0**4+LAMBDA**2*Z*Z)
     WRITE (6,555) CM
 555 FORMAT(1X'CM=',E15.6)
      DO 200 I=1,2
     H = HH(I)
     C = W0*H
      RMIN=-.25*Z
     DRZ = (-RMIN/(N-1))/Z
     RZ = 0.
     WRITE (6,530) Z,H,C
 530  FORMAT(1H0 'Z=',F6.0,2X'H=',F6.2,2X'C=',E13.6)
     BETA=2.0*(C/W0)**2
     DO 100 J=1,N
     R(J) = RZ*Z
     SQRTRZ = SQRT(Z*Z + R(J)*R(J))
      ALPHA=H*H+(0., 1.0)*PI*C*C/(LAMBDA*SQRTRZ)
     A = PI*2.0/LAMBDA*C*R(J)/SQRTRZ
      D = -A*A*.25
     CALL PCSUM      (ALPHA,D,BETA,P,L,CSUM,M)
     CC = BETA*.25*A*A
     IF(R(J) .EQ. 0. .AND. L.EQ.0) CC  = 1.0
     FACTOR = (Z*C*C)**2/(LAMBDA*(Z*Z+R(J)*R(J)))**2*(   CC
    1        )**L/(1.0+DEL)*TT
     TERM = CSUM
      U=FACTOR*CABS(TERM)**2*4.*PI/(W0*CM*W0)
      UU(J)=U
     RZ = RZ+DRZ
 100 CONTINUE
      WRITE (6,520) (R(J), UU(J), J=1,N)
 520 FORMAT(1X10E13.6)
      IF(I.GT.1) GO TO 160
      RMAX = -RMIN
       CALL MAXMIN(UU, N, YMAX, YMIN)
      CALL SCALE(YMAX, 0., TOP, BOT, 10,JJ)
       CALL LABEL(0., 0., RMIN, RMAX, 15., 15, 'R', 1, 0)
      CALL LABEL(0., 0., BOT, TOP, 10., 10, 'I', 1, 1)
      DIMENSION LINE(22)
 570   FORMAT('TEM',1X,I1,I1)
      CALL CUTCOR(LINE,NUM)
      WRITE (6,570) P,L
      CALL CUTCOR
      CALL SYSSYM( 7.0, 9.5, .1, LINE,4*NUM,0.)
 160 CONTINUE
       CALL XYPLOT(N, R, UU, RMIN, RMAX, BOT, TOP, DD, 0)
       CALL XYPLOT(N, R, UU, RMAX, RMIN, BOT, TOP, DD, 0)
 200 CONTINUE
      END
C
      SUBROUTINE PCSUM(ALPHA,D,BETA,P,L,PSUM,N)
      COMPLEX*16 PSUM
       COMMON/MISVA/RZ,A
      INTEGER P
      DOUBLE PRECISION TM
      COMPLEX * 16 ALPHA,Y,CSUM,TAB(900),T1,T2
      TM = 1.
      K = 0
      LL = 1
      IF(L.EQ.0) GO TO 15
      LL = L
      DO 10 I = 1,L
      TM = ((P+L-I+1)/FLOAT(L-I+1)**2)*TM
  10  CONTINUE
  15  CONTINUE
      PSUM = (0., 0.)
       N=IFIX(100.*BETA/2.+.5)
      TAB(1) = (1., 0.)
      DO 20 I = 2,N
      IF(CDABS(TAB(I-1)) .LT. 1.E-60) GO TO 30
  20  TAB(I) = TAB(I-1)*(-ALPHA)/(I-1)
      I = N+1
  30  CONTINUE
      IF (I-1 .LT. N) N = I-1
  35  CONTINUE
      T1 = (1.0, 0.)
      CSUM = (0., 0.)
      LK = L+K
      DO 40 I = 1,N
  40  CSUM = CSUM + TAB(I)/ (LK+I)
      KM=IFIX(100.*(-D)+.5)
       DO 60 M=1,KM
      T1 = T1*D/(M*(M+L))
      T2 = 0.
      DO 50 I = 1,N
  50  T2 = T2 + TAB(I)/(LK+M+I)
      CSUM = CSUM + T2  *T1
      IF(CDABS(T2*T1/CSUM) .LT. 1.E-8) GO TO 100
  60  CONTINUE
       WRITE (6,510)RZ,A,ALPHA,T2,CSUM
 510   FORMAT(1X,F5.1,2(1X,E11.4),1X6E15.6)
 100  CONTINUE
      PSUM = PSUM + CSUM*TM
      K = K+1
```

```
      IF(K.GT.P) GO TO 120
      TM = TM*(P-K+1)/(FLOAT(K*(K+L)))*(-BETA)
      GO TO 35
  120 CONTINUE
      RETURN
      END
```

APPENDIX B

```
      REAL FUNCTION TOTAL(N1,L1)
      IF (1-L1)49,52,52
 49   AA=1.
      LL=1
 50   AA1=N1+LL-1
      AA=AA1*AA
      LL=LL+1
      IF (LL-L1)50,51,51
 51   TOTAL=AA*.2
      GO TO 53
 52   TOTAL=.2
 53   CONTINUE
      RETURN
      END
C
C
      REAL FUNCTION FCN(X)
      COMMON/AFCN/N2,L2
      INTEGER P1
      DIMENSION EL(12,12)
 11   EL(L2,1)=1
      XL=L2
      EL(L2,2)=XL-X
 12   X2=P1
      P1=1
      EL(L2,P1+2)=((2.*X2+XL-X)*(EL(L2,P1+1))-(X2+XL-1.)*(EL(L2,P1)))
     * /(X2+1.)
      P1=P1+1
      IF (P1-N2+1)12,13,13
 13   IF (1-L2)14,15,14
 15   FCN=(EL(1,N2)**2)*EXP(-X)
      GO TO 16
 14   FCN=(EL(L2,N2)**2)*(X**(L2-1))*EXP(-X)
 16   CONTINUE
      RETURN
      END
C
C
      DIMENSION INT(10),RR(20), XX(20), DD(3)
      DATA DD/0., 0.0, 1.0/
      INTEGER P
      EXTERNAL FCN
      COMMON/AFCN/N3,L3
      Y=1.
      G=1
      T=1
      IF (G-1)7,23,7
 23   DO 200 L3=1,11
      IF (T-1)7,22,7
 22   DO 105 N3=1,11
      SW=0
      DEL=1
      P=N3-1
      L=L3-1
      A=TOTAL(N3,L3)
 9    B=SIMSON (FCN,0.0, Y, 1.0E-3, IT, INT)
      IF (ABS(1-B/A)-.01)13,13,11
 11   IF (B-A)14,13,12
 14   IF (SW)7,15,16
 15   Y=Y-DEL
      SW=0
      GO TO 9
 16   DEL=DEL/2.
      GO TO 15
 12   IF (SW)7,17,18
 18    Y=Y+DEL
      SW=1
      GO TO 9
 17   DEL=DEL/2.
      GO TO 18
 7    WRITE(6,102)
 13   R=SQRT(Y/2)
 101  FORMAT(1X,'R=',F6.3,2X,'P=',I3,2X,'L=',I3)
 102  FORMAT(1X,'ERROR')
      WRITE (6,101) R,P,L
      RR(N3)=R
      XX(N3)=N3-1
 105  CONTINUE
      CALL LABEL(0.0,0.0,0.0,10.,10.,10,'R/W',3,1)
      CALL LABEL(0., 0., 0., 10., 10., 10, 'P', 1, 0)
      CALL XYPLT(11,XX,RR,0.,15.,0.,10.,DD,0,L3)
 200  CONTINUE
      STOP
      END
```

APPENDIX C

```
      DIMENSION RR(20),XX(20),DD(3),ROOTS(1),ITER(1),FRT(1)
      DATA DD/0., 0., 1.0/
      EXTERNAL F
      COMMON/AF2/N3
      COMMON/AF1/M3
      DO 200 M3=1,11
      DO 105 N3=1,11
      M=M3-1
      N=N3-1
      CALL TROOT(F,0.,12.,12.,1.0E-2,20,NROOTS,ROOTS,ITER,FRT)
      R=ROOTS(1)*2./1.4142
      WRITE (6,101) R,N,M
  101 FORMAT(1X,'R=',F6.3,2X,'N=',I3,2X,'M=',I3)
      V=2.*R
      RR(N3)=V
      XX(N3)=N3-1
  105 CONTINUE
      IF (M3 .GT. 1) GO TO 137
      CALL LABEL(0.,0.,0., 7.,10., 7,'A/W0',4,1)
      CALL LABEL(0.,0.,0.,10.,10.,10,'N=',1,0)
  137 CALL XYPLT(11,XX,RR,0., 15.,0.,14.,DD,0,M3)
  200 CONTINUE
      STOP
      END
C
C
      REAL FUNCTION TOTAL(M1,N1)
      PI=3.1416
      FAM=1.
      MM=1
   10 FAM1=MM
      FAM=FAM1*FAM
      MM=MM+1
      IF (MM-M1)10,11,11
   11 FAN=1.
      NN=1
   12 FAN1=NN
      FAN=FAN1*FAN
      NN=NN+1
      IF (NN-N1)12,13,13
   13 TOTAL=2.**(N1+M1-2)*FAM*FAN*PI*(.5)/4.
      RETURN
      END
C
C
      REAL FUNCTION F1(X)
      DIMENSION H(110)
      COMMON/AF1/M2
      INTEGER P1
      H(1)=1
      H(2)=2.*X
      P1=1
   20 X2=P1
      H(P1+2)=2.*X*H(P1+1)-2.*X2*H(P1)
      P1=P1+1
      IF (P1-M2+1)20,21,21
   21 F1 =H(M2)**2*EXP(-X**2)
      RETURN
      END
C
C
      REAL FUNCTION F2(X)
      COMMON/AF2/N2
      DIMENSION H(110)
      INTEGER P2
      H(1)=1
      H(2)=2.*X
      P2=1
   30 X3=P2
      H(P2+2) =2.*X*H(P2+1)-2.*X3*H(P2)
      P2=P2+1
      IF (P2-N2+1)30,31,31
   31 F2 =H(N2)**2*EXP(-X**2)
      RETURN
      END
C
C
      REAL FUNCTION F(Y)
      DIMENSION INT(10)
      EXTERNAL F1,F2
      COMMON/AF2/N3
      COMMON/AF1/M3
      S1=SIMSON(F1,0.,Y,1.0E-3,IT,INT)*SIMSON(F2,0.,Y,1.0E-3,IT,INT)
      S2=TOTAL(M3,N3)
      F=S1-S2
      RETURN
      END
C
```

Reprinted from:

JOURNAL OF THE OPTICAL SOCIETY OF AMERICA VOLUME 62, NUMBER 9 SEPTEMBER 1972

Diffraction of Laguerre Gaussian Beams by an Aperture*

ALEXANDER C. LIVANOS AND NICHOLAS GEORGE
California Institute of Technology, Pasadena, California 91109
(Received 19 April 1972)
INDEX HEADINGS: Diffraction; Filter.

In recent articles the problem of the diffraction of the lowest-order gaussian beam truncated by a circular aperture has been treated.[1,2] We have extended these analyses to include any higher-order gaussian beams, using the associated Laguerre polynomial to describe the radial distribution of the electric field.

Consider an aperture located in the plane at $z=0$ having a transmittance function $T(\rho,\phi)$ given by

$$T(\rho,\phi)=\mathrm{circ}(\rho)=1 \quad (\rho\le a) \\ =0 \quad \text{otherwise}, \qquad (1)$$

with cylindrical coordinates ρ and ϕ. The scalar function $U_{pl}(\rho,\phi)$ is taken to describe the transverse component of the illumination at $z=0$,[3]

$$U_{pl}(\rho,\phi)=\frac{2}{(1+\delta_{0l})^{\frac{1}{2}}}\left[\frac{p!}{\pi(l+p)!}\right]^{\frac{1}{2}}\frac{1}{w_0}\left(\frac{\sqrt{2}}{w_0}\right)^l\rho^l \times L_p{}^l\left(\frac{2\rho^2}{w_0^2}\right)\begin{pmatrix}\cos l\phi\\ \sin l\phi\end{pmatrix}\exp(-\rho^2/w_0^2), \qquad (2)$$

where

$$\delta_{0l}=1 \quad \text{for} \quad l=0 \\ =0 \quad \text{for} \quad l\neq 0,$$

$L_p{}^l$ is the associated Laguerre polynomial, and w_0 = spot size of gaussian wave at plane $z=0$.

A transverse scalar component of the electric-field amplitude at $(\rho',\phi',z>0)$ (see Fig. 1) is given by the usual Fresnel-zone approximation of Sommerfeld's formula,[4]

$$V(\rho',r)=\frac{jz}{\lambda r^2}\exp(-jkr)\int_S\int U(\rho,\phi) \times\exp\left[-jk\left(\frac{\rho^2}{2r}-\frac{\rho\rho'\cos(\phi'-\phi)}{r}\right)\right]\rho\, d\rho\, d\phi. \qquad (3)$$

In order to have the result applicable for large values of ρ', we expand

$$r'=[r^2+\rho^2-2\rho\rho'\cos(\phi-\phi')]^{\frac{1}{2}},$$

factoring $r=(\rho'^2+z^2)^{\frac{1}{2}}$, instead of simply z. Combining Eqs. (1)–(3) and integrating with respect to ϕ gives

$$V_{pl}(\rho',r)=\frac{jz\exp(-jkr)}{\lambda r^2}\exp\left(\frac{jl\pi}{2}\right)\begin{pmatrix}\cos l\phi'\\ \sin l\phi'\end{pmatrix}\frac{4\sqrt{\pi}}{(1+\delta_{0l})^{\frac{1}{2}}} \times\left[\frac{p!}{(l+p)!}\right]^{\frac{1}{2}}\frac{1}{w_0}\left(\frac{\sqrt{2}}{w_0}\right)^l\int_0^a\rho^{l+1}J_l\left(\frac{K\rho\rho'}{r}\right) \times L_p{}^l\left(\frac{2\rho^2}{w_0^2}\right)\exp\left[-\rho^2\left(\frac{1}{w_0^2}+\frac{jk}{2r}\right)\right]d\rho, \qquad (4)$$

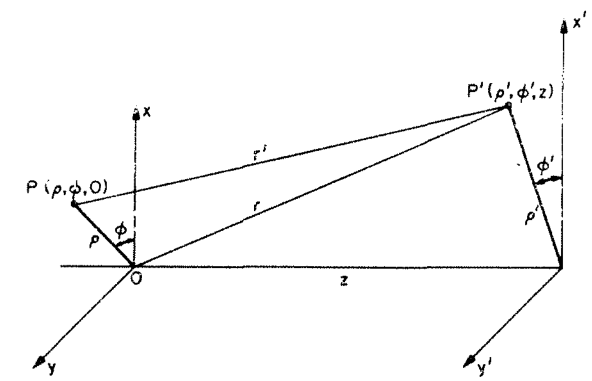

FIG. 1. Geometry of relationships between aperture and observation plane.

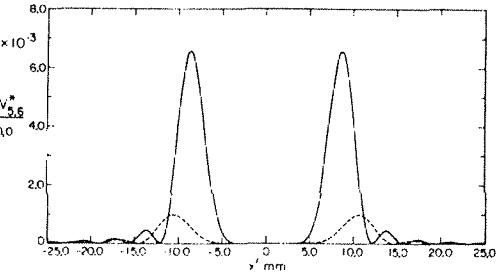

FIG. 2. Normalized transmitted irradiance $V_{5,6}V_{5,6}{}^*$ vs x'; $a/w_0=0.8$, 1.0 are dashed and solid curves, respectively, for $\lambda=0.6328$ μm, $z=0.1$ m, and $\phi'=0$.

where J_l is the Bessel function of order l. Expanding J_l and $L_p{}^l$ into infinite series, Eqs. (8.440) and (8.970) in Ref. 5, respectively, and integrating term by term gives the general result

$$V_{pl}(\rho',r)=\frac{2\sqrt{\pi}}{\lambda}\frac{a^2z}{r^2}\frac{1}{w_0}\left[\frac{p!(l+p)!}{1+\delta_{0l}}\right]^{\frac{1}{2}}h^l\exp(-jkr) \times\exp\left(\frac{jl\pi}{2}\right)\begin{pmatrix}\cos l\phi'\\ \sin l\phi'\end{pmatrix}\frac{1}{\alpha^{l+1}} \times\sum_{K=0}^{K=p}\frac{\xi^K}{(l+K)!(p-K)!}\sum_{m=0}^{m=\infty}\frac{g^m\gamma(l+m+K+1,\,a)}{m!(m+l)!}, \qquad (5)$$

where γ is the incomplete γ function and

$$b=\frac{K\rho' a}{r},\quad \frac{a^2}{w_0^2}+\frac{j\pi a^2}{\lambda r}=\alpha,\quad \xi=\frac{2a^2}{w_0^2\alpha},\quad g=\frac{-b^2}{4\alpha},\quad h=\frac{ab}{\sqrt{2}w_0}.$$

Restricting the radial dependence to $\rho^l\exp(-\rho^2/w_0^2)$ by setting $p=0$ gives

$$V_{0l}(\rho',r)=\frac{2\sqrt{\pi}}{\lambda}\frac{a^2z}{r^2}\frac{1}{w_0}\left[\frac{1}{l!(1+\delta_{0l})}\right]^{\frac{1}{2}}\frac{e^{-\alpha}}{\alpha}\beta^l\exp(-jkr) \times\exp\left(\frac{jl\pi}{2}\right)\begin{pmatrix}\cos l\phi'\\ \sin l\phi'\end{pmatrix}\sum_{m=1}^{m=\infty}\frac{J_{l+m}(b)}{d^m}, \qquad (6)$$

where $d=b/2\alpha$, $\beta=\sqrt{2}a/w_0$.

For comparison to Refs. 1 and 2, reducing to the single-lobe case, i.e., $p=0$ and $l=0$, in Eq. (5) gives the equivalent unnormalized result

$$V_{00}(\rho',r)=\frac{(2\pi)^{\frac{1}{2}}}{\lambda}\frac{a^2z}{r^2}\frac{1}{w_0}\frac{e^{-\alpha}}{\alpha}\exp(-jkr)\sum_{m=1}^{m=\infty}\frac{J_m(b)}{d^m}. \qquad (7)$$

An illustration of the radiation pattern for the higher-order modes is shown in Fig. 2. $V_{5,6}V_{5,6}{}^*/I_{00}$ from Eq. (5) for $V_{5,6}$, normalized to I_{00}, is plotted vs x' for $a/w_0=1.0$ and 0.8. I_{00} is the irradiance of the TEM$_{00}$ mode at any point $(0,z)$ in the absence of the aperture, given by

$$I_{00}=2\pi w_0^2/(\pi^2w_0^4+\lambda^2z^2). \qquad (8)$$

For $a/w_0=1.0$ only about 12% of the total power is transmitted through the aperture. By way of contrast, we note that with same aperture size 86% of the power is coupled for the TEM$_{0,0}$ mode. For $a/w_0=0.8$ as shown in Fig. 2, we see that the power transmitted in the TEM$_{5,6}$ mode drops sharply to a mere 2.5% of the incident power.

Also, we note the zero of irradiance at $\rho'=0$; this is characteristic of each of these modes for any p when $l\neq 0$. On the other hand, when $l=0$, the central lobe is a maximum.

To study the loss of power as a function of the aperture ratio a/w_0, we compute

$$P_{tr}/P_{in}=\int_0^{2\pi}\int_0^a|U_{pl}|^2\rho\, d\rho\, d\phi, \qquad (9)$$

where the incident and transmitted powers are denoted by P_{in},

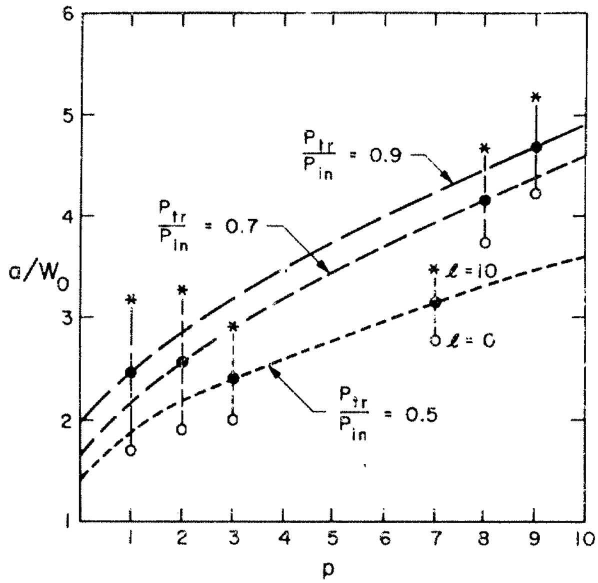

FIG. 3. Transmittance P_{tr}/P_{in} as a function of relative aperture size and mode index p for $\lambda = 0.6328\ \mu m$, $z = 0.1$ m. The dashed curves are for $l = 5$; range bars are shown on each curve to permit interpolation for mode indices from $l = 0$ (○) to $l = 10$ (*).

P_{tr}, respectively, noting that

$$P_{in} = \int_0^{2\pi} \int_0^{\infty} |U_{pl}|^2 \rho\, d\rho\, d\phi$$

is unity. Substituting Eq. (2) in Eq. (9) gives

$$\frac{P_{tr}}{P_{in}} \frac{(p+l)!}{p!} = \int_0^{2a^2/w_0^2} x^l (L_p^l(x))^2 e^{-x} dx. \tag{10}$$

Equation (10) was solved numerically and resulting curves for a wide range of modes $TEM_{p,l}$ are shown in Fig. 3. The dashed lines show relative aperture, a/w_0, plotted vs the mode index p for constant efficiency, P_{tr}/P_{in}, for values of 0.5, 0.7, and 0.9 with $l = 5$.

* Research supported in part by the Electronic and Solid State Sciences Division of the Air Force Office of Scientific Research.

[1] G. O. Olaofe, J. Opt. Soc. Am. 60, 1654 (1970).
[2] R. G. Schell and G. Tyras, J. Opt. Soc. Am. 61, 31 (1971).
[3] A. E. Siegman, *An Introduction to Lasers and Masers* (McGraw-Hill, New York, 1971), p. 330.
[4] For example, see Eq. (3) in Ref. 2.
[5] I. S. Gradshteyn and I. M. Ryzhik, *Table of Integrals, Series, and Products* (Academic, New York, 1965).